THE ADSORPTION OF CHEMICAL CONTAMINANTS ONTO ENVIRONMENTAL SURFACES WITH SPECIAL CONSIDERATION OF THE BACTERIAL SURFACE

A Dissertation

Submitted to the Graduate School

of the University of Notre Dame

in Partial Fulfillment of the Requirements

for the Degree of

Doctor of Philosophy

by

Drew Gorman-Lewis, Ph.D.

_____

Jeremy B. Fein, Director

Graduate Program in Civil Engineering and Geological Sciences

Notre Dame, Indiana

November 2005

THE ADSORPTION OF CHEMICAL CONTAMINANTS ONTO GEOLOGIC SURFACES WITH SPECIAL CONSIDERATION OF THE BACTERIAL SURFACE

Abstract

by

Drew Gorman-Lewis

Adsorption reactions are one of many processes to consider when attempting to predict and understand the movement of contaminants through the subsurface. This dissertation presents the work of four individual but related studies that measured and quantified adsorption reactions of chemical contaminants onto a variety of particulate subsurface media with special consideration of the reactivity of the bacterial surface. Chapter 2 describes the adsorption of an ionic liquid onto mineral oxides, clay, and bacteria. The experimental results reveal that 1-Butyl, 3-methylimidazolium chloride (Bmim Cl) is unstable in water below pH 6 and above pH 10 and that it exhibits pH independent and ionic strength dependent adsorption onto Na-montmorillonite with 0.4, 0.8, 1.0, 1.2, and 2.0 g/L of clay. We observed no adsorption of the Bmim Cl onto *Bacillus subtilis* (3.95 or 7.91 g (dry weight) bacteria/L) at pH 5.5 to 8.5 or onto gibbsite (500 or 1285 g/L) or

quartz (1000 and 2000 g/L) over the pH range 6-10. The measured adsorption was subsequently quantified using a distribution coefficient approach. Chapter 3 focuses specifically on the reactivity of the bacterial surface using the new technique of combining titration calorimetry with surface complexation modeling to produce site-specific enthalpies and entropies of proton and Cd adsorption. Our results provide mechanistic details of these adsorption reactions that are impossible to gain from previous techniques used to study the bacterial surface. Chapters 4 and 5 present work measuring and quantifying the adsorption of U and Np onto *B. subtilis* under a variety of conditions. Np adsorption exhibited a strong ionic strength dependence and unusual behavior under low pH high ionic strength conditions that was consistent with reduction of Np(V) to Np(IV). U adsorption, in constrast to Np adsorption, was extensive under all conditions studied. Thermodynamic modeling of the data suggests that uranyl-hydroxide, uranyl-carbonate and calcium-uranyl-carbonate species each can form stable surface complexes on the bacterial cell wall. These studies investigate a variety of adsorption reactions and provide parameters to quantify adsorption that may aid in integration of these reactions into geochemical models to predict contaminant transport in the subsurface.

CONTENTS

FIGURES

TABLES

ACKNOWLEDGMENTS

First I would like to thank Dr. Jeremy B. Fein for his guidance, patience, and friendship. I don't think it's possible to find a better advisor. A large portion of the research in this dissertation was conducted at Argonne National Lab in the Actinide Facility. I would like to thank Dr. Lynne Soderholm for making that collaboration possible. A special thanks to Dr. Mark P. Jensen from whom I have learned so much and truly enjoyed working with. You are a gifted scientist and an exceptional teacher. I would also like to thank the members of my committee Drs. Patricia A. Maurice, Peter C. Burns, and Clive R. Neal. Each of you have brought a unique perspective to my work and graduate career.

I would not have made it to graduate school if not for Drs. Michael M. Haley, Mark H. Reed, Karen Kelskey, and Nancy Deans. Thank you all for your support and taking the time to prepare me for my graduate career.

Drs. Jo Trigilio and Sal Johnston gave me the first glimpse of what my future may hold and I thank them for their friendship.

I received a GAANN fellowship and additional funding through the Environmental Molecular Science Institute during my graduate career. This funding provided me with travel and research experiences that otherwise would have been unavailable. Numerous portions of the research contained in this dissertation would not have been possible without the equipment and staff at the Center for Environmental Science and Technology at the University of Notre Dame.

CHAPTER 1

INTRODUCTION

Biogeochemical cycles, activities related to industry, weapons production, mining, nuclear energy, and other processes have introduced chemical contaminants into the environment. As contaminants migrate through the subsurface they encounter a range of geologic surfaces that may retard the mobility of the contaminants through a variety of chemical reactions. Adsorption reactions are one type of interaction to consider when examining the migration of contaminants through the subsurface. The mobility of chemical contaminants in the subsurface can be highly influenced by adsorption onto geological surfaces (Beveridge and Murray, 1976; Sposito, 1984; Waite et al., 1994; Fein et al., 1997; Macaskie and Basnakova, 1998; Rheinlander et al., 1998; Stipp et al., 2002; Stewart et al., 2003; Garelick et al., 2005). Since adsorption reactions can have such an impact on the mobility of pollutants, it is necessary to be able to quantify adsorption onto common geologic surfaces. This dissertation encompasses four individual research projects describing the adsorption and quantification of chemical contaminants onto geologic surfaces with special consideration of the reactivity of the bacterial surface.

Quantification of contaminant adsorption onto geologic media is crucial for incorporation of these reactions into geochemical models that attempt to predict contaminant transport. The most common methods of quantifying adsorption of aqueous contaminants are with the distribution coefficient approach or a surface complexation model. Each technique has strengths and weaknesses depending on the adsorption behavior of the solute and the surface properties of the sorbent. Bulk adsorption experiments and subsequent application of the distribution coefficient adsorption model to the data produces a parameter, a K_D value in the case of a distribution coefficient model or a stability constant with the application of a surface complexation model, which quantifies the observed adsorption.

The distribution coefficient approach is a more simplistic means of describing adsorption of introduced chemical contaminants in the environment than a surface complexation model. K_D values are partitioning coefficients between the aqueous and adsorbed solute. This modeling technique is most useful when adsorption behavior is relatively simple, i.e. there is no pH dependence, or when the surface properties of the sorbent are too heterogeneous to be described with balanced chemical equations. The distribution coefficient approach can typically describe adsorption accurately; however, its predictive properties for adsorption in systems not directly studied in the laboratory could be weakened due to its lack of grounding in thermodynamics (Bethke and Brady, 2000; Brady and Bethke, 2000; Koretsky, 2000).

Surface complexation models are a more sophisticated approach to describing adsorption onto geologic surfaces. This model has its basis in thermodynamics and describes adsorption with balanced chemical equations. Consequently, well-characterized surfaces, in which the acidity constants are known for the functional groups responsible for contaminant adsorption, are necessary in order to apply a surface complexation model to bulk adsorption data. This added complexity requires more knowledge of the sorbent surface than the K_D approach, which does not require any sorbent characterization. However, the surface complexation approach is a more flexible method because its basis in thermodynamics allows for prediction in systems not directly measured in the laboratory. The work presented in this dissertation uses both the K_D approach and surface complexation models to quantify the observed adsorption behavior of a variety of chemical contaminants described in the following chapters.

Green engineering efforts have led to development of new industrial solvents with little to no vapor pressure in an effort to reduce air pollution (Brennecke and Maginn, 2001). These new solvents, ionic liquids, hold promise as potential industrial replacements to volatile solvents that contribute air pollution and compromise worker safety (Anthony et al., 2001). Prior to these solvents being widely used in industry their potential impact on subsurface environments needs to be assessed. Chapter 2 of this dissertation describes the adsorption of an ionic liquid onto mineral and bacterial surfaces which are analogues for many types of surfaces that a contaminant might encounter if released into the environment. Consequently, these results can be interpreted to describe the potential mobility of the ionic liquid in the subsurface. This work has been published

in *Environmental Science and Technology* (Gorman-Lewis and Fein, 2004). I performed the experiments, data analysis, and wrote the manuscript. Jeremy B. Fein provided intellectual insight and manuscript editing.

Bacterial adsorption reactions have the potential to control the mobility of contaminants in the subsurface. Understanding the reactivity of bacterial surfaces is a key factor in determining the potential impact bacterial adsorption reactions may have on a system of interest. Traditional methods of investigating the reactivity of the bacterial surface include acid-base titrations, spectroscopic studies, and bulk adsorption measurements (Fein et al., 1997; Kelly et al., 2002; Martinez et al., 2002; Boyanov et al., 2003; Ngwenya et al., 2003; Yee et al., 2004; Fein et al., 2005). Although potentiometric titrations and bulk adsorption experiments provide constraints on the total reactivity of the cell wall, they do not provide complete or detailed information on the binding environments. Spectroscopic data provide more direct evidence of the metal coordination environment than do bulk adsorption measurements. However, due to the complexity of the cell wall binding environments, and due to the fact that xray adsorption spectroscopy (XAS) yields an averaged binding environment, the experimental results from XAS can be complex and difficult to interpret. New methods that could enhance our understanding of the reactivity of the bacterial surface include calorimetric measurements of proton and metal adsorption. Chapter 3 describes a study in which we measured the enthalpy of proton and Cd adsorption onto *B. subtilis*. This approach yields mechanistic details and the temperature dependence of these adsorption reactions which are impossible to gain from bulk adsorption experiments. This work has been submitted for publication. Mark

P. Jensen and I performed the experiments and data analysis. I wrote the manuscript and Mark P. Jensen and Jeremy B. Fein provided intellectual insight and manuscript editing.

Nuclear waste, mining activities and weapons production have led to the release of radionuclides into the environment. Np is a byproduct of nuclear reactors, and is considered to be one of the most problematic radionuclides during long term nuclear waste storage due its long half-life, high solubility, and potential mobility in the environment (Runde, 2002). The fate and transport of Np in the subsurface is difficult to predict because the adsorption of Np onto common mineral and organic surfaces has not been well characterized. In addition to Np, U is also problematic due to the high solubility of the uranyl ion and its complex aqueous speciation. This makes prediction of its behavior in the subsurface environment extremely difficult. Bacteria, which can adsorb a wide range of aqueous cations, are ubiquitous in near-surface environments. Thus, bacterial cell wall adsorption may affect the mobility of radionuclides (Boily and Fein, 2000). Consequently, it is crucial to quantify U and Np-bacterial adsorption in order to accurately predict the transport of these contaminants through bacteria-bearing groundwater systems. Chapter 4 and 5 of this dissertation describe studies in which we measured and quantified U and Np adsorption onto *B. subtilis*. The objective of this research is to measure the pH, concentration, and ionic strength dependence of Np adsorption onto a common bacterial cell wall. This work has been published in *Geochimica et Cosmicha Acta* (Gorman-Lewis et al., 2005b). I performed the experiments, data analysis, and wrote the manuscript. Jeremy B. Fein, Mark P. Jensen,

and Lynda Sodherholm provided intellectual insight and manuscript editing. Ming Chiang and Mark P. Jensen provided technical and experimental support.

The goal of chapter 5 was to conduct uranium adsorption experiments to determine the identity and thermodynamic stabilities of the important bacterial surface uranium species above pH 5, where the aqueous uranium speciation becomes complex. This work has been published in *Environmental Science and Technology* (Gorman-Lewis et al., 2005a). I performed the experiments, data analysis, and wrote the manuscript. Jeremy B. Fein provided intellectual insight and manuscript editing.

CHAPTER 2

EXPERIMENTAL STUDY OF THE ADSORPTION OF AN IONIC LIQUID ONTO BACTERIAL AND MINERAL SURFACES

2.1 Introduction

Most organic solvents used in industrial applications exhibit a measurable vapor pressure under their conditions of use, and therefore these solvents can constitute a substantial source of volatile organic compounds (VOCs) to the environment (Allen and Shonnard, 2002). A range of environmental problems such as air pollution and human health effects are linked to VOC pollution (Economopoulou and Economopoulos, 2002; Masjedi et al., 2003; Molhave, 2003). These environmental impacts have provided the impetus for the development of "green engineering", which represents research aimed at finding environmentally benign alternatives to harmful chemicals. Ionic liquids have received considerable attention as potential alternatives to volatile solvents. These liquids are organic salts with no measurable vapor pressure and with an extremely large liquidus

range. The large range of organic cation and inorganic anion pairs that can be used to build these salts makes it possible to design solvents with specific properties to suit specific applications. However, the primary advantage of ionic liquids over other organic solvents is that ionic liquids have immeasurably low vapor pressures, so that their widespread industrial use as solvents would dramatically reduce VOC release to the environment. To date, studies have demonstrated that ionic liquids can successfully substitute for traditional organic solvents in a wide range of industrial applications, including Diels-Alder, Heck, and Friedel-Crafts reactions, as well as others (Welton, 1999; Earle and Seddon, 2000).

Despite the potential for ionic liquids to reduce VOC emissions, the fate and mobility of these solvents in the environment is unknown. Although ionic liquids currently are not widely used in industrial applications, continued development and use of these solvents requires a better understanding of their effects on the environment. Little is know about the toxicity or mobility of ionic liquids in the environment. In this study, we concentrate on the adsorption behavior of one class of ionic liquids (dialkylimidazolium salts) in order to determine the mobility of these molecules should they ever be present as contaminants in groundwater systems. Virtually nothing is known concerning the adsorption of ionic liquids onto geologic media or the stability of ionic liquids in aqueous solutions. The adsorption of ionic liquids onto high concentrations of activated carbon is a potentially effective, but not necessarily efficient, remediation technique (Anthony et al., 2001). The objective of this study is to determine the adsorption behavior of one class of ionic liquids onto the biological and mineral surfaces

that are common in geologic systems. These adsorption reactions typically dominate the environmental fate and transport of non-volatile dissolved contaminants in groundwater systems (Sposito, 1984).

2.2 Experimental Procedure

We measured the adsorption of dissolved 1-Butyl, 3-methylimidazolium chloride (Figure 2.1) onto non-metabolizing *Bacillus subtilis*, gibbsite, quartz, and Na-montmorillonite. Figure 2.1 illustrates the basic structure of dialkylimidazolium salts. The R_1 and R_2 groups can be alkyl chains of varying lengths, and X^- can be a variety of inorganic anions. The dialkylimidazolium salts have received much attention because of their ease of synthesis and use in Friedel-Crafts reactions (Earle and Seddon, 2000). 1-Butyl, 3-methylimidazolium chloride (Bmim Cl) is a commercially available dialkylimidazolium salt. Other ionic liquids that should have similar surface adsorption behaviors to Bmim Cl are ones with the same organic cation group, i.e., Bmim PF_6 and Bmim BF_4. *B. subtilis*, an aerobic, Gram-positive bacterial species, is a common soil microorganism with well–characterized surface properties (Beveridge and Murray, 1976; Beveridge and Murray, 1980; Fein et al., 1997; Daughney and Fein, 1998a; Fowle and Fein, 2000), and we use it here to study typical sorptive properties of subsurface bacteria. Gram-negative bacterial cell walls possess an additional outer lipid membrane layer compared with Gram-positive cell walls. However, their general sorptive properties, with respect to organic and inorganic solutes, (e.g., 2,4-dichlorophenoxy-acetic acid and Cd(II)), appear to be similar to those of Gram-positive species (Paris et al., 1981; Yee and Fein, 2001).

Gibbsite and quartz are common near-surface minerals, and represent different ends of the spectrum of surface charge properties. The zero point of charge (pH_{zpc}) for quartz is approximately 2 - 3, meaning above this pH range, and in our experiments, the quartz surface is negatively charged. Conversely, the pH_{zpc} of gibbsite is approximately 9.8 (Sverjensky and Sahai, 1996), so under our experimental conditions, the gibbsite surface varies from being predominantly positively charged to neutral, and then negatively charged with increasing pH.

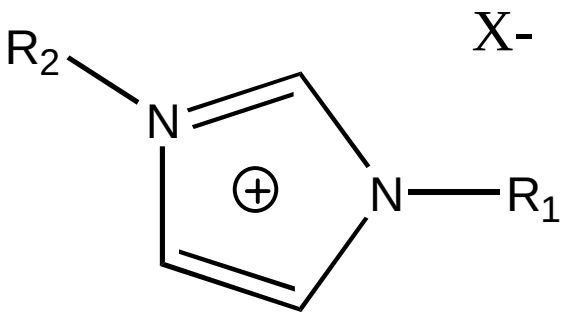

Figure 2.1: General structure of an imidazolium salt where R_1 and R_2 can be alkyl chains of varying lengths and X^- is an inorganic anion. In solution, the imidazolium ion and the anion completely dissociate.

Clay minerals in the smectite group that have a 2:1 structure (such as montmorillonite) typically exhibit two types of adsorption mechanisms: pH-dependent and pH-independent sorption. The pH-independent adsorption occurs through cation exchange reactions in the interlayer and from electrostatic interactions from the permanent charge on the clay (Turner et al., 1996). The pH dependent adsorption occurs

through site-specific surface complexation reactions involving clay edge sites, similar to reactions that occur on oxide surfaces (McKinley et al., 1995). Experimental measurements of cation adsorption onto montmorillonite demonstrate that the clay exhibits both pH-dependent and pH–independent sorption mechanisms (Johnston and Cardile, 1987; Kraepiel et al., 1999).

B. subtilis cells were cultured and prepared following the procedures outlined in Fein et al. (1997) and Fowle and Fein (2000), except the acid wash step in the cell preparation was not conducted. Cells were maintained on agar plates consisting of trypticase soy agar with 0.5% yeast extract added. Cells for the adsorption experiments were grown by first inoculating a test-tube containing 3 ml of trypticase soy broth and 0.5% yeast extract, and incubating it for 24 h at 32°C. The 3 ml bacterial suspension was then transferred to a 1 L volume of trypticase soy broth, also with 0.5% yeast extract, for another 24 h on an incubator shaker table at 32°C. Cells were pelleted by centrifugation at 4500 rpm for 15 min, and rinsed seven times with 0.1 M $NaClO_4$. The bacteria were then pelleted by centrifugation at 7500 rpm for 60 minutes to remove excess water to obtain a wet weight so that suspensions of known bacterial concentration could be created. The ratio of this wet weight to dry weight is 5.1:1 (Borrok et al., 2004a). 1-Butyl, 3-methylimidazolium chloride (Bmim Cl) was acquired from Sachem Inc. and used as received. Synthetic gibbsite [$Al(OH)_3$] powder from J.T. Baker was used as received. Quartz [SiO_2] from Industrial Quartz was intermittently agitated in 6M NaOH for 1 hour, decanted and intermittently agitated with 10% HNO_3 for 1 hour, and rinsed 15 times with 18 MΩ ultrapure water before use. SWy-1 (Na-Montmorillonite), with a

chemical formula of $(Ca_{.12}Na_{.32}K_{.05}([Al_{3.01}Fe(III)_{.41}Mn_{.01}Mg_{.54}Ti_{.02}][Si_{7.98}Al_{.02}]O_{20}(OH)_4$ (Chipera and Bish, 2001), was obtained from the Clay Minerals Society and washed with 0.1 M $NaClO_4$ 5 times and rinsed 5 times with 18 MΩ ultrapure water before use. The adsorption of Bmim Cl onto the four solids was measured separately in 10^{-4} M and 10^{-1}M $NaClO_4$ electrolyte solutions. Batch experiments were conducted at 25 ± 1°C as a function of pH, solid:solute ratio, and time. Aliquots of a 9.3 X 10^{-4} M Bmim Cl aqueous parent solution were added to a reaction vessel (polypropylene) with known amounts of gibbsite, quartz, Na-Montmorillonite, or *B. subtilis*. Clay concentrations varied from 0.8 to 1.2 g/L and gibbsite and quartz concentrations varied from 500 to 2000 g/L. Bacterial concentrations were 3.95 and 7.91 g/L (dry weight). Additional Na-Montmorillonite experiments with 2.0 and 0.4 g/L were performed with aliquots of a 5 X 10^{-4}M Bmim Cl aqueous parent solution with a 10^{-4}M ionic strength. The pH of the suspension in each vessel was adjusted using small volumes (less than 1% of total experimental volume) of concentrated HNO_3 or NaOH. The reaction vessels were placed on a rotating rack providing end-over-end agitation for 30 minutes and additional experiments were agitated for 3 hours. The equilibrium pH was recorded, and the suspension was then centrifuged and filtered through a .45 μm nylon filter membrane. The filtrate was analyzed for Bmim Cl concentration by UV-Vis spectroscopy at 211 nm and by dissolved organic carbon (DOC) analysis, both with matrix-matched standards. Samples were prepared for DOC analysis by acidifying the supernatant with 2M ultra pure HCl. The extent of adsorption was determined by difference between the known initial concentrations of Bmim Cl and the observed final concentrations in the filtrates. Due to lower analytical uncertainties, we used the DOC measurements to determine extent of adsorption for each experiment,

except for the bacterial samples, which were affected by DOC exudates from the bacteria (see below). For the bacterial samples, we used the UV-Vis results to determine extent of adsorption.

Isotherm experiments were performed to measure ionic liquid adsorption onto the montmorillonite at pH 6.7 and 7.0, with ionic strengths of 10^{-1}M and 10^{-4}M, respectively. The starting concentration of the Bmim Cl was 9.3 X 10^{-4}M and the clay concentration was varied from 0.1 to 1.2 g/L. pH in these experiments was held constant by using small volumes (less than 1% of total experimental volume) of concentrated HNO_3 or NaOH. The reaction vessels were agitated for 3 hours. Analysis of the Bmim Cl concentration in the supernatant was performed as described above.

We also conducted control experiments without bacteria or mineral sorbents in order to determine the pH range in which the ionic liquid was stable. Aliquots of a 9.3 X 10^{-4} M Bmim Cl solution were adjusted to pH 3-10 and agitated for 30 minutes and additional experiments were agitated for 3 hours. Samples were handled and analyzed using the UV-Vis procedure described above, as well as by thin layer chromatography conducted in 100% methanol. Control experiments, to determine the amount of dissolved organic carbon introduced into the supernatant solution from the sorbents, were conducted in the same manner as the Bmim Cl experiments but without the ionic liquid present in solution. These samples were analyzed with a dissolved organic carbon analyzer and UV-Vis spectroscopy.

2.3 Results and Discussion

The control experiments reveal that Bmim Cl is only stable in the pH range from approximately 6 to 10. There were no differences found between samples that were agitated for 30 minutes or 3 hours, thus Figure 2.2 only shows results for experiments agitated for 3 hours. After exposure of the Bmim Cl to conditions below pH 6 and above pH 10, the UV-Vis spectral trace and absorption at 211 nm changed substantially from that of the parent solution (Figure 2.2). The spectral trace for these low and high pH samples exhibited multiple erratic peaks with dramatically increased absorption. The spectral absorption for samples between pH 6 and 10 was identical to that of the parent solution, and these samples exhibited no decrease in absorption intensity at 211 nm, indicating that adsorption of the ionic liquid onto the reaction vessel and decomposition of the molecule were negligible under these pH conditions. Thin layer chromatography revealed that both the parent Bmim Cl and at least one other molecule were present in solution in the samples below pH 6 and above pH 10, while only the Bmim Cl was present in the pH 6-10 samples. These experiments constrain the pH stability range for aqueous Bmim Cl, and we use the results to guide our adsorption experiments.

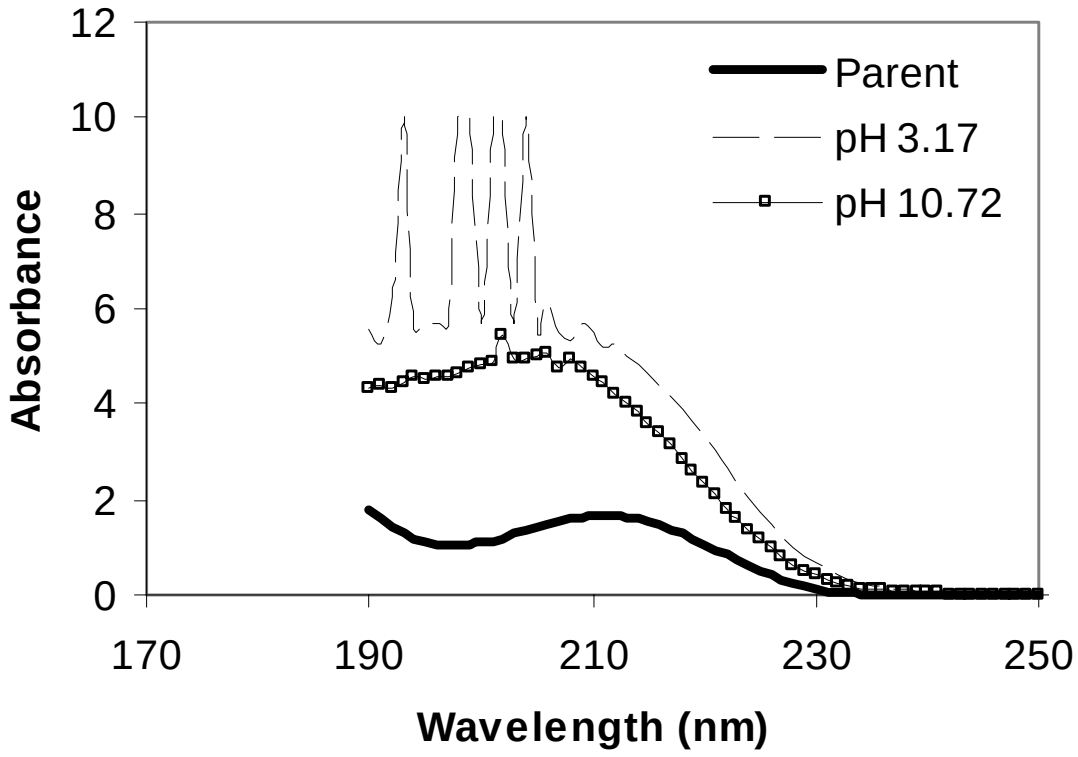

Figure 2.2: UV-Vis spectra of the stable Bmim Cl parent solution at pH 6.21 and the unknown products at pH 3.17 and 10.72

In the Bmim Cl-free control experiments, we measured elevated DOC concentrations in solutions in contact with each of the sorbents. The experiments with 1285 g/L of gibbsite and 2000 g/L quartz exhibited 25 ppm C and 7 ppm C, respectively. These results were independent of pH. DOC analysis of the 18 MΩ water revealed no dissolved carbon, indicating that introduction of DOC likely resulted from mineral surface impurities. Therefore, because the mineral contribution of DOC was constant as a function of pH and ionic strength, we could determine the concentration of Bmim Cl in the experimental samples by subtracting the DOC impurity concentration from the experimental DOC analysis for the mineral experiments. DOC in contact with the

bacteria ranged from 40 ppm C to 500 ppm C, and showed no consistent pattern with pH. Because a DOC background correction could not be applied to the bacterial samples, we used UV-Vis spectroscopy to determine the final concentration of Bmim Cl in these solutions. Control experiments showed negligible interference of the bacterial exudates molecules with the Bmim Cl at the wavelengths used to quantify the extent of Bmim Cl adsorption. There were no DOC impurities released from the Na-montmorillonite. Figure 2.3 depicts the results from the adsorption experiments involving gibbsite. As the figure demonstrates, we observed no change in the concentration of Bmim Cl during the course of the experiments. This observation held true regardless of solution pH, ionic strength, duration of exposure, and gibbsite concentration in the system, and thus Figure 2.3 only shows results for the system with the highest concentration of solids at the lowest ionic strength agitated for 3 hours. Figure 2.3 also illustrates the results from the quartz experiments. In these systems, too, we observed no change in the concentration of Bmim Cl during exposure to the quartz, with this observation holding regardless of the system pH, ionic strength, water:mineral ratio, or solid:solute contact time.

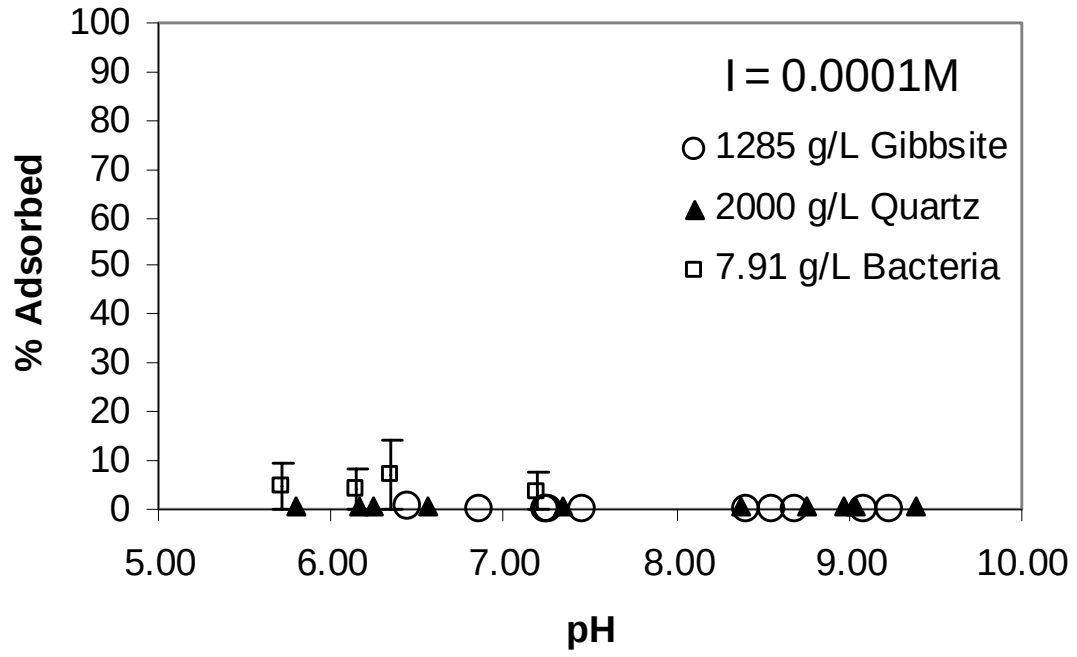

Figure 2.3: Percent of Bmim Cl adsorbed onto 1285g/L gibbsite, 2000g/L quartz, and 7.91g (dry weight)/L *B. subtilis* at an ionic strength of 10^{-4}M agitated for 3 hours (2σ error bars shown or are within data point).

The bacterial adsorption experiments exhibited similar results to those of the mineral-bearing systems. Figure 2.3 depicts the extent of adsorption of Bmim Cl onto the bacterial surface as a function of pH. Experiments in the bacterial systems were only conducted from pH 5.5 to 8.5; above pH 8.5 in the systems containing 7.91 g (dry weight)/L bacteria, the Bmim Cl samples exhibited similar spectral results to the low pH control experiments. That is, the trace showed increased light absorption at 211 nm, and an erratic spectral pattern, suggesting the presence of a pH active impurity in the solution. Results were similar for all bacterial systems studied; consequently, Figure 2.3 only

depicts the data for the systems with the highest concentration of bacteria at the lowest ionic strength agitated for 3 hours.

In contrast to the bacteria, gibbsite, and quartz systems, we observed substantial Bmim Cl adsorption onto the montmorillonite over a wide pH range. We observed adsorption that was independent of pH, but that increased with decreasing ionic strength and with increasing concentration of montmorillonite. These results suggest that interlayer cation exchange and/or the fixed negative surface charge on the clay account for adsorption, rather than pH-dependent surface complexation reactions. Figures 2.4, 2.5, and 2.6 illustrate the increase in adsorption with increasing amount of montmorillonite in the system, and that this effect is more pronounced under lower ionic strength conditions. Our isotherm results (Figure 2.7) indicate that the extent of adsorption is a linear function of clay concentration, and the results demonstrate that adsorption increases with decreasing ionic strength.

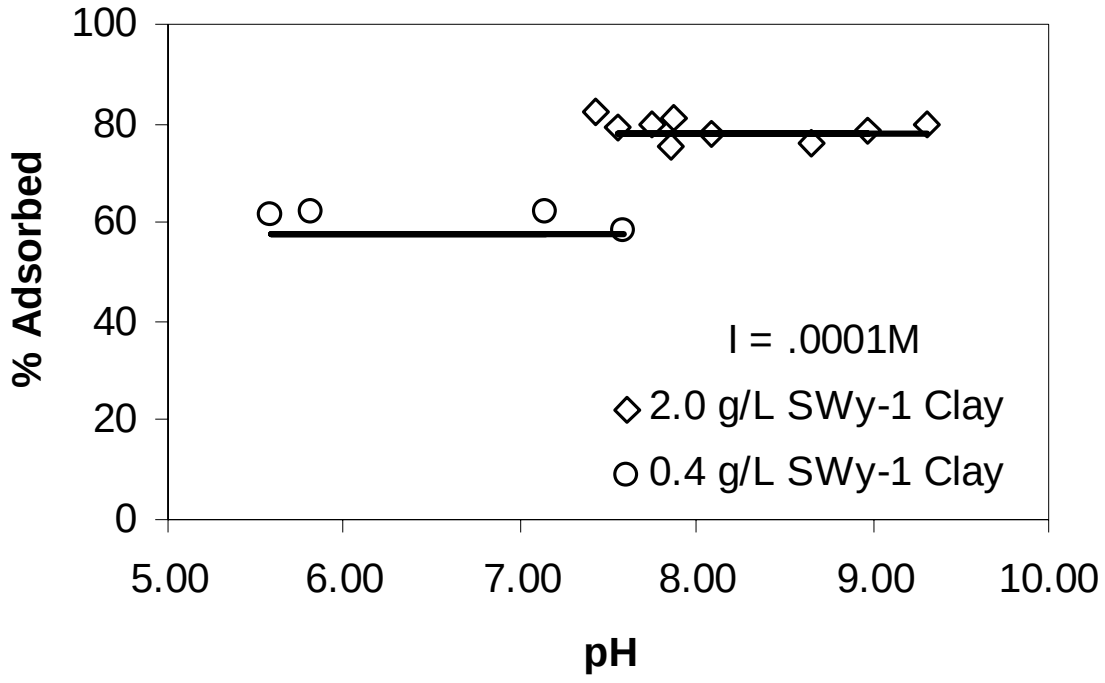

Figure 2.4: Percent of Bmim Cl (initial aqueous concentration 5 X 10^{-4}M) adsorbed onto 0.4. and 2.0 g/L SWy-1 at an ionic strength of 10^{-4}M agitated for 3 hours (2σ error bars shown or are within data point). The lines represent adsorption modeled with a K_D value of 1735 L/Kg.

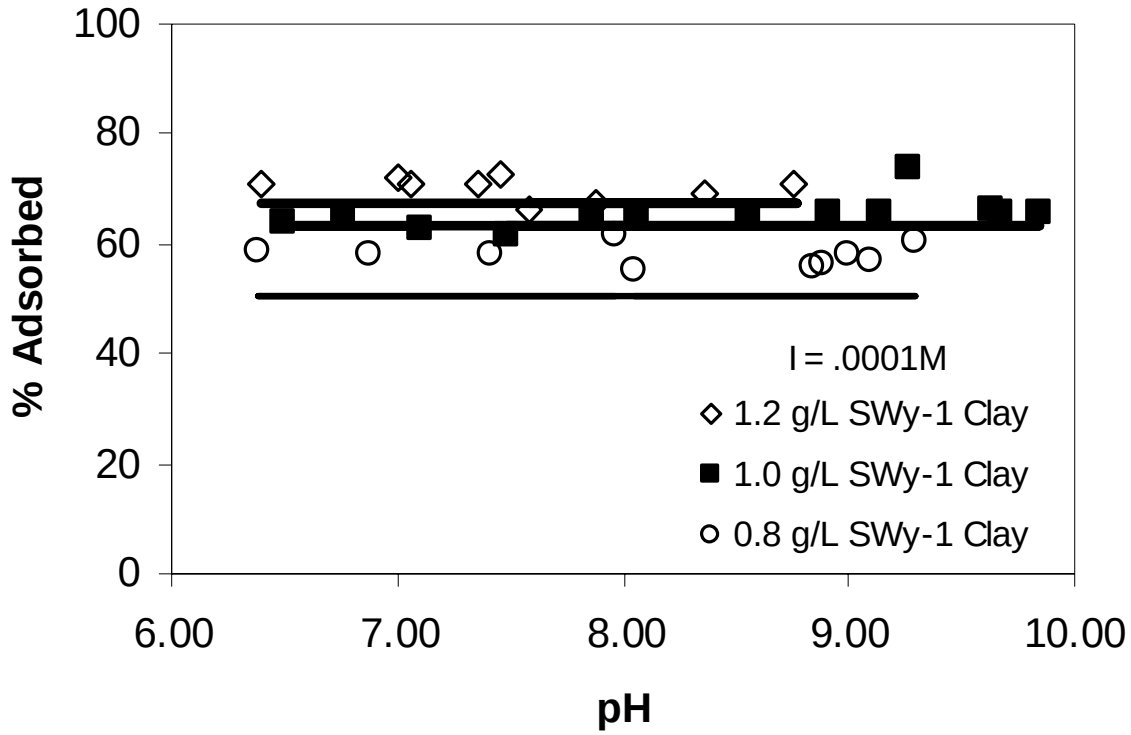

Figure 2.5: Percent of Bmim Cl (initial aqueous concentration 9.3 X 10^{-4}M) adsorbed onto 0.8, 1.0, and 1.2 g/L of SWy-1 with an ionic strength of 10^{-4}M agitated for 3 hours (2σ error bars shown or are within data point). The lines represent adsorption modeled with a K_D value of 1735 L/Kg.

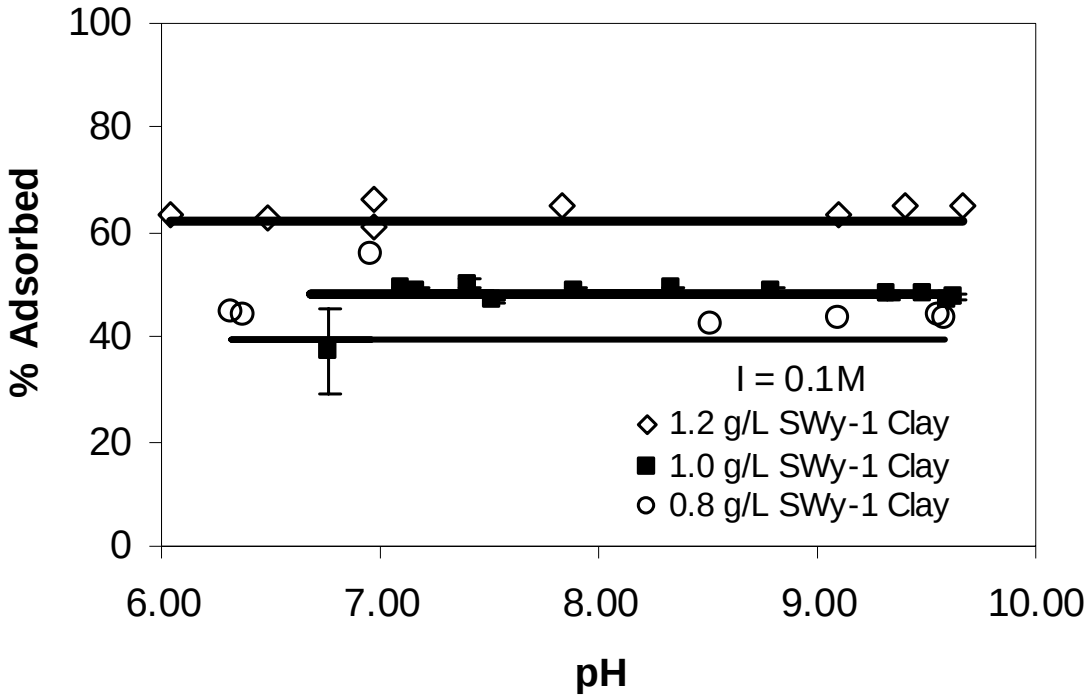

Figure 2.6: Percent of Bmim Cl (initial aqueous concentration 9.3 X 10^{-4}M) adsorbed onto 0.8, 1.0, and 1.2 g/L of SWy-1 with an ionic strength of 10^{-1}M agitated for 3 hours (2σ error bars shown or are within data point). The lines represent adsorption modeled with a K_D value of 1133 L/Kg.

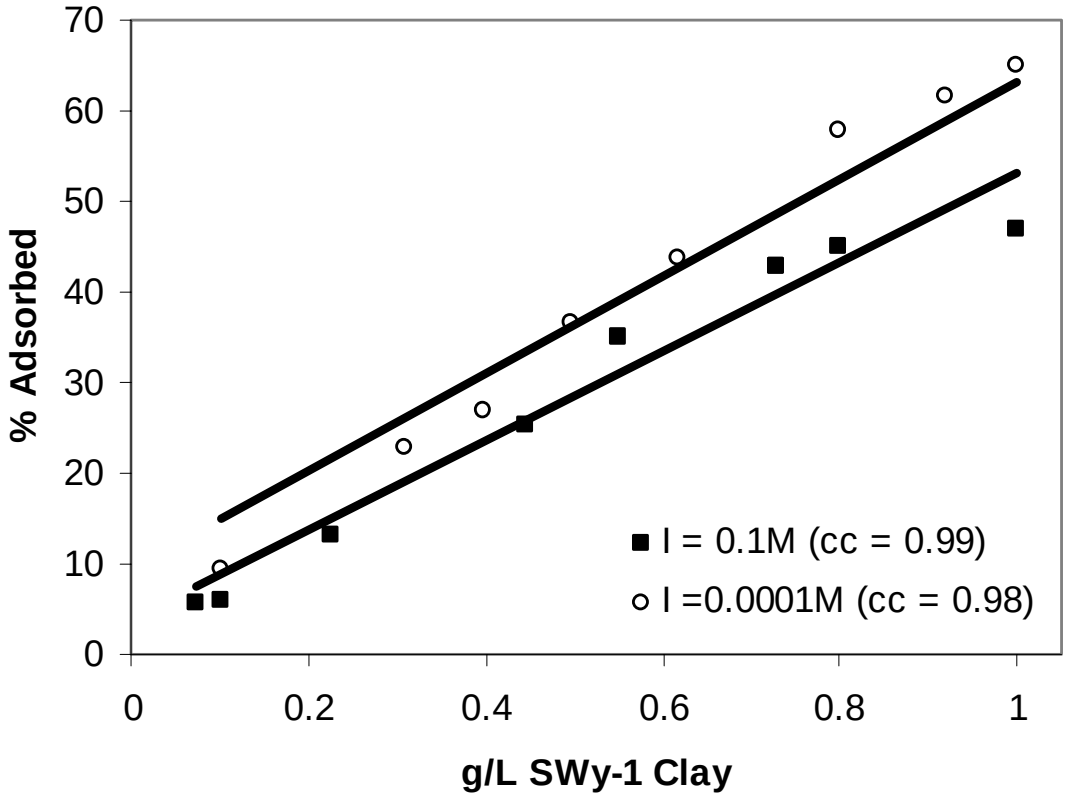

Figure 2.7: Percent of Bmim Cl (initial aqueous concentration 9.3 X 10^{-4}M) adsorbed onto varying concentrations of SWy-1 at an ionic strength of 10^{-1}M and 10^{-4}M agitated for 3 hours (2σ error bars shown or are within data point). The lines represent adsorption modeled with a K_D value of 1700 L/Kg and 1100 L/Kg for the10^{-4}M and 10^{-1}M ionic strengths respectively.

We model the Bmim Cl adsorption onto the montmorillonite using a distribution coefficient (K_D) approach:

$$K_D = \frac{[Bmim\,Cl]_{Adsorbed}}{[Bmim\,Cl]_{Aqueous}} \quad (1)$$

where the brackets for the adsorbed Bmim Cl represent the moles of Bmim Cl/Kg montmorillonite, and those for aqueous Bmim Cl are given in terms of moles/L, yielding the overall units for K_D values of L/Kg.

This approach provides a simple way to predict the amount of retardation of the ionic liquid. Distribution coefficients were calculated for every data point in the montmorillonite experiments. For each ionic strength, we averaged the calculated K_D values resulting in two distinct values for the distribution coefficient. The 10^{-1} M and 10^{-4} M ionic strength systems produced average K_D values, with 1-σ uncertainties, of 1100 ± 300 L/Kg and 1700 ± 300 L/Kg, respectively. That is, for a given ionic strength, experiments with different solute:sorbent ratios yield similar calculated values for K_D. These K_D values successfully account for the observed dependence of the adsorption on the clay concentration and on the Bmim Cl concentration, as illustrated by the solid black lines in Figures 2.4-2.7. The range of ionic strength values studied here reflects the ionic strength range that is typically seen in natural systems. Although we observe ionic strength dependence to the adsorption, it should be noted that the ionic strength dependence is not particularly strong. A change in ionic strength of three orders of magnitude from 10^{-4} M to 10^{-1} M $NaClO_4$ affects adsorption only by 10-20%.

Each batch adsorption experimental system was designed to contain relatively high concentrations of surface functional groups compared to the concentration of Bmim Cl present in each system. The properties of the *B. subtilis* cell wall are listed in Table 2.1. The most concentrated bacterial systems in this study, with 7.91 g/L of *B. subtilis*, contained functional group concentrations of 9.49 X 10^{-3}, 3.48 X 10^{-3}, and 4.90 X 10^{-3} moles of sites per liter of carboxyl, phosphoryl, and hydroxyl groups, respectively. Each of these site concentrations is greater than the 9.3 X 10^{-4} M concentration of Bmim Cl used in the experiments.

TABLE 2.1

SORBENT PROPERTIES

Sorbent	Surface Area (m^2/g)	Sites/nm^2
Gibbsite	0.217[a]	20[e]
Quartz	0.028[b]	20[e]
Swy-1 clay	31[c]	40[d]
	Moles of sites/g dry weight[f]	
B. subtilis	1.2×10^{-3} (carboxyl sites) 4.4×10^{-4} (phosphoryl sites) 6.2×10^{-4} (hydroxyl sites)	

[a](BET measurement). [b](Yee and Fein, 2002). [c & d](McKinley et al., 1995). [e](Hayes et al., 1991). [f](Fein et al., 1997).

Although we did not perform titrations of the gibbsite or quartz used in these experiments, mineral oxides typically have site densities ranging from 2 to 20 sites per nm^2 (Hayes et al., 1991). Using a value of 20 sites per nm^2 (Sverjensky and Sahai, 1996) and the properties listed in Table 2.1 yields a site concentration of 1.9×10^{-3} M available for adsorption with 2000 g/L quartz. Similarly, we calculate a site concentration of 9.3×10^{-3}M for gibbsite (properties listed in Table 2.1). With the bacteria, quartz, and gibbsite, we used enough sorbate to have approximately an order of magnitude difference between the Bmim Cl and the total available sites for adsorption. Even with this excess of sites available, we saw no change in the concentration of Bmim Cl during the experiments. Previous titrations of the SWy-1 clay (McKinley et al., 1995) yield edge site

concentrations of 4 X 10^{-5} moles of sites per liter for 1.2 g/L of clay. Therefore, the available number of edge sites cannot account for the total amount of adsorption of Bmim Cl. This implies that the fixed negative charge and/or the interlayer cation exchange capacity of the clay contribute at least to some extent to the adsorption of Bmim Cl. This result is also consistent with the pH-independent adsorption that we observed. Previous research of nitrogen heterocycle adsorption to clay has also found that adsorption primarily occurs through cation exchange reactions (Zachara et al., 1986; Ainsworth et al., 1987; Zachara et al., 1987; Zachara et al., 1990).

Our experimental results indicate that Bmim Cl has no affinity to adsorb to alumina or silica mineral surface sites or to the Gram-positive bacteria *B. subtilis*. The pH for the zero point of charge for gibbsite is 9.8 (Sverjensky, 1994). Although net electrostatic repulsion occurs between aqueous cations and the positively charged gibbsite surface below pH 9.8, a number of cations (e.g., lead(II), cadmium (II), and copper (II) (Weerasooriya et al., 2000; Weerasooriya et al., 2001; Weerasooriya et al., 2002)) adsorb onto the gibbsite surface at pH values less than the zero point of charge. The quartz surface is negatively charged at circumneutral pH values, and a wide range of cations adsorb onto the surface through the pH range 2-10 (Iler, 1979). Takeda and Usui observed substantial adsorption of the organic dodecylammonium cation onto quartz at pH 5 and 9.8 (Takeda and Usui, 1987). Their study used 5 g/L of quartz powder with a surface area of 2.62 m^2/g, resulting in a site concentration of 4.35 X 10^{-3} moles of sites per liter. This concentration is an order of magnitude higher than that of the dodecylammonium cation in their experiments, yielding a solute:sorbent ratio similar to

that used in this study. Clearly, the lack of observable adsorption in this study was not the result of insufficient sorbent concentration, but rather a result of the chemical properties of the dissolved ionic liquid molecules.

B. subtilis has carboxyl, phosphoryl, and hydroxyl functional groups covering its surface and as pH increases these sites deprotonate, creating a negatively charged surface. Although adsorption can result from electrostatic attraction of cations, the bacterial surface is also a site of hydrophobic adsorption of organics (Daughney and Fein, 1998b; Fein et al., 1999; Fein and Delea, 1999). Our experimental systems contained excess concentrations of functional groups relative to the concentration of Bmim Cl, so the lack of adsorption of Bmim Cl indicates that the electrostatic and hydrophobic attractive forces are not sufficient to affect Bmim Cl concentrations under realistic environmental conditions.

Despite the wide range of surface types studied, and the high mineral and bacterial functional group concentrations employed, the clay was the only sorbent that displayed substantial ability to adsorb Bmim Cl. Solution pH, solute:sorbent ratio, and ionic strength did not have any effect on the lack of adsorption on the other solids within our experimental conditions. Therefore, we conclude that it is likely that Bmim Cl could be retarded by interlayer clays in geologic systems, but that it is unlikely to adsorb onto most other common sorbents in geologic systems. Bmim PF_6 does adsorb onto activated carbon (Anthony et al., 2001). Do et al. (2002) describe the primary mechanisms of adsorption of benzene onto activated carbon as multi-layering and pore-filling due to

hydrophobic attractions. Typical K_D values for organic contaminants with a high affinity for adsorption onto clay range from 20,000 to 60,000 L/Kg (Haderlein et al., 1996). Cadmium (II) adsorbs onto soils with a high clay content, typically yielding K_D values between 300 to 3000 L/Kg (Holm et al., 2003). Our results yield K_D values between 1100-1800 L/Kg, suggesting that Bmim Cl adsorption behaves more like an inorganic cation in solution than a hydrophobic organic molecule. The hydrophobicity of Bmim Cl is not great enough to drive adsorption onto bacterial surfaces, and the electrostatic interaction is not strong enough to cause adsorption with a range of negatively charged surfaces.

2.4 Conclusions

Our work suggests that geologic retardation of the dialkylimidazolium class of ionic liquids due to adsorption reactions involving mineral and bacterial surfaces will be minimal if these types of ionic liquids are dissolved in groundwater systems with low concentrations of 2:1 smectite clays, and that the mobility of dissolved ionic liquids, if they ever reach the water table, would be high. Although ionic liquids offer a number of environmental benefits relative to traditional solvents, foremost of which is the low vapor pressure of these compounds, our experiments indicate that the widespread use of ionic liquids will require economic and technological consideration of disposal issues.

CHAPTER 3

ENTHALPIES AND ENTROPIES OF PROTON AND CADMIUM ADSORPTION ONTO *BACILLUS SUBTILIS* BACTERIAL CELLS FROM CALORIMETRIC MEASUREMENTS

3.1 Introduction

The adsorption of metals onto bacterial surfaces can control the mobility and speciation of metals in a wide range of environments. Despite recent advances made by bulk adsorption measurements and spectroscopic investigations, we still lack a full understanding of bacterial cell wall reactivity and the mechanisms that control cell wall adsorption. Calorimetric measurements of proton and metal adsorption onto bacterial cell walls not only can provide rigorous constraints on bulk proton and metal adsorption, but interpretation of these data can yield site-specific enthalpies and entropies of proton and metal adsorption onto the bacterial surface functional groups, yielding information on coordination environment, as well as the temperature dependence of the adsorption reactions.

A range of experimental techniques has been used to study bacterial surface adsorption reactions. Potentiometric titrations measure proton adsorption, and can be used to determine acidity constants and site concentrations of the important functional groups on the bacterial cell wall (Plette et al., 1995; Fein et al., 1997; Daughney and Fein, 1998b; Cox et al., 1999; Haas et al., 2001; Sokolov et al., 2001; Yee and Fein, 2001; Martinez et al., 2002; Ngwenya et al., 2003; Yee et al., 2004; Fein et al., 2005). Bulk metal adsorption experiments measure the affinity for metals to adsorb onto the bacterial surface, and surface complexation modeling of these results yields thermodynamic stability constants for the important bacterial surface complexes (Fein et al., 1997; Fowle and Fein, 1999; Fowle et al., 2000; Haas et al., 2001; Daughney et al., 2002; Ngwenya et al., 2003; Borrok et al., 2004a; Chatellier and Fortin, 2004; Gorman-Lewis et al., 2005b). Although potentiometric titrations and bulk adsorption experiments provide rigorous constraints on the total reactivity of the cell wall, they do not provide complete or detailed information on the binding environments, and hence the derived thermodynamic property values are dependent on the binding models chosen to represent the bacterial surface reactivity. Spectroscopic data provide more direct evidence of the metal coordination environment than do bulk adsorption measurements, and X-ray absorption spectroscopy (XAS) has been used to constrain the binding environment of metal cations on cell wall functional groups (Hennig et al., 2001; Kelly et al., 2002; Panak et al., 2002; Boyanov et al., 2003). However, due to the complexity of the cell wall binding environments, and due to the fact that XAS yields an averaged binding environment, the experimental results from XAS can be complex and difficult to interpret. For example, although XAS has been used successfully to demonstrate the importance of carboxyl and

phosphoryl binding sites for U and Cd on the bacterial cell wall of *Bacillus subtilis*, substantial uncertainties exist regarding the metal:ligand stoichiometry involved in binding (Kelly et al., 2002; Boyanov et al., 2003). Clearly, complementary lines of evidence are needed to constrain mechanisms of proton and metal adsorption onto bacterial cell walls.

Calorimetric measurements of proton and metal binding onto bacterial surfaces, interpreted using a surface complexation modeling approach, can be used to infer site-specific enthalpies and entropies of adsorption. Weppen and Hornburg (1995) used flow calorimetry and bulk adsorption experiments to compare the metal sequestration capability of cell wall suspensions harvested from a range of bacterial cells. Their measured bulk enthalpies of metal adsorption (for Cd, Cu, Zn, Pb, Mg, Ca, Sr, Ba) were all modestly endothermic (+ 3 to + 18 kJ/mol with a value of +10.4 kJ/mol for Cd), and in the expected range for divalent cations coordinated with anionic oxygen ligands. However, Weppen and Hornburg (1995) did not correct for the heat associated with protonation reactions, and used a bulk partitioning approach instead of a site-specific surface complexation model to quantify metal adsorption. In this study, we use calorimetric data, in conjunction with surface complexation models of the bacterial cell wall, to produce site-specific enthalpies of proton and Cd adsorption onto the cell wall of non-metabolizing *Bacillus subtilis*, a common Gram-positive aerobic soil bacterial species. Our calorimetric measurements, made using actual bacteria, allow the determination of site-specific metal adsorption enthalpies. In addition, the heats of proton adsorption, which are needed to correct the data from the metal adsorption

titrations, also may be used to constrain the nature and reactivity of cell wall binding sites, and to determine the site-specific enthalpies and entropies of proton adsorption. These data provide information regarding the likely structure of the functional groups on the bacterial surface, the usefulness of simple organic acids as proxies for these sites, and the temperature dependence of the acidity constants.

3.2 Experimental Procedures

3.2.1 Cell Preparation

B. subtilis cells (supplied originally by T.J. Beveridge, University of Guelph) were cultured and prepared following the procedures outlined previously (Fein et al., 1997; Fowle et al., 2000) except the acid wash step in the cell preparation was not conducted in order to avoid possible acid damage to the cell walls (Borrok et al., 2004b). Cells were maintained on agar plates consisting of trypticase soy agar with 0.5% yeast extract added. Cells for the adsorption experiments were grown by first inoculating a test-tube containing 3 ml of trypticase soy broth and 0.5% yeast extract, and incubating it for 24 h at 32 °C. The 3 ml bacterial suspension was then transferred to a 1 L volume of broth, also with 0.5% yeast extract, and allowed to grow for another 24 h on an incubator shaker table at 32 °C. Cells were pelleted by centrifugation at 1600 g for 15 min, and rinsed seven times with 0.1 M $NaClO_4$. The bacteria were then pelleted by centrifugation at 5000 g for 60 minutes to remove excess water to obtain a wet weight so that suspensions of known bacterial concentration could be created. The ratio of this wet weight to dry weight is 5.1:1 (Borrok et al., 2004b).

3.2.2 Bulk Adsorption Experiments

The calorimetric measurements made in this study yield the heat of adsorption that occurs upon titration of an adsorbate (either $HClO_4$ or $Cd(ClO_4)_2$ solutions) into a bacterial suspension. These data can be most simply interpreted if the experiments are conducted under conditions where virtually all of the adsorbate added to the system binds to the surface of interest, eliminating contributions to the measured total heat from other sources such as aqueous complexation reactions involving the added metal ions and organic exudates from the bacteria. In order to quantify the extent of Cd that adsorbs onto the bacterial cells under all of the conditions present during the calorimetry experiments, we conducted two types of preliminary adsorption experiments: 1) bulk adsorption measurements, conducted as a function of Cd concentration and pH to directly mirror the Cd calorimetry experimental conditions; and 2) Cd adsorption kinetics experiments to determine the time to reach adsorption equilibrium under the experimental conditions, and thus and the speed at which the calorimetric titrations could proceed. We needed to use a bacterial concentration of approximately 80 g wet mass/L in the calorimetry experiments in order to obtain a measurable response, so we used this same concentration in each of the adsorption control experiments. We measured the extent of Cd adsorption as a function of pH, suspending the bacteria in a solution containing 5.3 x 10^{-4} M $Cd(ClO_4)_2$ with 0.1 M $NaClO_4$ to buffer ionic strength, following a similar procedure outlined by Borrok et al. (2004a). Concentration dependent adsorption experiments were performed by suspending the bacteria in 0.1 M $NaClO_4$ adjusted to pH 6.18 and adding $Cd(ClO_4)_2$ to obtain total Cd concentrations ranging from 0.04 mM to

0.53 mM (the range of Cd concentrations encountered during the calorimetric titrations). Adsorption kinetics experiments were performed with the bacterial suspension containing a Cd concentration of 5.3×10^{-4} M adjusted to pH 6.30. Samples were extracted at 30 s time intervals, similar to the procedure outlined in (Fowle et al., 2000). Samples from each control experiment were analyzed for aqueous Cd by inductively coupled plasma optical emission spectroscopy with matrix-matched standards. The analytical uncertainty was $\pm$ 3.5 %.

We observed approximately 100% adsorption of Cd at or above pH 5.3 and at all Cd concentrations studied. The adsorption kinetics experiments demonstrated that virtually all of the Cd adsorbed onto the bacterial surfaces within 30 s after introduction of the Cd to the bacterial suspension. Because these control experiments were conducted under identical conditions to those employed in the calorimetry experiments, we conclude that all of the Cd that is added to the bacterial suspensions during each step of the calorimetric titration adsorbs onto the bacteria, and that the adsorption reaction goes to completion rapidly (in less than 30 seconds).

3.2.3 Titration Calorimetry

The calorimetric titrations were conducted with an isothermal titration microcalorimeter (Calorimetry Sciences Corporation, Model ITC 4200), which measures the heat flow between a reaction cell and a reference cell. The calorimeter's response to the heat flow was calibrated by electrical heating, a procedure that we have previously verified by checking the reported protonation heat of trishydroxymethylaminomethane

(TRIS/THAM) at 25 °C (Grenthe et al., 1970). Initially, both cells were filled with identical solutions (in this case, a bacterial suspension containing 0.1 M $NaClO_4$ to buffer ionic strength) and placed in the calorimeter bath. The bacterial suspension in the reaction cell was stirred at 300 rpm with a motor driven stainless steel paddle. After thermal equilibrium with the water bath (24.995 ± 0.005 °C) and a sufficiently constant background heat flow between the reaction and reference cells were achieved, a predetermined number of individual titrant doses were delivered into the reaction cell via a needle from a 100 or 250 µL syringe driven by a computer-controlled motor. Each titrant addition was followed by a period between 300 and 600 seconds, depending on the titrant, where the heat flow between the reaction and reference cells, due to addition and reaction of each dose, was measured continuously.

Two types of calorimetric measurements were conducted: 1) protonation experiments in which acid was titrated into the reaction cell to sequentially protonate bacterial cell wall functional groups; and 2) Cd adsorption experiments in which a Cd-bearing solution was titrated into the reaction cell at a nearly constant pH. All the titrations were performed with 900 µL of an 80 g/L bacterial suspension in 0.1 M $NaClO_4$. The pH of the suspension was adjusted to the appropriate pH by the addition of $HClO_4$ or carbonate-free NaOH prior to the titration. The titrant composition was either 0.170 M $HClO_4$ for the protonation titrations or 5.3×10^{-3} M $Cd(ClO_4)_2$ in 0.1 M $NaClO_4$, adjusted to match the pH of the bacterial suspension.

We gathered the protonation data under two different initial experimental conditions where the initial pH of the bacterial suspension was adjusted between pH 6.4 to 7.0 (low pH) or to pH 10.0 (high pH). A single titration from pH 10 to 2.5 that would measure the protonation heats for all four sites could not be conducted due to limitations on the number of possible titrant additions by the calorimeter. A wider pH range could have been covered using a more concentrated acid as the titrant, but this would have caused the magnitude of the heats generated by protonation of the bacterial surface to be well outside the ideal range of heats for the calorimeter. For the high pH titration, we used sequential 1 µL additions of 0.170 M $HClO_4$ and obtained a final pH of ca. 6. In order to optimize the calorimetric response for the low pH titrations, in which the heats generated by protonation of the bacterial suspension were smaller than those from the high pH titrations, we used 20 sequential 5 µL additions of 0.170 M $HClO_4$, obtaining a final pH between 2.50 and 2.61, depending on the initial pH of the solution. Low pH titrations were performed in triplicate and high pH titrations were performed in duplicate. Additional experiments measuring the background heats that were not caused by proton adsorption (i.e., the heat of dilution and other heats associated with the experimental apparatus such as the heat of titrant injection), were performed by titrating 0.170 M $HClO_4$ into a bacteria-free solution of 0.1 M $NaClO_4$ adjusted to pH 6.93.

For the Cd adsorption titrations, the reaction and reference cells were filled with 900 µL of an 80 g/L bacterial suspension in 0.1 M $NaClO_4$ adjusted to pH values of 6.01 or 5.33. The titrant used was a 5.3×10^{-3} M $Cd(ClO_4)_2$ solution in 0.1 M $NaClO_4$ adjusted to match the pH of the bacterial suspension. In each experiment, sequential 8 µL doses of titrant were added to the reaction cell, and the experiments were performed in duplicate at

each pH. Drift in the solution pH over the course of the experiment was minimal as indicated by the final pH value in the reference cell, which was 5.95 and 5.34, respectively, for experiments that started at pH 6.01 and 5.33. We measured the background heats in the Cd titration experiments (i.e., the heats that were not caused by Cd adsorption), by titrating the same Cd-bearing solution into a bacteria-free solution of 0.1 M $NaClO_4$ adjusted to pH 6.04 or 5.32.

In order to obtain the heat associated with a reaction on the bacterial cell wall after the *x*th addition of titrant, $Q_x{}^{corr}$, we subtracted the background heat that was measured for the addition of an identical amount of titrant to a bacteria-free system, $Q_x{}^{bkg}$, from the experimentally measured heat associated with a given titrant addition, $Q_x{}^{exp}$,:

$$Q_x{}^{corr} = Q_x{}^{exp} - Q_x{}^{bkg} \quad (1)$$

This background correction accounts for the heat of dilution and for other heats intrinsic to the titration process. When the solution exceeds pH ~ 8.5, it is also necessary to correct for the heat of hydroxide neutralization associated with the reaction $H^+ + OH^- \rightarrow H_2O$ that occurs on the addition of acid or liberation of protons from the bacterial surface by metal binding. The enthalpy for this reaction in 0.1 M $NaClO_4$ was estimated to be -56.48 ± 0.09 kJ/mol by interpolation of the heats of NaOH neutralization reported for HCl and $HClO_4$ in solutions with ionic strengths between 0.005 and 3 M (Hale et al., 1963; Vanderzee and Swanson, 1963; Martell et al., 1998). In our work, correction for the heat of hydroxide neutralization was only necessary for the high pH experiment protonation experiments. In those cases, the heat of hydroxide neutralization with each addition of

acid was calculated from the enthalpy of neutralization, the initial solution pH, the total amount of acid added, the concentration of protonatable bacterial surface sites, and the pK_a values of those sites and was included in the Q_x^{bkg} term in Equation 1. By convention, the calorimeter software assigns positive values to measured exothermic heats and negative values to endothermic heats. This is the opposite of the convention for enthalpies where the enthalpies of endothermic processes have positive values.

The concentration of each species in the suspension was calculated for each point in the titration using the program PSEQUAD (Zekany and Nagypal, 1985) with the known initial pH and the total concentrations of bacteria, and added metal and acid in the reaction vessel. Site-specific equilibrium constants for binding at each site on the bacteria surface were taken from the speciation models of Fein et al. (2005) for the protonation reactions and Borrok et al. (2004b) for the Cd-adsoprtion reactions. pH measurements during the titration are not possible. Therefore, the pH values we report for the individual titration points also come from the speciation calculations. The solution volume and the concentrations calculated by PSEQUAD for each point of the titration were then used as independent variables to derive the enthalpies of reaction from the calorimetric data as least-squares fitted parameters with the program Origin 5.0 (Microcal). Except as noted, the uncertainties in the thermodynamic parameters are given at the 95% (2σ) confidence level and are calculated for the enthalpies either as the standard error in the average, or from the inverse of the covariance matrix.

3.3 Results and Discussion

3.3.1 Protonation Reactions

The thin curve in Figure 1 depicts the raw calorimetry data from a typical low pH experimental run, illustrating the heat evolved for each addition of 5 µL of 0.17 M $HClO_4$ to the bacterial suspension. The heavy curve represents the background heat generated from the control titrations conducted under identical conditions only with no bacteria in suspension. The first addition of the titrant is not considered during data analysis due to the consistent anomalous behavior. The initial pH of the system was 6.87, and the pH after equilibration of the final addition was 2.61. The corrected heats for the protonation titration ($Q_x^{prot,corr}$) are the experimental heats (the integration of the area under the thin curve) minus the background heats. Figures 2 and 3 report the corrected heats generated from protonation of the low and high pH bacterial suspension, respectively.

The calorimetry measurements demonstrate that the protonation reactions are strongly exothermic and that substantial proton adsorption occurs continuously over the entire pH range studied. Proton adsorption at the lowest pH is consistent with the observations made by Fein et al. (2005), who used potentiometric titrations of *B. subtilis* suspensions to determine that proton uptake occurs at pH values at least as low as 2.5. Both the calorimetry data and the potentiometric titration data strongly suggest the presence of a cell wall functional group, or groups, with a pK_a (the negative logarithm of the acidity constant of this site), substantially below 4. Fein et al. (2005) modeled their data using a site with a pK_a value of 3.3, and we use this model as a basis for using the heats of protonation that were measured in this study to calculate site-specific enthalpies of protonation.

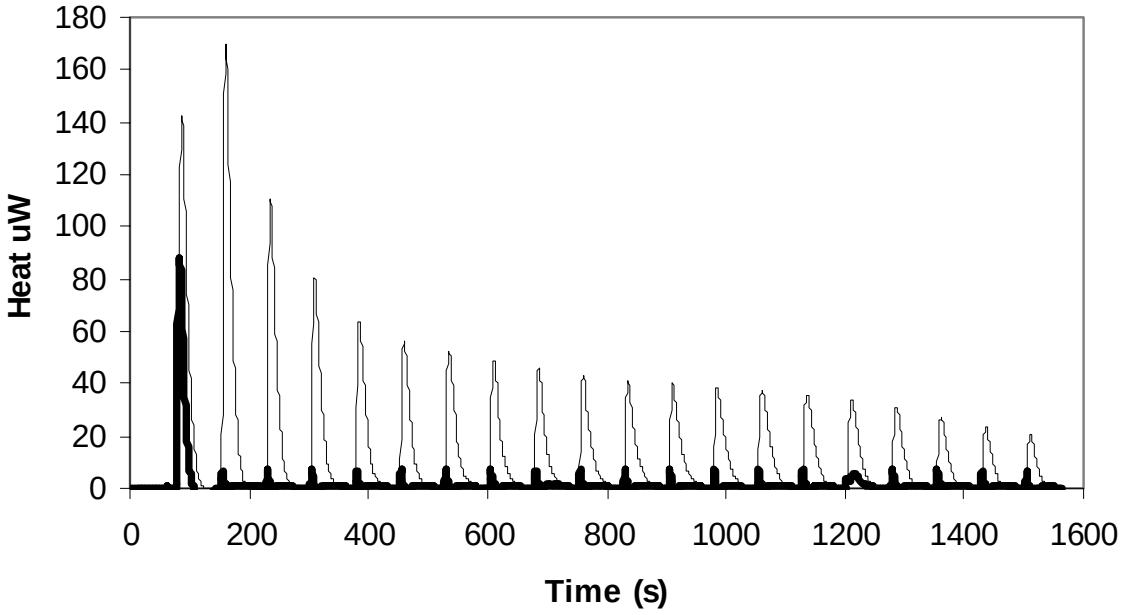

Figure 3.1: Raw data from a typical low pH proton adsorption titration (—) with heat of dilution multiplied by 10 for each corresponding addition of acid (▬).

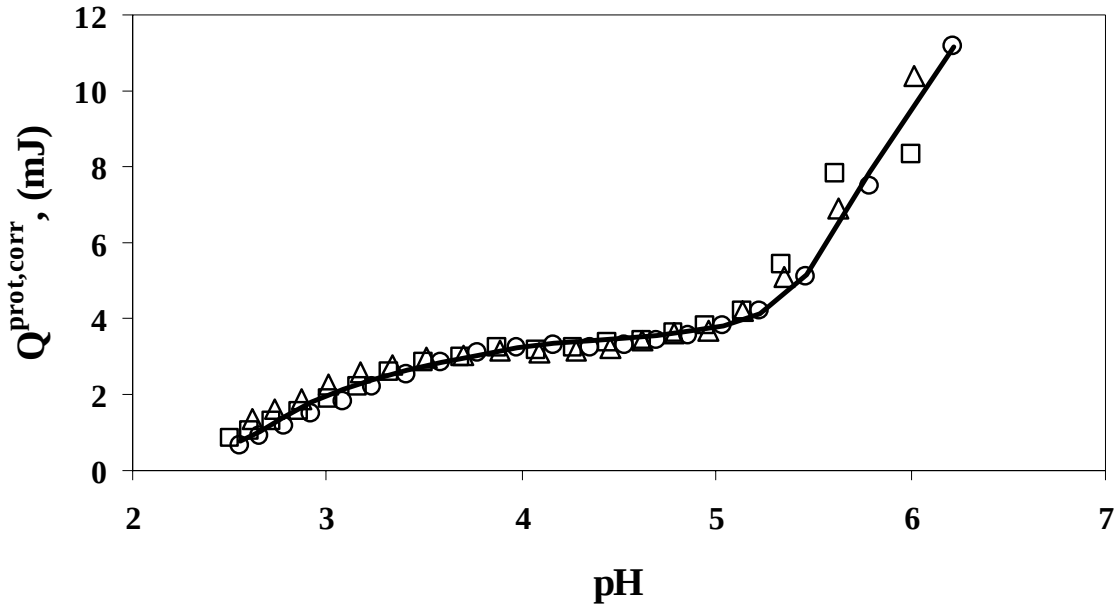

Figure 3.2: Corrected heat evolved (mJ), where positive Q represents exothermic heats, from three low pH proton adsorption titrations versus pH with the curve representing the fit of Equation 3.

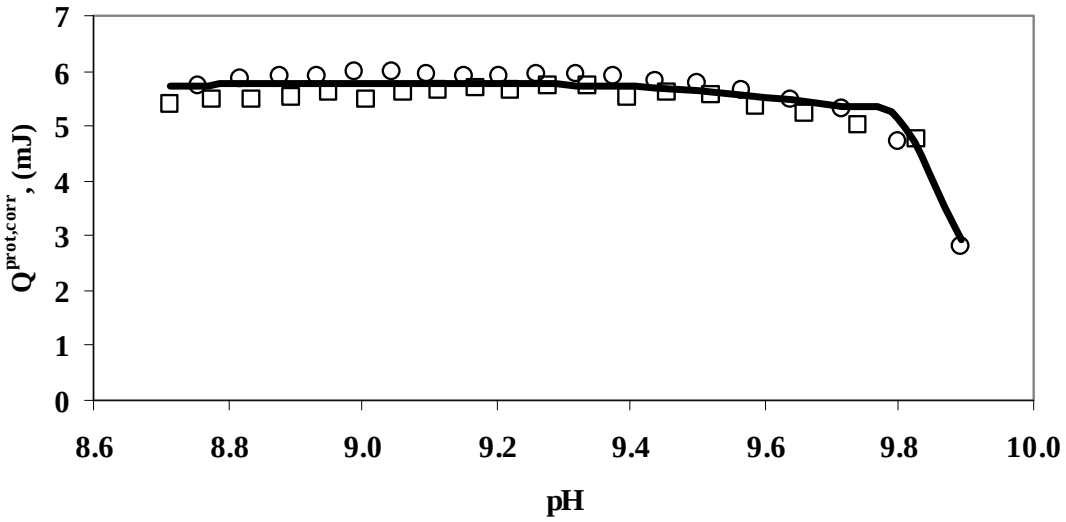

Figure 3.3: Corrected heat evolved (mJ), where positive Q represents exothermic heats, from two high pH proton adsorption titrations versus pH with the curve representing the fit of Equation 3.

The calculation of site-specific enthalpies provides thermodynamic data that can be used to constrain specific binding mechanisms involving specific functional groups on the bacterial surface. Using the model of Fein et al. (2005) to describe the proton-active sites on the bacterial surface, proton binding is ascribed to four distinct reactions of the following stoichiometry:

$$R - L_i^- + H^+ \longleftrightarrow R - L_i H^O \quad (2)$$

where *R* is a bacterium to which a proton-active functional group type, L_i^-, is attached. Fein et al. (2005) interpreted potentiometric titration data using a four discrete site non-electrostatic model, and the data constrain the site concentrations and acidity constants

for the pertinent protonation reactions with pK_a values of 3.3, 4.8, 6.8, and 9.1 for Sites 1 - 4, respectively. We use the calorimetric pH titration data, in conjunction with the protonation model of Fein et al. (2005), to calculate the site-specific enthalpy of protonation, ΔH_{HL_i}, with units of kJ/mol for Reaction 2. It represents the heat generated by protonation of Site L_i^- per mole of protonated Site L_i^-. For each step of the titration, the protonation enthalpies of each Site L_i^-, ΔH_{HL_i}, are related to the corrected protonation heat, $Q_x^{prot,corr}$, by the equation

$$-Q_x{}^{prot,\,corr} = \sum_{i=1}^{4} \Delta H_{HL_i} \Delta n_{HL_i}{}^{x}, \qquad (3)$$

where $\Delta n_{HL_i}{}^{x}$ is the change in the number of moles of the protonated species HL_i caused by the x-th addition of titrant.

It should be noted that although we use the bacterial surface complexation model proposed by Fein et al. (2005) to determine $\Delta n_{HL_i}{}^{x}$ values, and hence site-specific enthalpies. Any such treatment is model dependent. The calculated site-specific enthalpies of protonation are directly dependent on the model chosen to describe the acidity of the cell wall functional groups, and other surface complexation models of *B. subtilis* would yield different site-specific enthalpy values consistent with the differing speciation of the other complexation models and our measured bulk protonation heats.

Comparison of the data from the high and low pH calorimetric titrations between pH 6 and 7 suggests that a small, variable amount of carbonate contamination, from

atmospheric CO_2, was present in the high pH titrations. The construction of the calorimeter provides no convenient way to maintain a CO_2-free atmosphere in the reaction vessel, and high pH solutions can absorb large amounts of CO2 from the air (the $[CO_3^{2-}]$ in a hypothetical pH 10, 0.1 M ionic strength solution in equilibrium with the atmosphere is 0.097 M (Martell et al., 1998)). From the maximum deviation of the experimental protonation enthalpy of Site L_4^- between pH 8.8 and 9.9, and the reported enthalpy for CO_3^{2-} protonation, -18.8 kJ/mol (Martell et al., 1998), we estimate the *maximum* concentration of CO_3^{2-} at the start of the high pH titrations to be 0.001 M. While the presence of 0.001 M CO_3^{2-} would cause a 10% systematic error in ΔH_{HL_4} determined from the initial points of the high pH titrations, this level of carbonate contamination would have a much larger impact on ΔH_{HL_3}, which normally should be determinable between pH 5.8 and 7.8. This is due to the very large uncertainty in the solution speciation caused by the inaccuracy of the proton balance introduced by failing to quantitatively account for the presence of CO_3^{2-}. Any carbonate contamination will be much smaller in the low pH titrations where the equilibrium total carbonate capacity is much lower, and at the same time, the solution speciation is better constrained by the initial measured pH.

Consequently, the analysis of the site-specific enthalpies of proton adsorption was split in two parts. First, the data from the high pH titrations below pH 8.7 was discarded, and the data between pH 8.7 and 9.9 were used to determine ΔH_{HL_4} from Equation 3, with the approximations that $\Delta n_{HL_i}^{x} = 0$ for Sites 1-3 and that the influence of CO_3^{2-} on

ΔH_{HL_4} is small (≤ 10%) in that pH range. The model of Fein et al. (2005) suggests that the uptake of protons on Sites 1 - 3 is negligible (≤1%) when titrating the bacterial suspension from pH 10 to pH 8.7, as we do in the high pH titration. Despite these approximations, our high pH titration calorimetry data allow us to constrain the enthalpy of protonation of Site 4 and to determine the influence that Site 4 exerts on protonation reactions occurring below pH 8. The calculated enthalpy of Site 4 from the two high pH experiments is -35 kJ/mol, shown in Figure 3 and reported in Table 1, with the uncertainty increased to ±5 kJ/mol to account for the potential systematic errors composition caused by the likely CO_2 contamination of the high pH solutions.

TABLE 3.1

SITE-SPECIFIC THERMODYNAMIC PARAMETERS

Reaction	log *K*	ΔG^0 / kJ mol^{-1}	ΔH^0 / kJ mol^{-1}	ΔS^0 / J mol^{-1} K^{-1}
$H^+ + L_4^- \rightarrow HL_4$	9.1	-51.9 ± 1.1	-35 ± 5	+60 ± 20
$H^+ + L_3^- \rightarrow HL_3$	6.8	-38.8 ± 1.7	-15.4 ± 0.9	+79 ± 6
$H^+ + L_2^- \rightarrow HL_2$	4.8	-27.4 ± 0.6	-4.2 ± 0.2	+78 ± 2
$H^+ + L_1^- \rightarrow HL_1$	3.3	-18.8 ± 1.1	-3.5 ± 0.2	+51 ± 4
$Cd^{2+} + L_2^- \rightarrow CdL_2^+$	3.43	-19.6 ± 1.1	-0.2 ± 0.4	+65 ± 4
$Cd^{2+} + L_3^- \rightarrow CdL_3^+$	4.59	-26.2 ± 1.1	+14.4 ± 0.9	+136 ± 5

Parameters for the reaction of H^+ and Cd^{2+} with the surface of *B. subtilis* in 0.1 M $NaClO_4$ at 25.0 °C derived from calorimetric titration and the speciation models of Fein et al. (2005) and Borrok et al. (2004)

In the second part of the data analysis, we calculated the site-specific enthalpies of protonation of Sites 1, 2, and 3 from Equation 3 using the data from the low pH titrations and the value of ΔH_{HL_4} determined from the high pH titrations. The combination of the speciation model and Equation 3 produces an excellent fit (Figure 2) to the observed corrected heats of protonation. The calculated enthalpies of proton adsorption are -3.53 ± 0.22, -4.15 ± 0.20, and -15.4 ± 0.9 kJ/mol for Sites 1, 2, and 3, respectively. Despite the much larger uncertainty associated with the enthalpy of proton absorption at Site 4,

the pK_a of Site 4 is sufficiently different from the pK_a values of the other sites that Site 4 does not substantially influence the other enthalpies. The exact value used for ΔH_{HL_4} can be varied over a wide range (between 0 and -50 kJ/mol) without changing the protonation enthalpies derived for Sites 1 and 2, and with minimal impact (< 0.5 kJ/mol, or 1σ) on the protonation enthalpy of Site 3. Protonation reactions of Site 4 are also unimportant in the pH ranges used for the Cd titrations.

Site-specific standard-state entropies of protonation can be calculated from known values of the standard-state Gibbs free energy and enthalpy of protonation:

$$\Delta G^{o}(HL_i) = \Delta H^{o}(HL_i) - T\Delta S^{o}(HL_i)$$

(4)

where T is absolute temperature, $\Delta G^{o}(HL_i)$ is the change in the standard-state Gibbs free energy, $\Delta H^{o}(HL_i)$ is the change in the standard-state enthalpy, and $\Delta S^{o}(HL_i)$ is the change in the standard-state entropy from the protonation of Site L_i^- as described by Equation 2. The determination of the site-specific enthalpy values required for these calculations is described above; the standard-state Gibbs free energy value for each site is determined directly from the acidity constant for each type of functional group on the bacterial surface through the mass action equation:

$$LogK_{HL_i} = \frac{\Delta G^{O}(HL_i)}{-2.303RT}$$

(5)

where K_{HL_i} is the acid *dissociation* constant of protonated Site HL_i, R is the universal gas constant. The calculated entropies of proton adsorption, with propagated uncertainties, are +51 ± 4, +78 ± 4, +79 ± 5, and +60 ± 20 J/mol K for Sites 1, 2, 3, and 4, respectively.

Each of the four types of acidic sites previously identified on the surface of *B. subtilis* is comprised of many similar, individual functional groups (e.g., R-COO$^-$ moieties), with similar pK_a values, which interact with each other and with other components of the cell surface. These interactions are important because the environment experienced by the first protons to go onto a particular type of site (L_i^-) will be substantially different from the environment encountered by the last protons to bind to that type of site. Thus, the "microscopic" enthalpy and entropy of the first proton bound to a particular L_i^- is likely to be substantially different from that of the last proton bound to that type of site. Since the calorimetric protonation titrations span large degrees of protonation at each site, the site-specific thermodynamic parameters derived from the calorimetric experiments are the average values for the ensemble of microscopic protonation events at each type of site.

Despite this, previous workers have been able to use the characteristic thermodynamic parameters of various ligand groups to identify and quantify acidic sites in large, complex molecules such a proteins or humic acids (Jespersen and Jordan, 1970; Perdue, 1978). For the surface of *B. subtilis*, Spectroscopic evidence suggests that Site 2 is likely composed of carboxylate functionalities, while Sites 1 and 3 are likely

phosphoryl groups with different degrees of protonation (Kelly et al., 2002; Boyanov et al., 2003).

The protonation of simple monofunctional carboxylic acids, e.g. acetate, and the first protonation of simple organic phosphates ($R\text{-}OPO_3^{2-}$) are characterized by endothermic to thermoneutral protonation enthalpies and protonation entropies on the order of +80 to +120 J/mol K (Christensen et al., 1967; Christensen et al., 1976; Martell et al., 1998). This is not in good agreement with our site-specific thermodynamic parameters (exothermic enthalpies and entropies < 80 J/mol k). However, while the entropies for the addition of the first proton to multifunctional carboxylic acids, such as citrate or malonate, usually are similar to those of the monofunctional acids, the addition of subsequent protons to other acid groups within the molecule is marked by sequential smaller, though still positive, protonation enthalpies (Christensen et al., 1967; Christensen et al., 1976; Martell et al., 1998) because of statistical and physical effects (King, 1965; Nancollas, 1966). This trend in the entropies for successive protonations is also observed for other multifunctional acids such as the derivatives of methane-1,1-diphosphonic acid (Nash et al., 1995). The protonation of subsequent sites in multifunctional acids has a less consistent impact on protonation enthalpies, but for carboxylic acids, it generally leads progressively less endothermic/more exothermic protonation enthalpies, as typified by citric or malonic acid.

Consequently, the thermodynamic parameters derived from this work support the previous assignments of Sites 1-3, suggesting that the functional groups on the bacterial

surface behave more like multifunctional organic acids with nearby proton-active sites rather than simple monofunctional acids with a single isolated functional group and that multifunctional organic acids are likely better analogues than monofunctional acids in modeling the acidity behavior of the functional groups present on bacterial surfaces. This perspective is also supported by the thermodynamic parameters for the protonation of the carboxylate sites of humic and fulvic acid, highly multifunctional acids (Choppin and Kullberg, 1978; Perdue, 1978; Rao and Choppin, 1995). The protonation enthalpies are exothermic, just as we observe for the bacterial surface. Likewise the protonation enthalpies, +66 to +86 J/mol K, are somewhat smaller than the values found for the first protonation step of most carboxylic acids.

3.3.2 Cd Adsorption Reactions

The cumulative background correct heat evolved when a solution of Cd is titrated into the bacterial suspension is shown as a function of the total moles of Cd added in Figure 4. In contrast to the protonation experiments, where we observed exothermic heats, the bulk heats produced as Cd adsorbs onto the bacterial surface are endothermic. The continued uptake of heat at the highest Cd concentrations illustrates that the bacterial surface did not reach saturation and continued to adsorb Cd throughout the titration experiment.

For the calorimetry measurements of protonation of the bacterial surface, the background corrected heat is only a product of proton adsorption reactions; however, for the Cd adsorption titrations the background corrected heat includes the heat from Cd-

bacterial wall adsorption reactions as well as from protonation / deprotonation reactions that occur as the bacterial suspension comes to equilibrium after each addition of Cd. In the pH ranges studied, the pH change caused by each Cd addition is small (the total pH change over an entire titration was ≤ 0.1 in both cases), because the pH of the bacterial suspension and the titrant were well matched. Nevertheless, Cd adsorption alters the concentration of free adsorption sites, L_i^-, which causes the concentration of the HL_i sites to shift accordingly. In the Cd-adsorption titrations, changes in the degree of protonation are responsible for ca. 30% of the background corrected heat and must be accounted for when calculating the enthalpies of Cd adsorption.

Equation 6 describes the relationship between the cumulative background corrected heat at the *x*-th addition of Cd, and the individual contributions from each adsorption site (omitting charges on the Cd species for simplicity):

$$-\sum_{x=1}^{n} Q_x{}^{corr} = \sum_{i=1}^{4}\left(\Delta H_{CdL_i} n_{CdL_i}^{x} + \Delta H_{HL_i} n_{HL_i}^{x}\right) \qquad (6)$$

where ΔH_{CdL_i} is the enthalpy of adsorption of Cd onto Site L_i^- per mole of CdL_i formed, $n_{CdL_i}^{x}$ represents the total number of moles of Cd adsorbed onto site L_i^-, and $n_{HL_i}^{x}$ represents the change in the number of moles of species HL_i from the beginning of the titration. Values for $n_{CdL_i}^{x}$ at each point of the titration are determined from the Cd adsorption model of Borrok et al. (2004b), who used measurements of Cd adsorption onto *B. subtilis* to constrain stability constants for the important Cd-bacterial surface complexes. Their model was based on the bacterial surface protonation model of Fein et

al. (2005), and involved Cd adsorption onto bacterial surface Sites 2 and 3 with the following reaction stoichiometry:

$$L_i^- + Cd^{2+} \longleftrightarrow CdL_i^+ \quad (7)$$

Using Fein's protonation constants, Borrok's stability constants, and the known total concentrations of Cd, protons, and each of the L_i sites, one can calculate the values of $n^x_{CdL_i}$ and $n^x_{HL_i}$ associated with each addition of Cd-containing titrant during the experiment. Since $n^x_{CdL_1}$ and $n^x_{CdL_4}$ are zero in the Borrok model of Cd adsorption, Equation 6 contains two unknown parameters, ΔH_{CdL_2} and ΔH_{CdL_3}. The best fit of these parameters to the Cd titrations at pH 5.34 and 5.95 gives enthalpies of -0.2 ± 0.4 and +14.4 ± 0.9 kJ/mol for Cd adsorbing onto Sites 2 and 3, respectively (Figure 4). Given the nearly constant pH values encountered within each Cd titration and the large excess of bacterial sites relative to the Cd concentration, the contribution of protonation/deprotonation equilibria to the measured reaction heats are small. Therefore, the Cd adsorption enthalpies derived from our calorimetric measurement are relatively insensitive to the uncertainties in the protonation enthalpies of Sites 1-3. Inaccuracies in the protonation enthalpy of Site 3 would have the largest impact on the derived Cd-binding enthalpies, but varying ΔH_{HL_3} within its 2σ uncertainty limits changes the Cd adsorption enthalpies by 0.3 kJ/mol, which is substantially less than the uncertainty in the fit. Using the same approach that we used to calculate the protonation entropies, we calculate the following entropies of Cd adsorption, +65 ± 4 and +136 ± 5 J/mol K, at Sites 2 and 3, respectively.

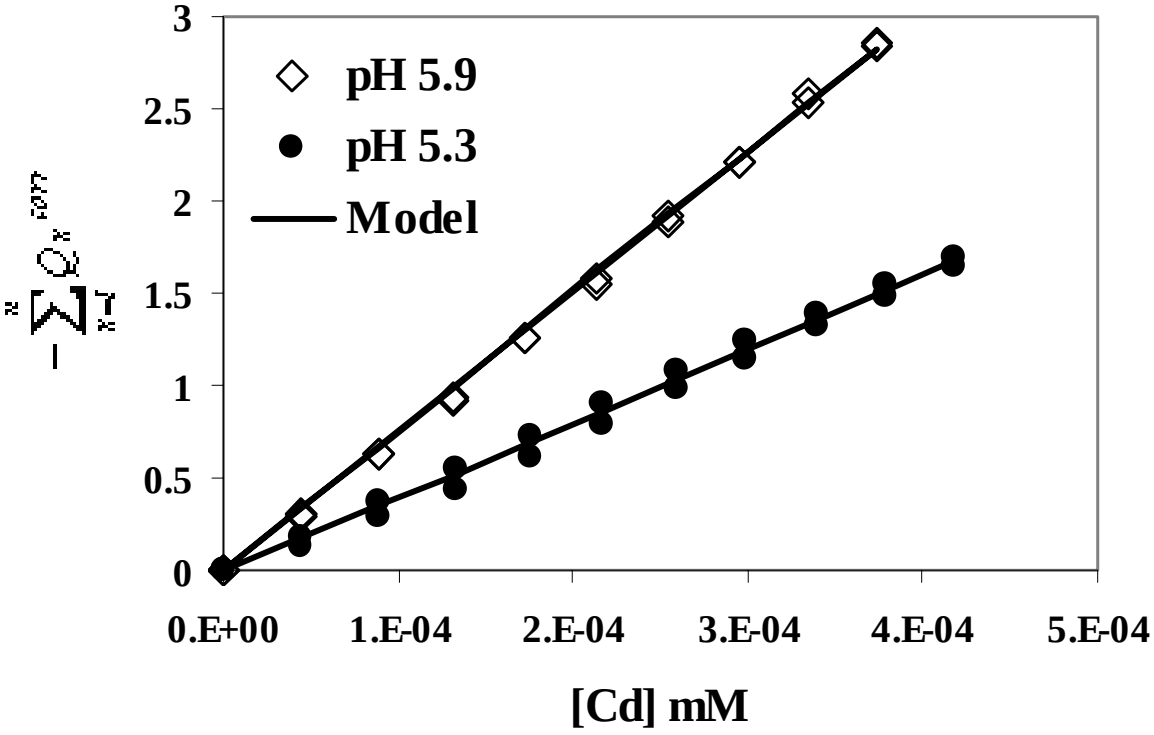

Figure 3.4: $-\sum_{x=1}^{n} Q_x{}^{corr}$, where negative Q represents endothermic heats, versus total Cd added (mM) for the Cd adsorption titrations at pH 5.9 and 5.3 with the curve representing the fit of Equation 6.

3.4 Implications of Derived Enthalpies and Entropies

The calculated values for the enthalpies of Cd adsorption by the bacterial surface are similar to those expected for Cd complexation by anionic oxygen ligands, which are typically endothermic to slightly exothermic (Martell et al., 1998). The similarity in enthalpies suggests that the binding mechanisms between metals and the anionic oxygen's on organic acids such as citrate and acetate are similar to those which are responsible for Cd binding to the organic acid functional group sites on the bacterial

surface. This explains the success of predictive tools such as the linear free energy correlations invoked by Fein et al. (2001), who demonstrated a relationship between measured stability constants for metal-bacterial surface complexes and corresponding metal-organic acid anion stability constants. Similarities in binding environments make these predictive tools possible and are likely the cause of the similar enthalpies of Cd adsorption onto the bacterial surface functional groups.

Entropies of complexation can provide information on the coordination environment of complexed metals, e.g. inner sphere versus outer sphere complexation and metal-ligand stoichiometries. The formation of a metal-ligand complex in solution would initially seem to decrease the number of particles in a solution, thus imparting order and causing a decrease in the entropy of the system ($\Delta S < 0$). This is often untrue. Inner sphere complexes have *positive* entropies of complexation because the complexation event displaces solvating water molecules from the coordination sites of the metal and ligand. The displacement of water molecules from the coordination site increases the disorder of the system, causing large positive entropies of complexation (Nancollas, 1966). Negative complexation entropies, on the other hand, characterize outer sphere complexes because the formation of outer sphere complexes does not displace or dehydrate any water molecules as it coordinates with the functional group. In addition to the lack of dehydration during outer sphere complexation, the association of the metal and ligand decreases the number of particles in the solutions, further increasing the order in the system and resulting in more negative entropies of complexation. The

entropies of Cd complexation onto bacterial surface Sites 2 and 3 derived from our experiments are both positive, which is indicative of inner sphere coordination.

The magnitude of the entropy of complexation is related to the extent of dehydration caused by complexation and consequently to the identity and number of ligands binding the metal (Choppin, 1997; Jensen et al., 2000). Therefore, the entropy of complexation can provide information not only on the nature of complexation, but also on the number of ligands involved in the complexation. Typical entropies of complexation of inner sphere binding of Cd with a single deprotonated carboxyl ligand, acetic, ethoxyacetic, or (phenylthio)acetic acid, for example, range between +30 and +50 J/mol K (Martell et al., 1998), with an average of +35 ± 5 J/mol K per carboxylate. This can be compared to the value reported for a more weakly hydrated divalent cation, Ca^{2+}, which was +25 ± 4 J/mol K per bound carboxylate (Rizkalla and Choppin, 1992). Entropies for the inner sphere binding of Cd to deprotonated phosphoryl ligands ($R\text{-}PO_3^{2-}$) are expected to be approximately +65 J/mol K per bond phosphoryl, based on empirical ratios of the complexation entropies obtained for the 1:1 complexes of other divalent metal cations with related dicarboxylate and diphosphonate ligands (Martell et al., 1998). While these values are approximate, they provide some constraints on the mechanism for Cd binding onto the bacterial cell wall. For example, since the binding of Cd to two phosphoryl groups will displace approximately twice the number of water molecules as binding to a single group, the entropies associated with Cd-bisphosphoryl binding should be twice that of Cd-phosphoryl binding, and would therefore likely be ca. +130 J/mol K,.

Within this framework, the measured entropy of Cd adsorption onto bacterial surface Site 2 (+65 J/mol K), suggests that each Cd ion is bound to an average of two Site 2 ligands, if as suggested by EXAFS experiments, Site 2 is composed of carboxyl functionalities (Kelly et al., 2002; Boyanov et al., 2003). Our calculated entropy of Cd adsorption onto bacterial surface Site 3 (+135 J/mol K), which is most likely a phosphoryl functional group, would then suggest that Cd also is bound to approximately two Site 3 ligands. Our results are consistent with the EXAFS study by Boyanov et al. (2003), who examined Cd adsorption onto *B. subtilis* cells, and found evidence for binding of Cd onto phosphoryl sites under pH conditions above 5.9. The entropies of Cd adsorption at Site 2 from our study provide additional constraints on the binding that occurs below pH 5.9, experimental conditions at which the stoichiometry of binding could not be resolved using EXAFS (Boyanov et al., 2003).

Estimations of the temperature dependence of proton adsorption based on the enthalpies suggests that little change in the acidity constants occurs with increasing temperature between 25 and 75°C for Sites 1 - 3 and a modest change occurs for Site 4. These estimates for Sites 1 - 3 are consistent with the only experimental data available on protonation behavior of *B. subtilis* at elevated temperatures. Potentiometric titrations of *B. subtilis* at elevated temperatures have shown there to be little if any temperature dependence, up to a temperature of 75° C, of the protonation constant for functional groups whose p*K*a is below 7.7 (Wightman et al., 2001). If we assume that the ΔCp values, the relative heat capacities of the products and the reactants, are zero for the protonation reactions, we can use the van't Hoff equation, in conjunction with the

enthalpies from this study to calculate the expected temperature dependence of the protonation constants. The calculated acidity constants for the *B. subtilis* functional groups decrease approximately 0.1 log units between 25 and 75° C for Sites 1 – 3, and 0.9 log units for Site 4. The expected changes in acidity constants for Sites 1 – 3 are too small to be detected by acid – base titrations at elevated temperature. The expected change to the Site 4 acidity constant is more substantial, but may also reflect the relatively higher uncertainties associated with the Site 4 enthalpy of protonation compared to the values for the other sites. The titrations in the Wightman et al. (2001) study did not exceed pH 9; therefore, their model of the bacterial surface did not include a fourth site with a p*K*a above 7.7. Consequently, our results are consistent with the results from Wightman et al. (2001) for Sites 1 - 3. Performing similar calculations with the van't Hoff equation using our enthalpies of Cd adsorption and assuming a Cp of zero for the Cd adsorption reactions yields a predicted decrease in the log *K* value of Cd adsorbing onto Site 2 of 0.005 log units and an increase of 0.4 log units for Site 3 between 25 and 75° C. This suggests that Cd adsorption onto Site 2 at elevated temperatures can be determined reasonably accurately using the stability constant for Cd adsorption reactions from 25° C experiments. Our predicted stability constant for Cd adsorption onto Site 3 at 75° C suggests that there is a slight increase in Cd uptake, although the extent may not be detectable by bulk adsorption experiments.

3.5 Conclusions

Titration calorimetry of bacterial surface adsorption reactions is a powerful technique for gaining a new understanding of the reactivity of bacterial cell walls. Bulk calorimetry data are useful in gaining a qualitative view of the enthalpies and entropies, e.g. they differentiate between exothermic and endothermic reactions and provide constraints on bulk adsorption. The bulk heat measurements of bacterial surface protonation reactions in this study indicate that bacterial surface functional groups are not fully protonated under the pH conditions studied, even at pH values as low as 2.5. Interpretation of the measured bulk heats in this study, using a surface complexation model of the bacterial surface to determine the relative contributions to the bulk heat from individual functional groups, yields site-specific enthalpies and entropies of protonation and Cd adsorption onto *B. subtilis*. These data provide mechanistic details of proton and Cd adsorption that are impossible to glean from bulk adsorption experiments, spectroscopic approaches, or from thermodynamic modeling alone. The molecular-scale information that calorimetry offers substantially enhances our understanding of bacterial cell wall reactivity, and improves our ability to incorporate bacterial adsorption reactions into geochemical models of mass transport in geologic systems.

CHAPTER 4

EXPERIMENTAL STUDY OF NEPTUNYL ADSORPTION ONTO *BACILLUS SUBTILIS*

4.1 Introduction

Neptunium (Np, atomic number 93) is a 5f, manmade element that is produced as a byproduct of nuclear fission in nuclear fuel. Like the other light actinides, it has complex solution chemistry and can be found as dissolved Np^{3+}, Np^{4+}, NpO_2^+, or NpO_2^{2+} ions under aqueous conditions relevant to natural systems (Fahey, 1986). The neptunyl(V) ion (NpO_2^+) is expected to be the most common species in natural environments. Np(V) is readily soluble and therefore mobile, which together with the long lifetime of ^{237}Np, makes it one of the most problematic elements for long term nuclear waste storage. The long-term performance of geologic nuclear repositories is dependent on the environmental mobility of Np, but the fate and transport of Np in the subsurface is difficult to predict because of its complex redox chemistry and because its tendency to adsorb onto common mineral and organic surfaces has not been well characterized. Bacteria, which can adsorb a wide range of aqueous cations, are ubiquitous in near-

surface environments and, therefore, bacterial cell wall adsorption may affect the mobility of Np.

The redox potential (E_h) of a system controls whether Np is present as the soluble neptunyl(V) cation (NpO_2^+), or as relatively insoluble Np^{4+} species. Np(V), the dominant solution species, tends to form less stable complexes (Keller, 1971) and therefore is less likely to adsorb to surfaces than is Np(IV). Np(IV) also is generally less soluble than Np(V), (Lemire et al., 2001) and both of these properties suggest that the mobility of Np(IV) is considerably lower than that of Np(V) in the subsurface. To date, most Np-related geomicrobiological research has focused on the microbial reduction of Np(V) to Np(IV) (Banaszak et al., 1998; Banaszak et al., 1999; Lloyd et al., 2000; Soderholm et al., 2000; Rittmann et al., 2003). Np(V) adsorption onto bacterial cell walls has received relatively little attention. Songkasiri et al. (2002) measured Np(V) adsorption onto the Gram-negative species *Pseudomonas fluorescens* at pH 6, 7, and 8 at a fixed ionic strength of approximately 0.1 M, using both batch adsorption and x-ray absorption spectroscopy experiments (XAS). Adsorption results showed rapid uptake of Np (i.e., 15 min for equilibrium to be attained) and increasing adsorption with increasing pH and biomass concentration. Sasaki et al. (2001) measured Np(V) adsorption onto mixed anaerobic bacteria at 35˚C and 5˚C. The pH of their systems varied in the pH ranges: 1 - 2, 5 – 6, and 9 – 11. Np adsorption increased with time in all systems except for the pH 5 – 6 system at 5˚C which steadily decreased after the first day and continued to decrease for at least ten days. Songkasiri et al. (2002) used a Freundlich isotherm approach to model the experimental data and Sasaki et al. (2001) used a distribution

coefficient approach to model their data. While these approaches enable accurate modeling of the observed adsorption behavior, they cannot be used to estimate the extent of adsorption that occurs in systems that differ substantially from those investigated in the laboratory. Conversely, surface complexation modeling, through the determination of thermodynamic stability constants of metal-bacterial surface species, has the potential to be a more flexible approach allowing the extrapolation of experimental results to more complex systems.

The objective of this research is to measure the pH, concentration, and ionic strength dependence of Np adsorption onto a common bacterial cell wall. We use the experimental measurements to constrain the important adsorption reaction stoichiometries and we solve for the values of the thermodynamic stability constants for the Np-bacterial surface complexes.

4.2 Materials and Methods

4.2.1 Cell Preparation

B. subtilis cells (supplied originally by T.J. Beveridge, University of Guelph) were cultured and prepared following the procedures outlined previously (Fein et al., 1997; Fowle et al., 2000), except the acid wash step in the cell preparation was not conducted in order to avoid possible acid damage to the cell walls (Borrok et al., 2004b). Cells were maintained on agar plates consisting of trypticase soy agar with 0.5% yeast extract added. Cells for the adsorption experiments were grown by first inoculating a test-tube containing 3 ml of trypticase soy broth and 0.5% yeast extract, and incubating it for 24 h

at 32°C. The 3 ml bacterial suspension was then transferred to a 1 L volume of broth, also with 0.5% yeast extract, for another 24 h on an incubator shaker table at 32°C. Cells were pelleted by centrifugation at 1600 *g* for 15 min, and rinsed seven times with 0.1 M $NaClO_4$. The bacteria were then pelleted by centrifugation at 5000 *g* for 60 minutes to remove excess water to obtain a wet weight so that suspensions of known bacterial concentration could be created. The ratio of this wet weight to dry weight is 5.1:1 (Borrok et al., 2004a). Autolysis of cells in a circumneutral pH solution has been previously shown to occur only after approximately 72 hours of cell suspension (Lee and Fein, 2000). Adsorption and desorption experiments were conducted as functions of time, pH, ionic strength, and solid:solute ratio in batch reaction vessels at 23 ± 1 ˚C, using an electrolyte solution of recrystallized $NaClO_4$ to buffer ionic strength.

4.2.2 pH and Ionic Strength Dependent Adsorption Experiments

Bacteria were suspended in a Np-bearing electrolyte solution diluted from a 5.75 X 10^{-3} M $^{237}Np(V)$ solution. A bacterial concentration of approximately 25 g/L (wet weight) was chosen to provide an approximately 3-orders of magnitude molar excess of surface sites relative to total Np in the system. The exact ionic strengths, pH ranges, and Np concentrations used in these experiments are listed in Table 4.1. We divided the bacterial suspension into separate 1.5 ml centrifuge cones and adjusted the pH of the solution in each to be between pH 2.5 and 8 using small volumes of concentrated NaOH and $HClO_4$. Reaction vessels were slowly agitated end over end for 1 hour and the equilibrium pH was measured. Each sample then was centrifuged for 2 minutes at 2100 *g* to pellet the bacteria, and the supernatant was filtered through a 0.45 μm nylon membrane filter. We

transferred 100 μL of the filtered supernatant to 5 mL of scintillation cocktail (Ultima Gold AB, Perkin Elmer Life and Analytical Sciences) for Np analysis. Each sample was counted for 2.5 hours with a Beckman 6000IC liquid scintillation counter with α/β discrimination. The uncertainty in the resulting Np concentration is approximately $\pm$ 4 % (at the 95% confidence level) from the combined counting and pipetting uncertainties. By subtracting the aqueous Np concentration in the supernatant from the initial concentration, we determined the concentration of Np bound to the bacteria. Bacteria-free control experiments were performed in the same manner to ensure that Np was not adsorbed onto the nylon membrane filter or other experimental apparatus.

4.2.3 Concentration Dependent Adsorption Experiments

Experiments were performed with a 25.01 g/L bacterial suspension in 0.1 M electrolyte initially adjusted to pH 5.5. This bacterial suspension was divided in equal portions into separate reaction vessels and aliquots of a 1.64 X 10^{-3} M pH 4.8 Np solution were added to each bacterial suspension to obtain total Np experimental concentrations ranging from 4.47 X 10^{-6} to 2.25 X 10^{-4} M. The amount of excess surface sites available for adsorption varied from 3 orders of magnitude to 1 order of magnitude over the concentration range of these experiments. The suspensions were adjusted to a pH of 5.3 $\pm$ 0.08. Unfiltered samples that included Np adsorbed onto the bacteria and in solution were taken to determine the total initial Np concentration. Reaction vessels were slowly agitated end over end for 1 hour and the equilibrium pH was measured. After the hour of equilibration, samples were taken and filtered, and analysis of the Np concentration in each supernatant was performed as previously described.

4.2.4 Desorption Experiments

Desorption experiments were conducted to determine the reversibility of the Np-bacterial adsorption reaction. Two Np-bacterial suspensions in 0.1 M electrolyte were adjusted to pH 2.5 and pH 6.2 and agitated for 1 hour. The final equilibrium pH of each suspension was 2.5 and 6.3, respectively. Aliquots were taken from these parent solutions, adjusted to higher and lower pH values, respectively, and agitated for an additional hour. Sampling and Np analyses were performed as previously described.

4.2.5 Kinetics Experiments

Adsorption kinetics experiments were performed with two Np-bacterial suspensions in 0.1 M electrolyte. The suspensions were adjusted to pH 2.5 and 6.2, with final equilibrium pH values of each suspension of 2.5 and 6.3, respectively. Aliquots were taken at various time intervals and Np analyses were performed as previously described.

4.3 Results

4.3.1 Kinetics Experiments

At pH 6.3 and 0.1 M ionic strength, the amount of Np adsorbed from solution in the kinetics experiments (Figure 4.1) reaches a plateau, with no continued adsorption of Np after approximately 15 minutes. In contrast, however, the extent of Np adsorption does not plateau during the course of the pH 2.5 kinetics experiments (also shown in Figure

4.1), continually increasing for at least 24 hours. The kinetics of Np removal from solution under low pH and 0.1 M ionic strength conditions are markedly different from that observed for pH 6.3 and 0.1 M ionic strength, suggesting dramatically different mechanisms for Np uptake under the different pH conditions.

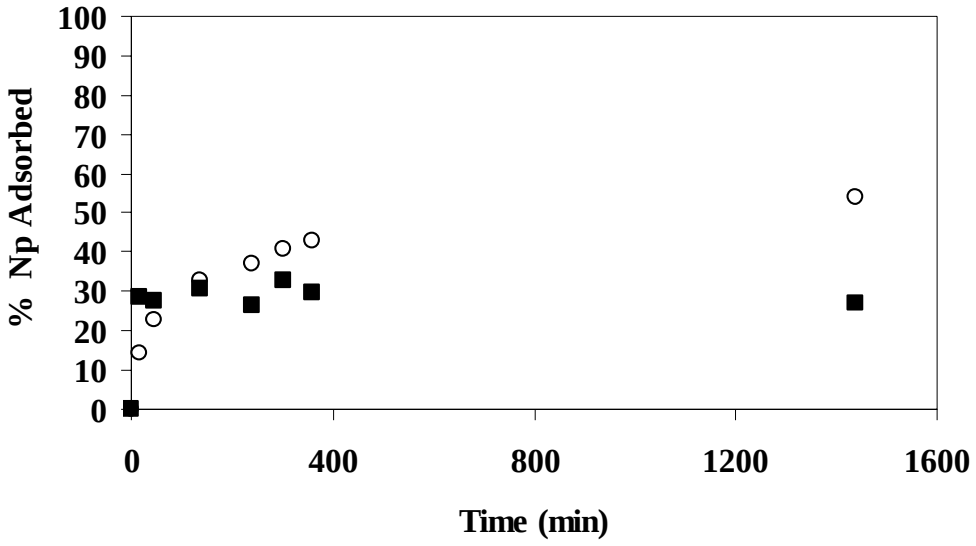

Figure 4.1: Percent Np adsorbed by *B. subtilis* as a function of time in 0.1 M $NaClO_4$. Open circles (O) depict kinetics experiment at pH 2.5 with 24.95 g/L (wet mass) bacteria and 4.17 X 10^{-6} M Np. Closed squares (■) depict kinetics experiment at pH 6.3 with 24.95 g/L (wet mass) bacteria and 4.17 X 10^{-6} M Np.

4.3.2 Adsorption Experiments

The concentration of Np bound to the surface is highly dependent on both ionic strength and pH. Experiments conducted as a function of ionic strength at a pH of approximately 6 illustrate a substantial decrease in Np adsorption as ionic strength increases (Table 4.1). Figures 4.2 depicts the observed extent of Np removal from solution for the 0.1 M ionic strength experiments as a function of pH. From pH 2.5 to 4.5 there is a decrease in Np removal with increasing pH. Np removal increases with pH above pH 4.5 and plateaus at pH values above approximately 5.5, with maximum removal being approximately 16 %.

Figure 4.3 depicts the dependence of Np adsorption on the total Np concentration in 0.1 M ionic strength experiments in which the bacterial concentration and pH were held constant. The data exhibit a sub-linear trend and do not plateau at high Np concentrations. The lack of a plateau on this adsorption isotherm confirms that the bacterial surface functional groups were considerably undersaturated with respect to adsorbed Np, even at the highest Np concentrations studied here, a result consistent with the excess of bacterial surface sites relative to the total Np concentration.

Figure 4.4 illustrates the pH dependence of Np adsorption at 0.001 M ionic strength. Adsorption at low pH is substantial and increases strongly with pH up to pH 7, with a weaker pH dependence above pH 7. Similar increases in metal cation adsorption with increasing pH have been observed for a wide range of cations and bacterial species (Fein et al., 1997; Yee and Fein, 2001), however the pH dependence observed here is considerably weaker than for any previously studied multivalent cation.

TABLE 4.1

EXPERIMENTAL CONDITIONS FOR Np ADSORPTION DATASETS

Ionic Strength	Total Np (M)	Np Adsorbed (M)	Bacteria (g/L wet mass)	pH
0.001	5.62×10^{-6}	See Figure 4.4	26.38	See Figure 4.4
0.005	3.80×10^{-6}	1.82×10^{-6}	24.70	6.04
0.01	3.24×10^{-6}	9.77×10^{-7}	24.70	5.98
0.05	3.39×10^{-6}	7.41×10^{-7}	24.70	6.08
0.10	4.17×10^{-6}	See Figure 4.2	24.16	See Figure 4.2
0.10	See Figure 4.3	See Figure 4.3	25.01	5.3 ± 0.08
0.30	3.02×10^{-6}	6.46×10^{-7}	24.70	6.00
0.50	2.69×10^{-6}	3.98×10^{-7}	24.70	5.69

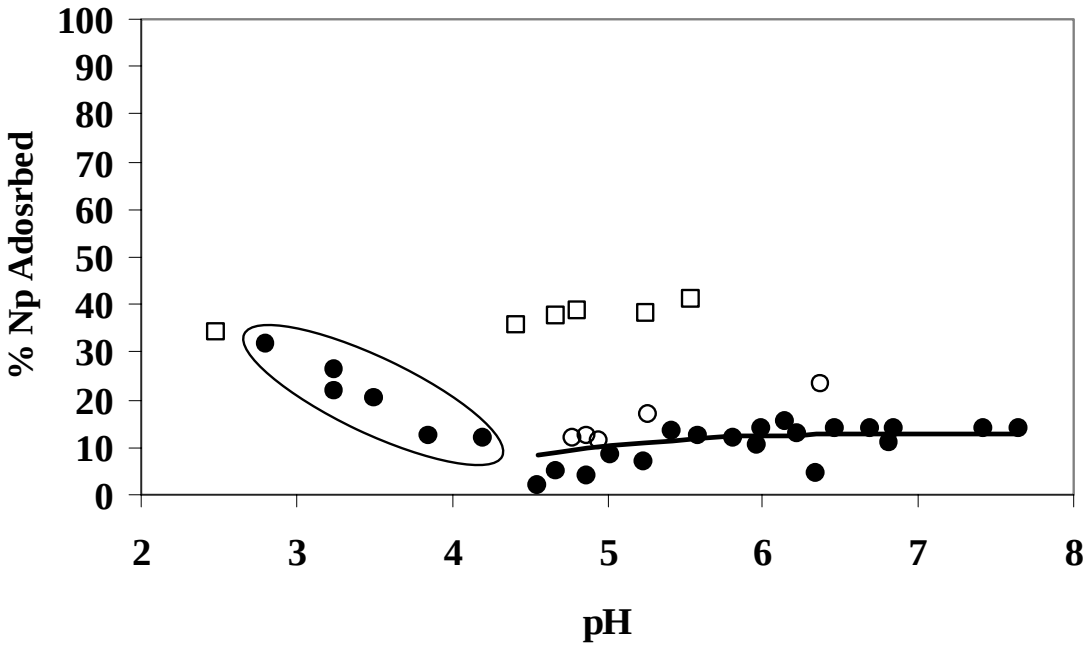

Figure 4.2: Percent Np adsorbed by *B. subtilis* as a function of pH in 0.1M $NaClO_4$. Closed circles (•) depict adsorption experiments with 24.16 g/L (wet mass) bacteria and 4.17 X 10^{-6} M Np. Open circles (O) depict desorption experiment with 24.95 g/L (wet mass) bacteria, 4.57 X 10^{-6} M Np, and initial pH 6.3. Closed circles (•) enclosed in oval depict irreversible adsorption/reduction of Np with 24.16 g/L bacteria (wet mass) and 4.17 X 10^{-6} M Np. Open squares (□) depict attempted desorption with 24.95 g/L (wet mass) bacteria, 4.57 X 10^{-6} M Np, and initial pH 2.5. The solid line represents the best-fit surface complexation model (see text).

4.3.3 Desorption Experiments

Adsorption in the 0.1 M system above pH 4.5 appears to be reversible. Figure 4.2 depicts results from a desorption experiment in which a parent solution containing a Np-bacteria suspension was adjusted to pH 6.2 and allowed to reach equilibrium. We sampled the solution after this adsorption step, and observed that approximately 25% of the Np was bound to the bacteria. Next, we took aliquots of this solution, adjusted the pH to lower values between 4.5 and 5.5, and allowed these samples to re-equilibrate. Analysis of the samples indicates the extent of adsorption decreases to yield a similar shaped adsorption edge to that observed in the adsorption-only experiments (see open circles Figure 4.2). This suggests that the Np was bound to the bacterial surface and subsequently desorbed rapidly when the pH was lowered. Our desorption results do not plot directly on top of the adsorption-only data because the bacterial and Np concentration in the two experiments were not identical.

In our low pH desorption experiment, a Np-bacterial solution was initially equilibrated at pH 2.5, and under these conditions, we measured approximately 35% removal of Np from solution. After adjusting aliquots of this equilibrated solution to higher pH (see open squares in Figure 4.2), the amount of Np bound to the bacteria increased slightly, rather than decreasing to the levels of Np removal observed in the adsorption experiments at the same pH values. This result indicates that the mechanism responsible for the observed Np removal from solution under low pH, high ionic strength conditions is non-reversible, at least on the timescale of these experiments. Data below pH 4.5 exhibit an increase in adsorption with a decrease in pH, a trend consistent with the

initial data point of the desorption experiment. We depict these data as separate from the adsorption edge above pH 4.5, and neglect them in subsequent adsorption modeling, because it is likely that a similar irreversible reaction controls the Np removal under each of these low pH, high ionic strength experimental conditions.

The above observations suggest that Np removal from solution at high ionic strength and low pH is not purely an adsorption process, and is likely influenced by reduction of Np(V) to Np(IV). The decrease in Np removal from pH 2.5 to 4.5 (Figure 4.2 data shown enclosed by the oval) and the increasing Np removal with time for the pH 2.5 system (open circles in Figure 4.1) are both consistent with reduction of Np(V) to Np(IV) and continued reduction over the course of the experiments. If indeed this reduction does occur, our experiment cannot provide information on whether the reduction leads to enhanced adsorption of Np^{+4} relative to NpO_2^+, or whether precipitation of a Np(IV) phase causes the enhanced Np removal at low pH. Nevertheless, Cr(VI) exhibits similar behavior under comparable experimental conditions (Fein et al., 2002). Non-metabolic *B. subtilis* cells, grown and harvested in a similar manner to the cells used in our experiments, reduce Cr(VI) to Cr(III) in the absence of an external electron donor. Fein et al. (2002) observed continuously increasing Cr(VI) removal from solution by *B. subtilis* at pH 2.3 for at least 100 hours. Fein et al. (2002) also determined that the removal was irreversible and that the kinetics of removal increased with decreasing pH. X-ray adsorption near edge spectroscopy (XANES) confirmed the reduction of Cr(VI) to Cr(III) by the bacterial cell wall in these experimental systems. While we do not have spectroscopic confirmation of Np reduction

in this study, the lack of reversibility and the results from the bulk adsorption experiments strongly suggest that reduction controls Np removal in the low pH, high ionic strength systems. In contrast, in the low ionic strength systems, XANES of samples similar to those in our 0.001 M system indicates that the Np adsorbed on the bacterial surface is predominantly present as Np(V) (Skanthakumar et al., 2004). Clearly, ionic strength and pH influence both the extent and the mechanism of Np removal in these bacteria-bearing systems.

4.4 DISCUSSION

4.4.1 Thermodynamic Modeling

We apply a surface complexation approach to model the adsorption of Np to the *B. subtilis* cell wall. Using the model of Fein et al. (2005) to describe the proton-active sites on the bacterial surface, proton binding is ascribed to four distinct reactions of the following stoichiometry (1):

$$R - L_i H^0 \quad \longleftrightarrow \quad R - L_i^- \quad + \quad H^+ \qquad (1)$$

where R is a bacterium to which a proton-active functional group type, L_i, is attached. Fein et al. (2005) use potentiometric titration data to constrain the site concentrations and acidity constants for the pertinent protonation reactions, and we employ their discrete pK_a 4-site non-electrostatic model with pK_a values of 3.3, 4.8, 6.8, and 9.1. XAS results of metal adsorption (Kelly et al., 2002; Boyanov et al., 2003) suggest that the L_1 and L_2 sites, with pKa values of 3.3 and 4.8, are phosphoryl and carboxyl groups, respectively.

The identities of the other surface sites, with pK_a values of 6.8 and 9.1, are less certain, and we refer to them as site 3 (L_3) and site 4 (L_4), respectively.

We test the ability of a range of reaction stoichiometries to account for the observed adsorption behavior, using the program FITEQL (Herbelin and Westall, 1994) to determine the model that best fits the experimental data. Although we have no spectroscopic data to constrain the dominant binding mechanisms, adsorption measurements conducted as a function of pH and solute:sorbent ratio can provide constraints on the stoichiometry and thermodynamic stability of the important bacterial surface species. The neptunyl ion is the dominant aqueous species over the entire pH and neptunium concentration range studied, and aqueous Np-hydroxide and Np-carbonate complexes are negligible under the experimental conditions (VanBriesen, 1998). Consequently, the important Np adsorption reactions most likely involve adsorption of NpO_2^+ onto one or more of the bacterial surface functional groups according to the following generic reaction (2):

$$NpO_2^+ + \quad R-L_i^- \quad \longleftrightarrow R-L_i-(NpO_2)^\circ \qquad (2)$$

where L_i represents one of the four surface functional group types present on the bacterial surface. We tested all possible reaction stoichiometries and solved for each proposed stability constant as defined by (3):

$$K = \frac{[R-L_i-NpO_2^\circ]}{a_{NpO_2^+}[R-L_i^-]} \qquad (3)$$

where *a* represents the aqueous activity of the subscripted species, and the brackets represent surface site concentrations in moles per kilogram of solution. Activity

coefficients were calculated by FITEQL using the Davies equation (Herbelin and Westall, 1994). The misfit of each model was quantified by the variance function, V(Y), in FITEQL (4):

$$V(Y) = \frac{\sum \left(\frac{Y_{calc} - Y_{exp}}{S_{exp}}\right)^2}{n_p n_{II} - n_u} \qquad (4)$$

where Y_{calc} and Y_{exp} are the calculated and experimental data, S_{exp} is the error associated with the experimental data, n_p is the number of data points, n_{II} is the number of group II components (for which total and free concentrations are known), and n_u is the number of adjustable parameters. We used the default FITEQL values for S_{exp} values since the relative and absolute errors associated with uncertainties associated with the radioactive counting procedure were judged to be small, and likely negligible compared to the uncertainties that arise from other experimental variables. The model with the lowest calculated V(Y) value was taken to be the model that could best account for the observed adsorption behavior.

4.4.2 Adsorption Experiment Modeling

When modeling our data, we were unable to account for the observed ionic strength effects through the application of aqueous species activity coefficients alone. We attempted to model the ionic strength effects on Np adsorption using a diffuse double layer electrostatic model, however this approach also could not account for the changes in adsorption that we observed as a function of ionic strength. Consequently, we used a non-electrostatic model of the reactivity of the bacterial surface and we report individual

conditional stability constants for each ionic strength of interest. Fein et al. (2005) found that bacterial surface deprotonation constants and site concentrations vary little as a function of ionic strength from at least 0.01 to 0.3 M, so we use a single set of deprotonation constants as determined by Fein et al. (2005) to model data from each ionic strength condition in this study.

We modeled the 0.001 M ionic strength data first because those provide the greatest pH dependence with which we could constrain the model and because of the unequivocal XAS evidence for un-reduced Np(V) on the cell wall (Skanthakumar et al., 2004). First, we attempted to fit a one-site model to the pH adsorption edge for the 0.001 M experimental data, meaning that the model invokes only one type of Np bacterial surface complex. We tested all possible 1-site models that are represented by reaction (2). Adsorption of Np onto the first deprotonated site (phosphoryl) gave the best fit to the low pH data. This model slightly under-predicts the extent of adsorption below pH 3.5, and more substantially under-predicts the extent of adsorption above pH 5. The low pH misfit is likely due to Np binding onto another functional group with a lower acidity constant than could be elucidated from the titration data that were used to define the bacterial surface protonation model. We then added another Np adsorption reaction to our 1-site model in order to account for the misfit between the 1-site model and the observed extent of adsorption above pH 5. Of all the possible 2-site models involving deprotonated surface sites, the model involving Np adsorption onto both site 1 (phosphoryl) and site 2 (carboxyl sites) produces the best fit over the entire pH range. The respective stability constants (log K values) for the surface complexes R-PO-NpO_2^o

and R-COO-NpO_2^o are 2.3 ± 0.3 and 2.3 ± 0.2. Models involving adsorption onto sites 3 and 4 in addition to sites 1 and 2 either do not substantially improve the fit or do not converge because the system was over-constrained. Low pH adsorption of NpO_2^+ by phosphoryl groups is consistent with XAS studies of UO_2^{+2} and Cd^{+2} adsorption onto *B. subtilis* (Kelly et al., 2002; Boyanov et al., 2003). Kelly et al. (2002) used extended x-ray absorption fine structure (EXAFS) analysis to determine that the uranyl ion binds exclusively to phosphoryl groups at low pH, with an increasing contribution from carboxyl binding with increasing pH. Similarly, Boyanov et al. (2003) used EXAFS to determine that below pH 4.4, Cd^{+2} binds predominately to phosphoryl groups and that, with increasing pH, carboxyl groups increasingly contribute to cadmium adsorption. In addition, a number of bulk adsorption studies of metal adsorption onto bacteria account for a mid-pH increase in adsorption with increasing pH by modeling it as cation adsorption onto deprotonated carboxyl sites (Ferris et al., 1989; Fein et al., 1997; Fowle and Fein, 2000; Markai et al., 2003; Ngwenya et al., 2003).

We used our model for the 0.001 M ionic strength data to help constrain our model for the 0.1 M pH dependent data where the Np adsorption was reversible (i.e., pH 4.5 to 8). Similar to the 0.001 M system, a 1-site model involving NpO_2^+ adsorbed onto a deprotonated site 1 (phosphoryl) provides the best fit of the possible 1-site models for the data between pH 4.5 and 5.2. Above pH 5.2, the 1-site model under-predicts the observed adsorption, as was the case for the 0.001 M ionic strength system. Since our 0.1 M ionic strength data cover a more limited pH range than for the 0.001 M system, we could not use the data to independently constrain the bacterial functional groups

responsible for the adsorption as we did for the 0.001 M data. Consequently, we assumed that the same 2-site model for the 0.001 M data applies to the 0.1 M data, and we solved for the NpO_2^+-bacterial stability constants by keeping the adsorbed NpO_2^+-bacterial surface site concentration ratios (that is, the concentration of R-PO-NpO_2^o relative to that of R-COO-NpO_2^o) the same at each pH as in the 0.001 M model. Adding the NpO_2^+-carboxyl surface complex to the 1-site model, we successfully account for the observed adsorption from pH 4.5 to 8 (Figure 4.2). The calculated stability constants for the R-PO-NpO_2^o and R-COO-NpO_2^o surface species are 1.7 ± 0.2 and 1.6 ± 0.2, respectively. Our modeling results suggest that low pH adsorption is due to binding onto phosphoryl sites and that mid-pH adsorption is due to binding onto carboxyl sites.

We model the 0.1 M ionic strength concentration-dependent data separately from the pH dependent data to constrain the reaction stoichiometry of the adsorption reactions. We tested bidentate binding (a 1:2 molar ratio of NpO_2^+ to binding sites) as well as a model involving a 2:1 NpO_2^+:binding site ratio, however neither of these models yield acceptable fits to the data (Figure 4.3). The model involving monodentate adsorption of NpO_2^+ (a 1:1 molar ratio of NpO_2^+ to binding sites) onto deprotonated phosphoryl and carboxyl groups (with log K values of 1.7 ± 0.2 and 1.6 ± 0.2 respectively) provides an excellent fit to the data (Figure 4.3). This is consistent with the best-fitting model of the pH dependent data in that both ascribe adsorption to deprotonated phosphoryl and carboxyl sites. The calculated stability constants are similar for both data sets, indicating that the same set of stability constants can account for both the pH and the concentration dependences of the adsorption behavior.

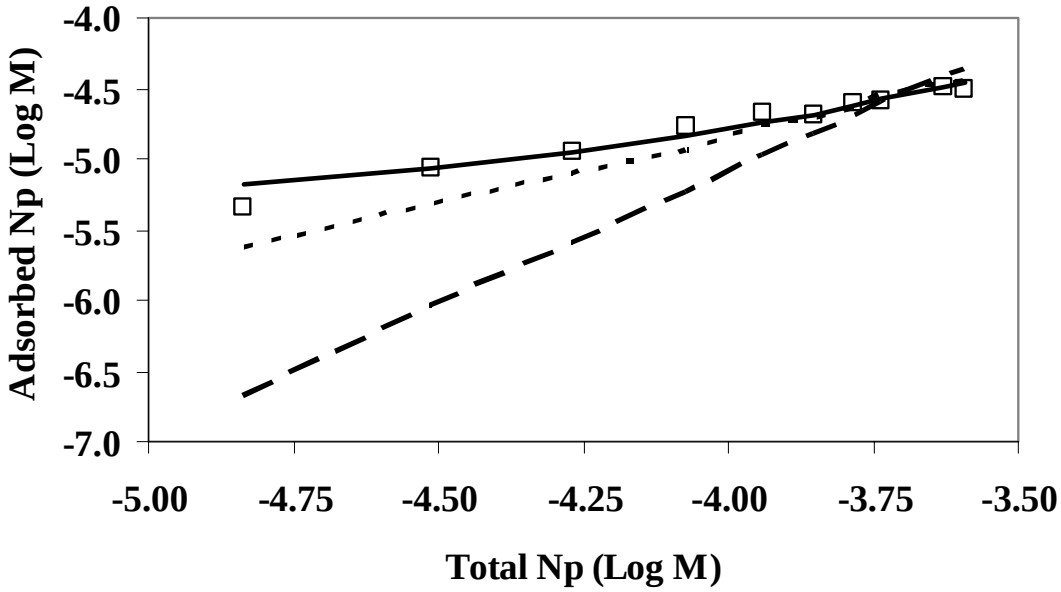

Figure 4.3: Np adsorbed by *B. subtilis* as a function of total Np concentration in 0.1 M $NaClO_4$ at pH 5.3 ± 0.08. Open squares (□) depict adsorption of Np with 25.40 g/L bacteria (wet mass). The solid curve (———) represents the best-fit surface complexation model (see text), the smaller dashed curve (– – – –) depicts bidentate binding (1:2 molar ratio of NpO_2^+ to binding sites), and the larger dashed curve (—— ——) depicts binding of 2:1 NpO_2^+:binding site ratio.

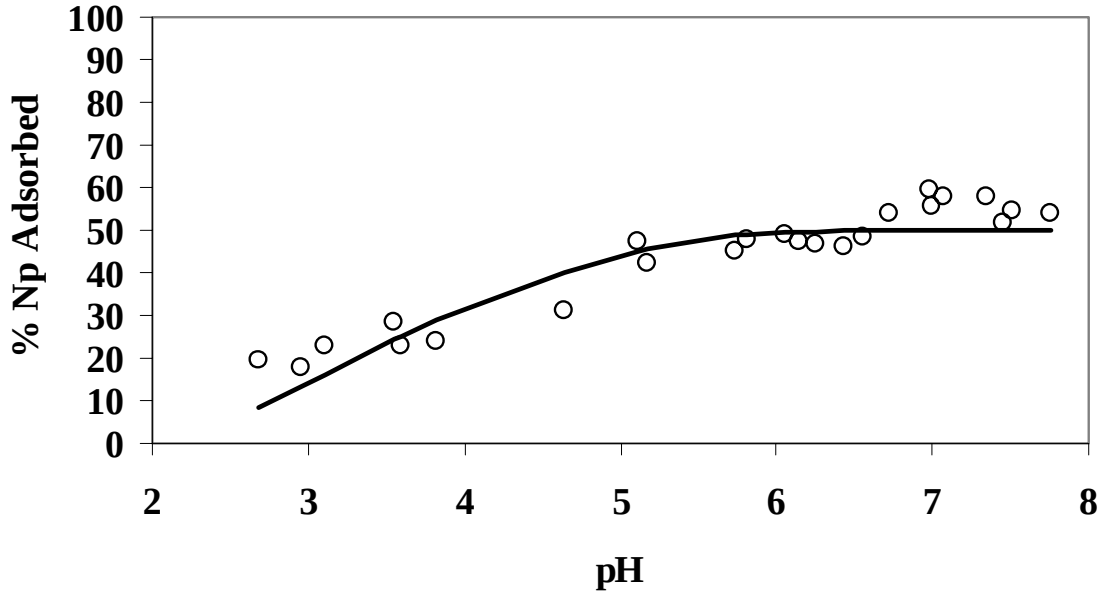

Figure 4.4: Percent Np adsorbed by *B. subtilis* as a function of pH in 0.001M $NaClO_4$. Open circles (O) depict adsorption experiment with 26.38 g/L (wet mass) bacteria and 5.62 X 10^{-6} M Np. The solid curve represents the best-fit surface complexation model (see text).

4.4.3 pH and Ionic Strength Effects

As Table 4.1 and comparison of Figures 4.2 and 4.4 illustrate, ionic strength and pH exert a substantial effect on the extent of bacterial surface adsorption of Np. Under low pH conditions, ionic strength affects the type of reaction responsible for Np uptake. Reduction is likely responsible for Np uptake under low pH, high ionic strength conditions. *B. subtilis* under low pH and 0.1 M ionic strength conditions releases more dissolved organic carbon (DOC) than under circumneutral pH (Borrok et al., 2004b), and the DOC may play a role through Np complexation and precipitation. Adsorption of Np(V) can explain Np uptake throughout the pH range studied in the low ionic strength systems. Under mid- to high-pH conditions, where the Np adsorption reaction is both rapid and reversible, ionic strength exerts a different effect. For example, decreasing the ionic strength from 0.1 M to 0.001 M at pH 7 increases Np adsorption by 40%. This ionic strength effect suggests that electrostatic forces represent a substantial component of the total binding energy, and that changes to the thickness of the bacterial surface electric double layer can markedly affect the extent of Np adsorption. While we do not intrinsically account for these ionic strength effects in our modeling approach, we use our adsorption measurements that were conducted as a function of ionic strength to calculate stability constant values for a range of ionic strength conditions (Table 4.2). We employ the same technique for modeling our ionic strength dependent data as we do for modeling the 0.1 M systems. That is, we use the same 2-site model that best-fits the 0.001 M data, making the assumption that the concentration ratio of the two NpO_2^+-bacterial surface complexes remains fixed at a given pH condition. The results of these calculations are compiled in Table 4.2.

TABLE 4.2

BEST-FITTING LOG *K* VALUES FOR NP ADSORPTION DATASETS

Ionic Strength	$R-PO-NpO_2^\circ \pm 2\sigma$	$R-COOO-NpO_2^\circ \pm 2\sigma$
0.001	2.3 ± 0.2	2.3 ± 0.2
0.005	2.3 ± 0.3	2.3 ± 0.2
0.01	2.0 ± 0.2	2.0 ± 0.2
0.05	1.9 ± 0.2	1.8 ± 0.2
0.10	1.7 ± 0.2	1.6 ± 0.2
0.10[a]	1.7 ± 0.2	1.6 ± 0.2
0.30	1.7 ± 0.2	1.7 ± 0.2
0.50	1.7 ± 0.2	1.7 ± 0.2

Log *K* values are for a stoichiometry as shown in Reaction 2. 2σ error calculated by determining the range of log *K* values that encompasses 95% of the experimental data. [a] Log *K* values from concentration dependent adsorption.

4.4.4 Linear Free-Energy Correlation

Fein et al. (2001) demonstrated that stability constants for bacterial surface metal-carboxyl complexes can be estimated using a linear free energy approach (Langmuir, 1979). Previously measured bacterial metal-carboxyl stability constants for a range of divalent and trivalent metal cations can be correlated to the corresponding stability constants for aqueous metal-organic acid anion complexes for the same metals. Based on this correlation, unknown metal-carboxyl bacterial stability constants can be estimated with reasonable accuracy if the corresponding metal-organic acid anion stability constant is known. Fein et al. (2001) calibrated this approach for *B. subtilis* by measuring a range of divalent and trivalent bacterial metal-carboxyl stability constants in a 0.1 M background electrolyte, and correlating the constants to their respective acetate-, oxalate-, citrate-, and tiron-metal stability constants. We extend this treatment to the NpO_2^+-carboxyl stability constant from this study, calculated from the 0.1 M ionic strength data. Although there is some uncertainty concerning the low pH Np-bacterial binding mechanism, the stability constant for the NpO_2^+-carboxyl surface species does not vary substantially from model to model, and is primarily constrained by the extent of mid-pH adsorption. The aqueous NpO_2^+-tiron stability constant has not been measured, but we create correlation plots for acetate, oxalate, and citrate (Figure 4.5).

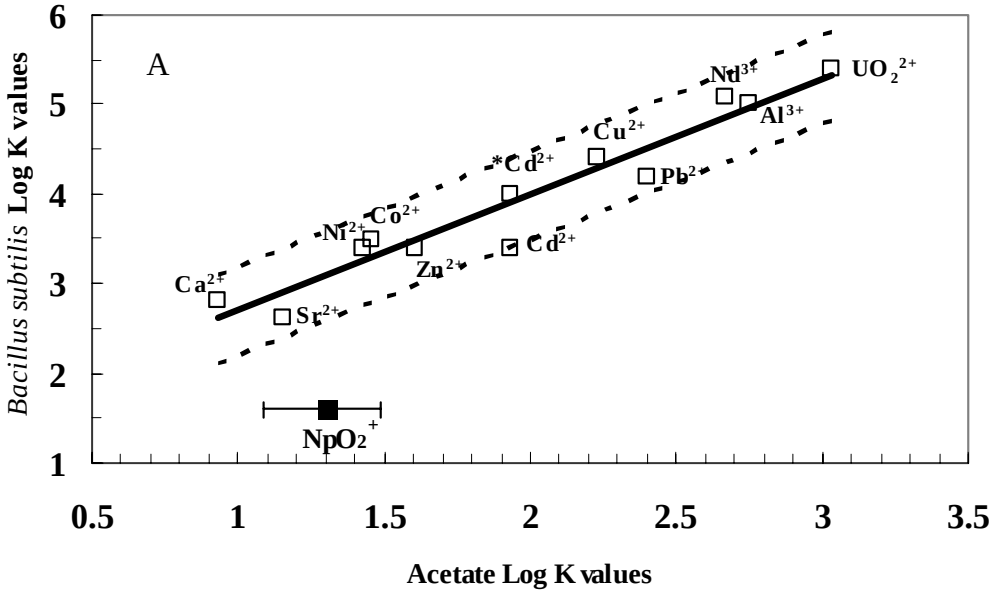
A
Bacillus subtilis Log K values
Acetate Log K values
6
5
4
3
2
1
0.5
1
1.5
2
2.5
3
3.5
UO2 2+
Nd3+
Al3+
Cu2+
*Cd2+
Pb2+
Co2+
Ni2+
Cd2+
Zn2+
Ca2+
Sr2+
NpO2+

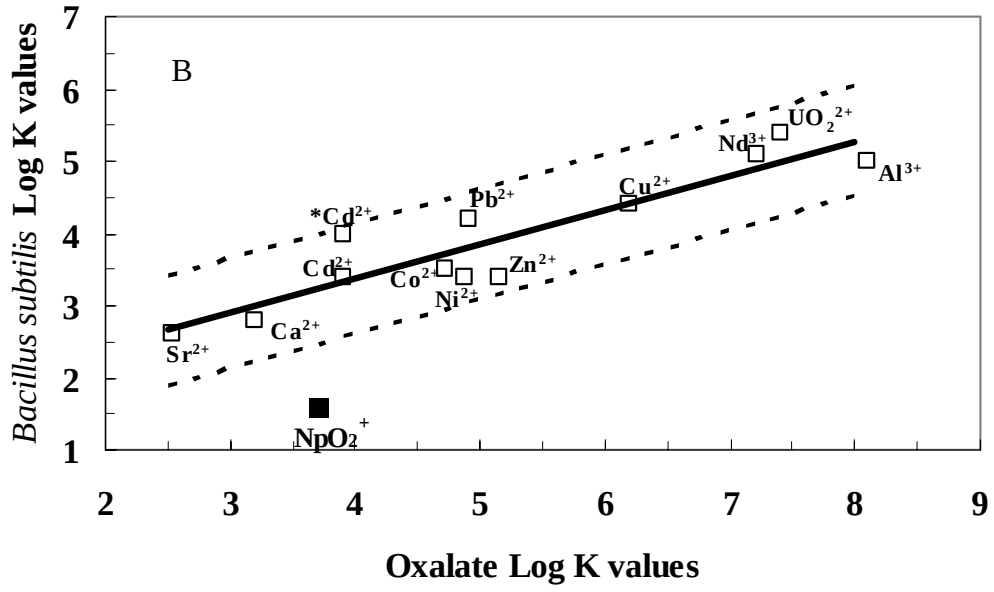
B
Bacillus subtilis Log K values
Oxalate Log K values
7
6
5
4
3
2
1
2
3
4
5
6
7
8
9
UO2 2+
Nd3+
Al3+
Cu2+
Pb2+
*Cd2+
Cd2+
Co2+
Zn2+
Ni2+
Ca2+
Sr2+
NpO2+

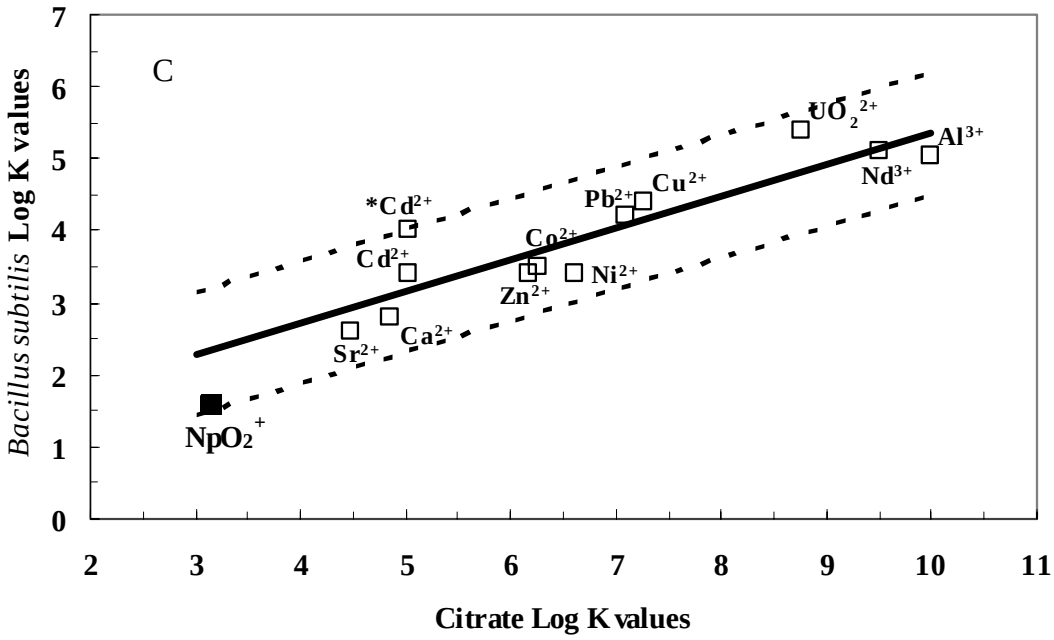

Figure 4.5: Correlation plots showing calculated and previously published metal-carboxyl stability constants for *B. subtilis* as functions of aqueous metal-organic acid anion stability constants for acetate (A), oxalate (B), and citrate (C). The Np-carboxyl stability constant for *B. subtilis* (I = 0.1 M) is shown as a filled square, and error bars are within the data point. Horizontal error bars on the Np data point represent the range of literature values for the Np-acetate stability constant. Dashed lines represent 2 standard deviation units for the correlation.

Figure 4.5 illustrates that the bacterial NpO_2^+-carboxyl stability constant lies more than two standard deviation units (dashed lines) off the acetate and oxalate correlation lines. The bacterial NpO_2^+-carboxyl stability constant lies within two standard deviation units of the citrate correlation plot. However, the citrate correlation exhibits substantially

greater uncertainty (larger data scatter and associated two standard deviation values) than is associated with the oxalate or acetate correlations, and therefore the citrate correlation is unlikely to be the most precise predictive tool. Linear free energy relationships such as those depicted in Figure 4.5 likely exist due to similar binding mechanisms between the two organic functional groups involved. Our results suggest that NpO_2^+ is anomalous, interacting with the cell wall carboxyl groups in a fundamentally different way than all the other metal cations studied thus far (Fein et al., 2001). This behavior is rather surprising considering that these types of plots for purely aqueous complexation of NpO_2^+ with various organic and inorganic complexes suggest that Np aqueous complexation with these ligands is similar to that observed for a wide range of other aqueous cations (Jensen and Nash, 2001). The chemistry of NpO_2^+ differs from the other cations in three distinct ways. The neptunyl ion is redox active; however, redox reactions would tend to make Np adsorb more strongly to the bacterial wall and preliminary XAS data indicate that the Np would sorb as Np(V) under these conditions (Skanthakumar et al., 2004). NpO_2^+ has a well-known propensity for forming cation-cation (i.e., NpO_2^+-NpO_2^+) complexes (Sullivan et al., 1961; Guillaume et al., 1982; Stout and Choppin, 1993; Stoyer et al., 2000). However, at the Np concentrations of these experiments, the formation of such cation-cation complexes cannot account for the observed deviation from the general correlation. Last, the geometry of the neptunyl ion together with its low charge leads to weakly coordinated complexes (Keller, 1971). In the case of bacterial surface complexes, it is likely the low charge on the neptunyl ion cannot overcome the steric hindrance caused by the bacterial cell wall. As a result, the NpO_2^+-bacterial stability constants are much lower than those observed for other metals. The ionic

strength dependence that we observe is considerably stronger than that observed for Cd, Cu, and Pb adsorption onto *Bacillus subtilis* (Daughney and Fein, 1998a). These lines of evidence suggest that the adsorption of NpO_2^+ is dominantly electrostatic and depends directly on the thickness of the electric double layer that surrounds the bacterial cells.

4.5 Conclusions

Our experimental results indicate that the neptunyl ion adsorbs onto *B. subtilis* cell walls more weakly than do divalent and trivalent cations such as Cd^{+2}, UO_2^{+2}, Al^{+3}, etc. Np adsorption is highly ionic strength dependent, and ionic strength appears to control the extent of possible Np(V) reduction that we observed under low pH conditions. Our modeling results for both the 0.1 and 0.001 M systems suggest that binding is due primarily to attachment of the neptunyl cation onto phosphoryl and carboxyl surface groups on the bacterial cell wall, a result consistent with previous bulk adsorption and XAS experiments of bacterially adsorbed metal cations. This study yields a detailed understanding of the effects of pH and ionic strength on NpO_2^+ adsorption onto a common bacterial surface type, and we determine thermodynamic stability constants for the important NpO_2^+-bacterial surface complexes. Accurate modeling of the environmental fate of Np requires the determination of thermodynamic stability constants for environmentally-important Np species, including complexes with important mineral surfaces and humic/fulvic acids. Our results suggest that, under select conditions, bacterial surface adsorption can affect the overall Np speciation and mobility in bacteria-water-rock systems. However, the relatively weak adsorption of Np(V) by *B. subitilis*

also implies that the presence of competing ions will tend to mitigate the effect of bacterial surface complexation on Np solution chemistry.

CHAPTER 5

THE ADSORPTION OF AQUEOUS URANYL COMPLEXES ONTO *BACILLUS SUBTILIS* CELLS

5.1 Introduction

The release of radionuclides into the environment from mining activities, nuclear weapon production and nuclear energy production, and the storage of radioactive waste has focused research on the development of accurate and adaptable tools to predict the fate and transport of these contaminants in the subsurface (Zhang et al., 2002). The solubility and structural complexity of U(VI) mineral phases, and the complex speciation of aqueous uranium, make the prediction of uranium mobility difficult. The adsorption of aqueous uranium species onto mineral and bacterial surfaces can influence the speciation, and hence the mobility, of uranium in the subsurface (Nakajima et al., 1982; Atun and Kilislioglu, 2002). Considerable attention has been paid to uranium adsorption onto a range of mineral surfaces of environmental interest. However, very little research has focused on uranium adsorption onto bacteria, especially under the circumneutral pH conditions where aqueous uranium speciation is so complex.

Under oxidizing conditions, uranium is present in aqueous solutions as the highly soluble uranyl ion, UO_2^{+2}. Because the uranyl ion forms a number of stable hydroxide and carbonate complexes in the pH range 5 – 10, the circumneutral uranium adsorption behavior can be complicated. Above pH 5, neutral and negatively charged uranyl-carbonates dominate the aqueous uranium speciation, typically causing a substantial decrease in uranium adsorption onto mineral surfaces (Hsi and Langmuir, 1985; Lieser and Thybusch, 1988; Lieser et al., 1992; Waite et al., 1994). In groundwater systems, high calcium concentrations are common, and an aqueous calcium-uranyl-carbonate complex has been identified that can dominate uranium speciation in mid- to high-pH solutions. The tendency for these uranyl complexes to remain in solution has led to the common assumption that such aqueous complexation causes a high degree of uranium mobility (Giblin et al., 1981; Yanase et al., 1995). Furthermore, the presumed mobility of these uranyl complexes represents the basis of proposed remediation strategies that rely on the formation of uranyl-carbonate complexes to mobilize uranium (Longmire et al., 1994; Turney et al., 1994; Buck et al., 1996). Although there is some evidence that uranyl-carbonate complexes can adsorb onto mineral surfaces (Bargar et al., 1999; Bargar et al., 2000; Bencheikh-Latmani et al., 2003; Stamberg et al., 2003), the assumptions of uranium mobility persist, and there have been no studies that have determined whether these complexes adsorb to any substantial extent onto negatively charged bacterial surfaces.

Most previous studies of bacterial surface uranyl adsorption have focused on low pH conditions where UO_2^{+2} is the predominant aqueous uranium species. These studies typically model adsorption by invoking a bulk partitioning approach that cannot be extrapolated to conditions that differ substantially from those investigated in the laboratory (Hennig et al., 2001; Sar and D'Souza, 2001). Surface complexation approaches offer a more mechanistic and flexible approach. Fowle et al. (2000) used a surface complexation approach to model their measurements of low pH uranium adsorption onto the Gram-positive bacterial species *Bacillus subtilis*, ascribing the observed adsorption behavior to UO_2^{+2} binding onto two distinct types of bacterial surface sites. Kelly et al. (2002) confirmed the stoichiometry proposed by Fowle et al. (2000) through an x-ray absorption spectroscopy study performed on similar uranium-*Bacillus subtilis* samples. Haas et al. (2001) also applied surface complexation modeling to open atmosphere measurements of uranyl adsorption onto the Gram-negative bacterium *Shewanella putrefaciens.* These experiments extended over a wide pH range, and Haas et al. (2001) modeled the results by invoking binding of the uranyl cation and a uranyl-hydroxide species onto the bacterial surface. However, both uranyl hydroxide and uranyl carbonate complexes were present in solution in their experiments, so the experimental results alone cannot be used to uniquely determine how much of the adsorption should be ascribed to each type of complex. X-ray absorption spectroscopy offers a more direct view of uranyl-bacterial coordination environments, but studies are limited in number and have not examined uranium binding under pH conditions higher than pH 5 (Hennig et al., 2001; Kelly et al., 2002).

In this study, we conducted uranium adsorption experiments to determine the identity and thermodynamic stabilities of the important bacterial surface uranium species above pH 5, where the aqueous uranium speciation becomes complex. We measured aqueous uranium adsorption onto *B. subtilis* in the pH range 1.5 - 9 in both closed (no CO_2) and open atmospheres, with and without aqueous calcium. We use the adsorption experiments, in conjunction with thermodynamic modeling, to test for the presence of adsorbed uranyl-carbonate and calcium-uranyl-carbonate bacterial surface complexes. We used *B. subtilis*, an aerobic Gram-positive bacterial species, in these experiments because it is a common soil microorganism with well–characterized surface properties (Beveridge and Murray, 1980; Fein et al., 1997; Fein et al., 2005).

5.2 Experimental Section

5.2.1 Bacterial Growth

B. subtilis cells were cultured and prepared following the procedures outlined in previous studies (Fein et al., 1997; Fowle et al., 2000), excluding the acid wash step in the cell preparation. Cells were maintained on agar plates consisting of trypticase soy agar with 0.5% yeast extract added. Cells for the adsorption experiments were grown by first inoculating a test-tube containing 3 ml of trypticase soy broth and 0.5% yeast extract, and incubating it for 24 h at 32 °C. The 3 ml bacterial suspension was then transferred to a 1 L volume of trypticase soy broth, also with 0.5% yeast extract, for another 24 h on an incubator shaker table at 32 °C. Cells were then harvested after reaching the early stationary growth phase, pelleted by centrifugation at 1600 g for 15 min, and rinsed seven

times with 0.1 M $NaClO_4$. The bacteria were then re-pelleted by centrifugation at 5000 *g* for two 30-minute intervals to remove excess water and create a wet weight that was used to produce suspensions of known bacterial concentrations. The ratio of this wet weight to dry weight is 5.1:1 (Borrok et al., 2004a). Subsequent suspensions of the bacteria after washing does not release substantial amounts of calcium (Figure 5.1) or other cations in solution that would affect the charge on the bacterial surface (Borrok et al., 2004b). The washing procedure does not lyse the bacterial cells nor do the cells sporolate or multiply during the course of the experiments.

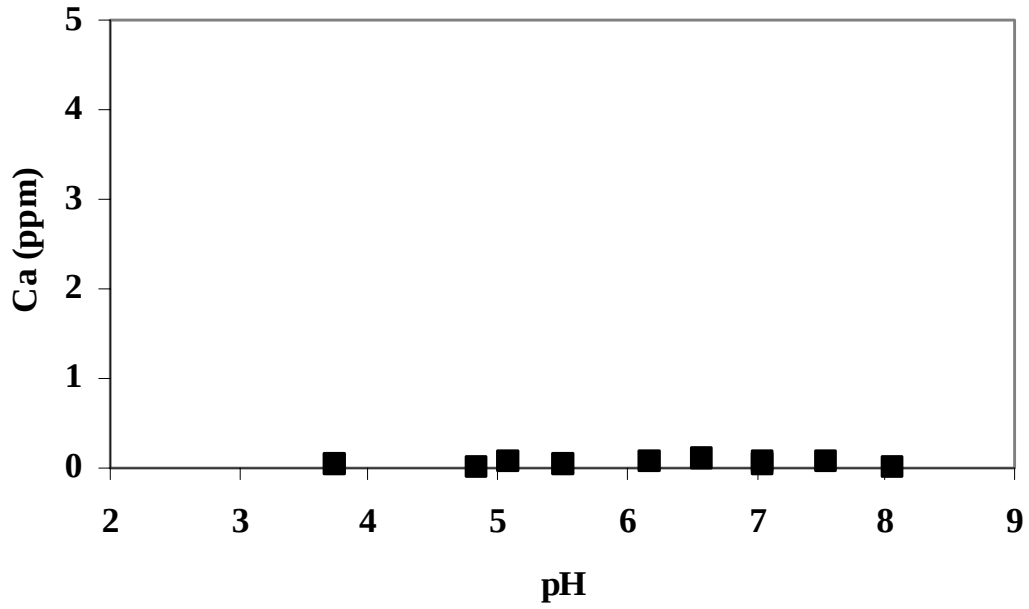

Figure 5.1: Ca released by *B. subtilis* (10 g/L wet weight) as a function of pH.

5.2.2 Control Experiments

The adsorption and desorption experiments were all conducted as functions of pH and solid:solute ratio in batch reaction vessels at 25 ± 1° C, using a 0.1 M $NaClO_4$ electrolyte solution to buffer ionic strength. Bacteria were suspended in a 4.2 X 10^{-6} M uranium-bearing electrolyte solution diluted from an acidic 4.2 X 10^{-3} M uranium atomic absorption spectroscopy aqueous standard. The experimental uranium concentration was chosen, based on control experiments, to avoid precipitation of any uranium mineral phases. The initial uranium-bacterial suspension was pH 3.5 for all experiments. Control experiments were performed in the same manner as the bacterial adsorption experiments described below, except without bacteria in order to test for loss of uranium due to precipitation or adsorption onto the reaction vessel. Control experiments using polypropylene reaction vessels revealed substantial uranium loss from solution with starting concentrations above 4.2 X 10^{-6} M. We did not observe any substantial loss of uranium in 4.2 X 10^{-6} M control experiments run in Teflon reaction vessels, so all subsequent experiments were conducted using this material.

5.2.3 U Adsorption Experiments

For the bacteria-bearing experiments, we divided the bacterial suspension into separate 10 ml Teflon centrifuge tubes and adjusted the pH of the solution in each to be between pH 1.5 and 9 using small volumes (less than 1% of total volume) of concentrated NaOH and HNO_3. Kinetics experiments (Figure 5.2) and previous studies (Fowle and Fein, 2000) indicated that steady-state adsorption was reached within 30 minutes and persisted

for at least 24 hours, so to insure the attainment of equilibrium in the remaining adsorption experiments, the reaction vessels were slowly agitated end over end for 2 hours. Prior to sampling of the experimental fluids, the equilibrium pH was measured in each vessel. Samples were centrifuged for 15 minutes at 10,000 *g* to pellet the bacteria. Approximately 6 ml of solution was pipetted off the top of the supernatant so as not to disturb the bacterial pellet, and each sample was acidified with 15 μ L of concentrated HNO_3 to maintain the uranium in solution prior to analysis. Calcium-bearing experiments were conducted in a similar manner, except 10 mM of calcium nitrate was added to the parent solution that contained bacteria and uranium prior to pH adjustment. Analysis for the total aqueous uranium and calcium concentrations in the supernatant of each sample was performed by inductively coupled plasma optical emission spectroscopy with matrix-matched standards with an analytical uncertainty of ± 3.5 %. Open and closed atmosphere experiments were conducted following the same procedures, except that the open atmosphere experiments were conducted with solutions in equilibrium with atmospheric CO_2, whereas CO_2 was excluded from the closed atmosphere experiments by conducting the experiments in a glove box purged with a 95% N_2, 5% H_2 gas mixture atmosphere. We used a Coy Model 10 gas analyzer to verify the glove box atmospheric composition. Glove box atmospheric preparation entailed purging the box until the oxygen levels were down to 100 ppm, then using a Plas-lab anaerobic chamber catalyst heater until oxygen levels were 0 ppm. In addition, all solutions used in the closed atmosphere experiments were purged for 1 h with N_2 immediately prior to use.

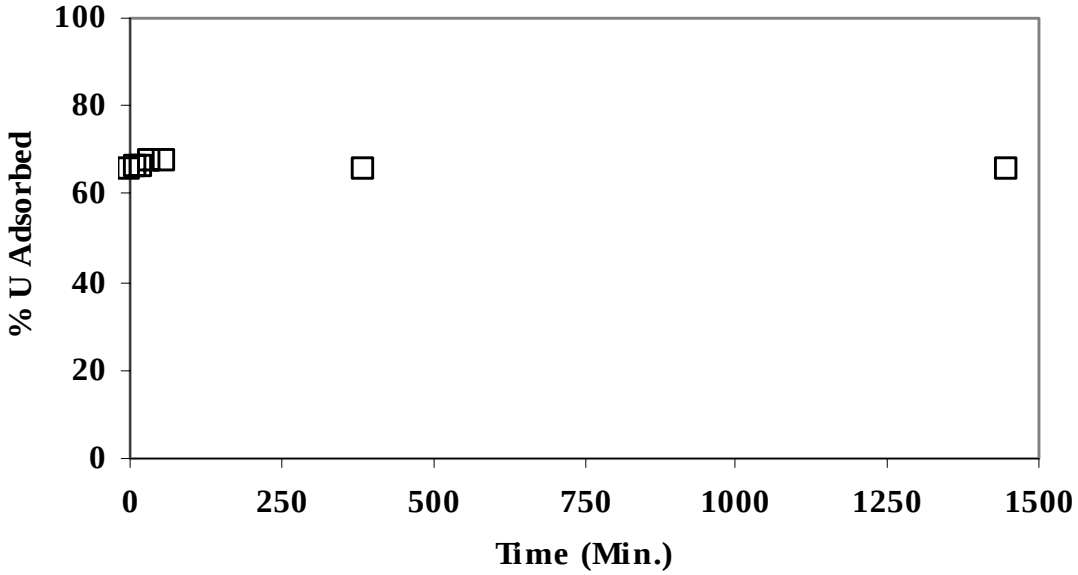

Figure 5.2: U adsorbed by *B. subtilis* (0.125 g/L wet weight) as a function of time at pH 5.5 in an open system.

5.2.4 U Desorption Experiments

These experiments were conducted with 0.125 g/L bacteria in the presence and absence of CO_2. An initial adsorption step was conducted in which a U-bacteria parent solution, prepared as described above, was adjusted to pH 6.3 in an open atmosphere system, and to pH 7.1 in a CO_2-free system, and each system was allowed to equilibrate for 2 h. Aliquots of these two parent solutions were placed into separate reaction vessels and subsequently adjusted to higher and lower pH conditions to promote U desorption from the bacteria. The systems were allowed to re-equilibrate for an additional 2 h. Samples were taken from these vessels, and U concentrations were determined, as described above.

5.2.5 Ca Adsorption Experiments

Adsorption experiments were conducted to determine the extent of Ca adsorption onto the bacteria in the absence of U, and to constrain the thermodynamic stabilities of the important Ca-bacterial surface complexes. Fowle and Fein (2000) conducted similar Ca adsorption experiments, but they used an acid-wash procedure which may have affected the cell wall adsorption properties (Borrok et al., 2004a). In this study, a Ca-bacterial parent solution in 0.1 M $NaClO_4$, with 10 g/L bacteria (wet weight) and 15 ppm Ca, was prepared similar to the U-bacterial parent solution previously described. We divided the bacterial suspension into separate 10 ml Teflon centrifuge tubes and adjusted the pH of the solution in each to be between pH 2 and 9 using small volumes of concentrated NaOH and HNO_3. The reaction vessels were slowly agitated end over end for 2 hours. Prior to sampling of the experimental fluids, the equilibrium pH was measured in each vessel. Samples were filtered with 0.45 μ nylon membranes and the supernatant was acidified with 15 μL of 15 M HNO_3. Ca concentration was determined by ICP-OES. Control experiments were also conducted to determine if Ca is released from the bacterial cells during experimentation, affecting the total Ca in the experimental systems. The control experiments were performed in a similar manner as the Ca adsorption experiments except without aqueous Ca present. Results, shown in Figure 5.1, indicate that Ca release to solution is negligible under the experimental conditions.

5.3 Modeling of Metal-Bacteria Adsorption

We applied a surface complexation approach to model the adsorption of U and Ca onto the *B. subtilis* cells. A surface complexation approach quantifies adsorption using balanced chemical equations. This approach enables prediction of adsorption in systems not directly measured in the laboratory. Using the model of Fein et al. (2005) to describe the proton-active sites on the bacterial surface, proton binding is ascribed to four distinct reactions of the following stoichiometry:

$$R - LiH^0 \quad \longleftrightarrow \quad R - Li^- \quad + \quad H^+ \tag{1}$$

where *R* is a bacterium to which a proton-active functional group type, *Li*, is attached. Fein et al. (2005) use potentiometric titration data to constrain the site concentrations and acidity constants for the pertinent protonation reactions, and we employed their discrete pK_a 4-site non-electrostatic model with pK_a values of 3.3, 4.8, 6.8, and 9.1. Electrophoretic mobility measurements of *B. subtilis* cells demonstrate that the bacteria exhibit a negative surface charge above pH 2, with increasing negative charge with increasing pH. These observations are consistent with successive deprotonation of bacterial surface sites with increasing pH, and suggest that neither Na^+ from the electrolyte, nor elements such as Ca and Mg, which may be released to some extent from the cell wall, substantially affect the bacterial surface charge under the conditions of the experiments. X-ray absorption spectroscopy results (Kelly et al., 2002; Boyanov et al., 2003) suggest that the *L1* and *L2* sites, with pKa values of 3.3 and 4.8, are likely phosphoryl and carboxyl groups, respectively. The identities of the other surface sites, with pK_a values of 6.8 and 9.1, are more uncertain, and we refer to them as site 3 (*L3*) and site 4 (*L4*), respectively.

We tested the ability of a range of reaction stoichiometries to account for the observed adsorption behavior, and used the program FITEQL (Herbelin and Westall, 1994) to determine the model that best fits the experimental data. Although we have no spectroscopic data to help constrain the dominant binding mechanisms above pH 5, adsorption measurements conducted as a function of pH and solute:sorbent ratio provide constraints on the stoichiometry and thermodynamic stability of the important bacterial surface species.

A generic metal adsorption reaction can be represented with the balance chemical equation:

$$M^{m+} + \quad R - LiH_z^{(z-1)} \quad \longleftrightarrow R - LiH_z - M^{(z-1+m)} \tag{2}$$

where *Li* represents one of the four surface functional group types present on the bacterial surface, and *z* can equal 0 or 1. We tested a range of possible reaction stoichiometries and solved for each proposed stability constant as defined by:

$$K = \frac{[R - LiH_z - M^{(z-1+m)}]}{a_{M^{m+}}[R - LiH_z^{(z-1)}]} \tag{3}$$

where *a* represents the aqueous activity of the subscripted species, and the brackets represent surface site concentrations in moles per kilogram of solution. Activity coefficients are calculated by FITEQL using the Davies equation (Herbelin and Westall, 1994).

5.4 Results and Discussion

5.4.1 Adsorption and Desorption Results

Bacteria-free control experiments do not exhibit any measurable loss of U in the open or closed system from pH 1.5 to 9 (not shown). In the CO_2-free experiments, uranium adsorption increases with increasing pH up to approximately pH 5 - 6 for each of the three bacterial concentrations studied, reaching adsorption plateaus above approximately pH 6 (Figure 5.3). The system containing 0.125 g/L bacteria displays a slight decrease in adsorption above pH 8. In the open-atmosphere experiments (Figure 5.4), we observed similar low pH increases in adsorption with increasing pH to approximately pH 6. However, at higher pH values, each system studied exhibits a substantial decrease in adsorption with increasing pH, with more pronounced decreases in the systems with lower bacterial concentrations. The calcium-bearing experiments exhibit no measurable loss of calcium, which is expected under high Ca concentrations combined with the low affinity for Ca to adsorb onto the bacterial surface. The Ca-bearing data exhibit similar increases in adsorption with increasing pH to approximately pH 6 (Figure 5.5). However, above pH 6, the presence of the calcium leads to dramatically enhanced adsorption relative to the open-atmosphere calcium-free systems. Each calcium-bearing system exhibits a decrease in adsorption above pH 6, but the decrease is less than that observed for the open atmosphere calcium-free systems. As expected in all three systems, we observe an increase in adsorption as bacterial concentrations increase.

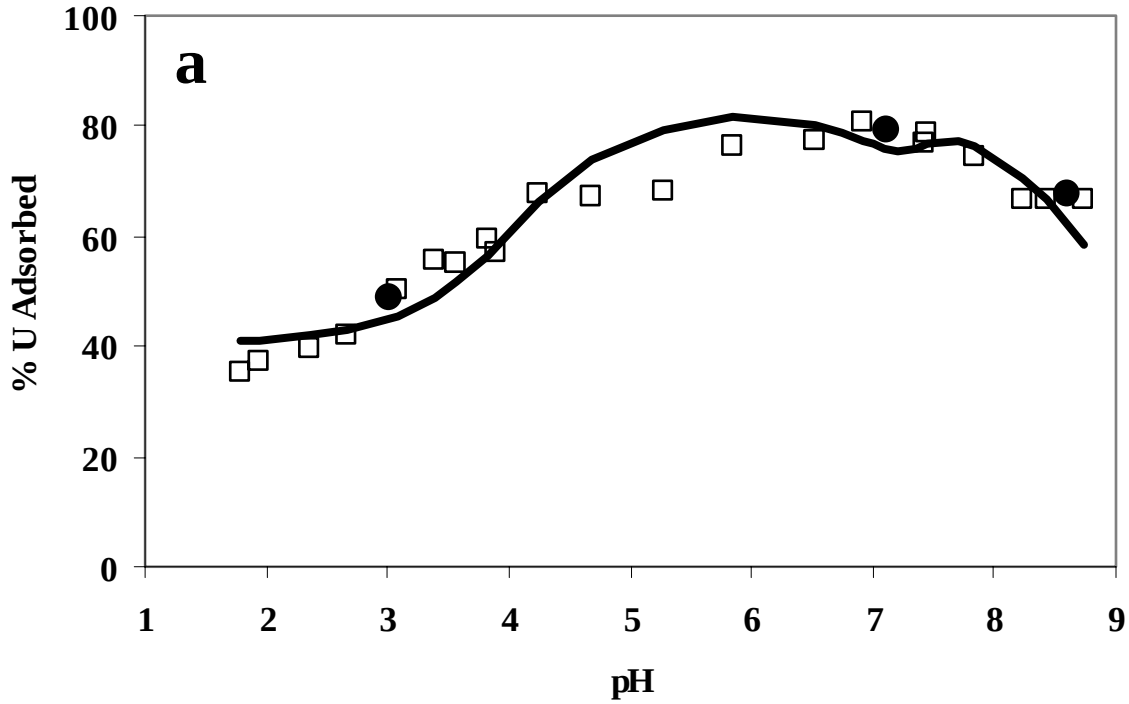
a
100
80
60
40
20
0
% U Adsorbed
1
2
3
4
5
6
7
8
9
pH

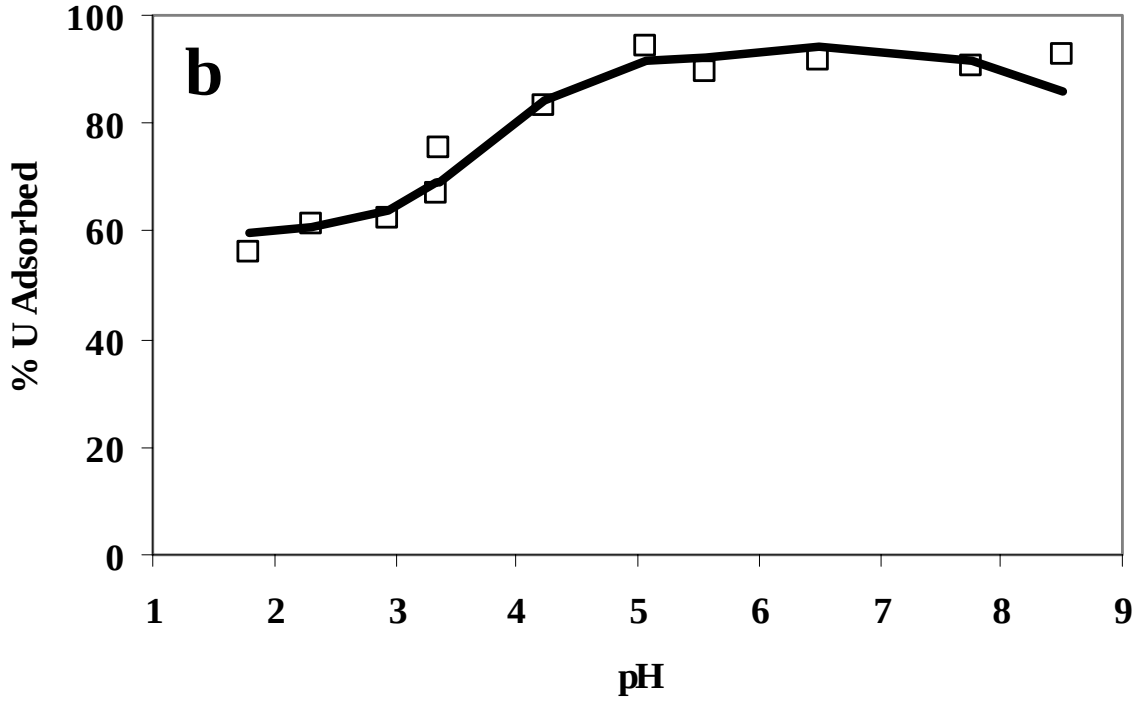
b
100
80
60
40
20
0
% U Adsorbed
1
2
3
4
5
6
7
8
9
pH

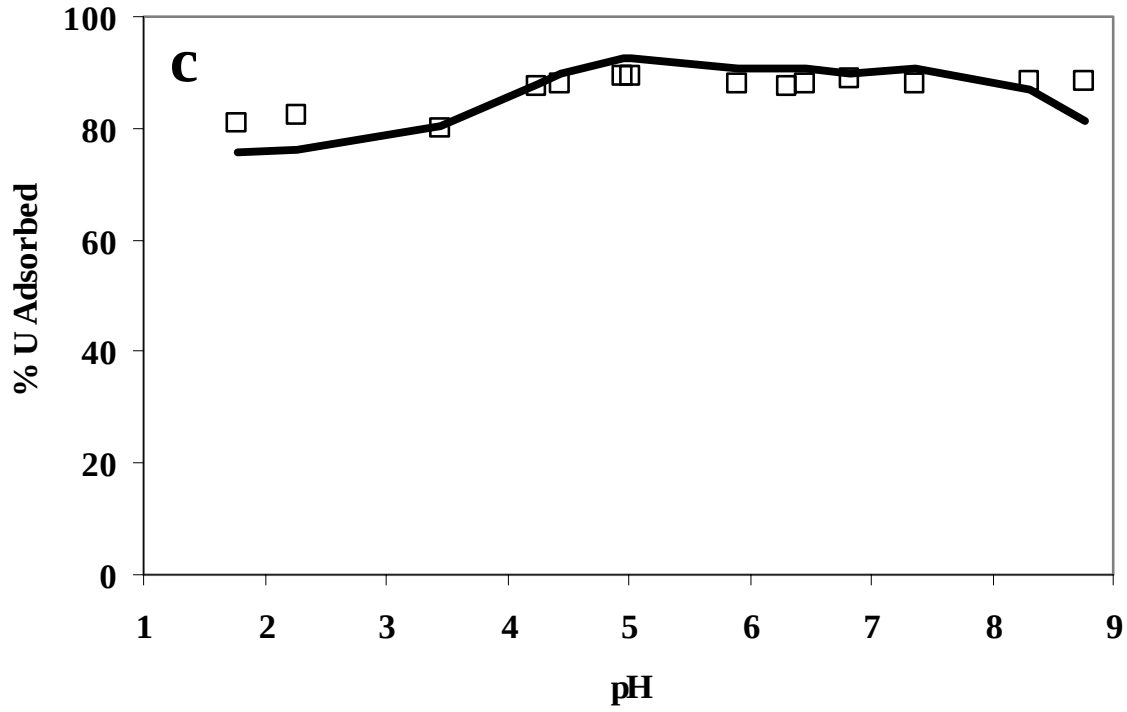

Figure 5.3: U adsorbed by *B. subtilis* as a function of pH and bacterial concentration, (a) 0.125, (b) 0.25, and (c) 0.5 g/L (wet mass), in a closed system (no CO_2). The curve (—) represents the best-fit surface complexation model (see text). Closed circles represent results from desorption experiments conducted with an initial adsorption step at pH 7.1.

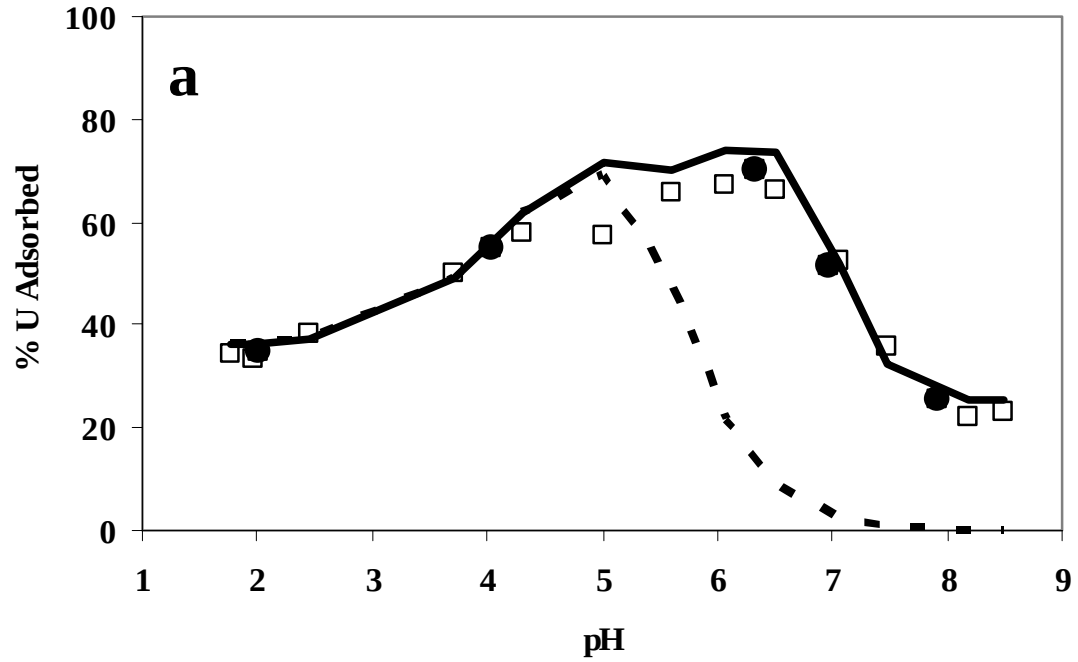
a
100
80
60
40
20
0
% U Adsorbed
1
2
3
4
5
6
7
8
9
pH

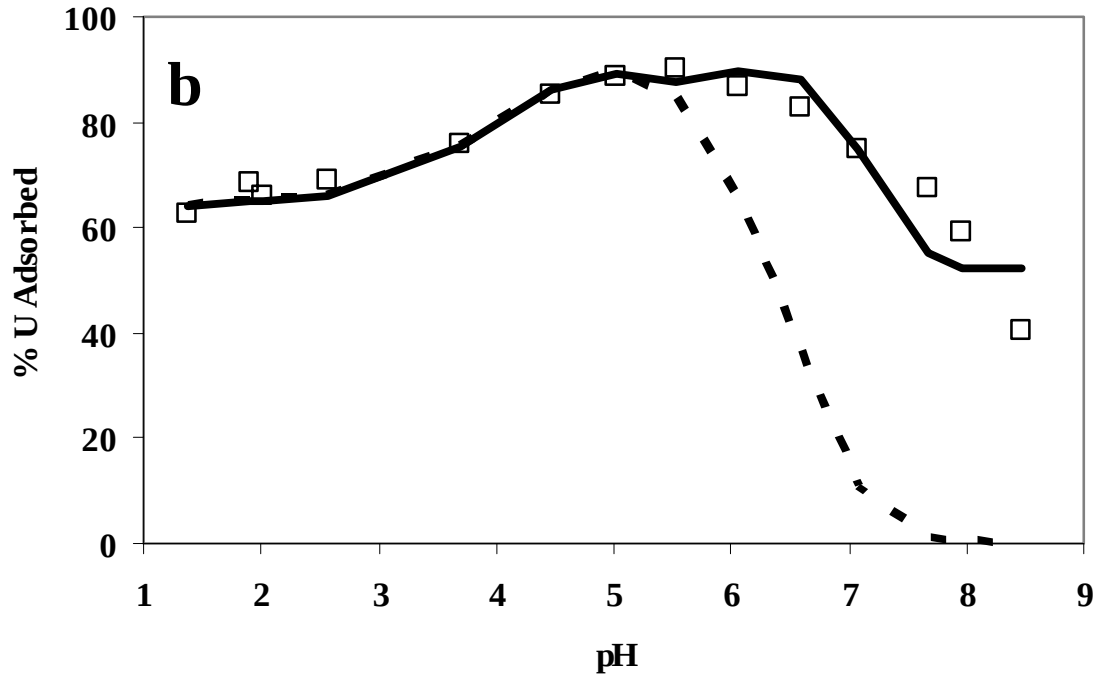
b
100
80
60
40
20
0
% U Adsorbed
1
2
3
4
5
6
7
8
9
pH

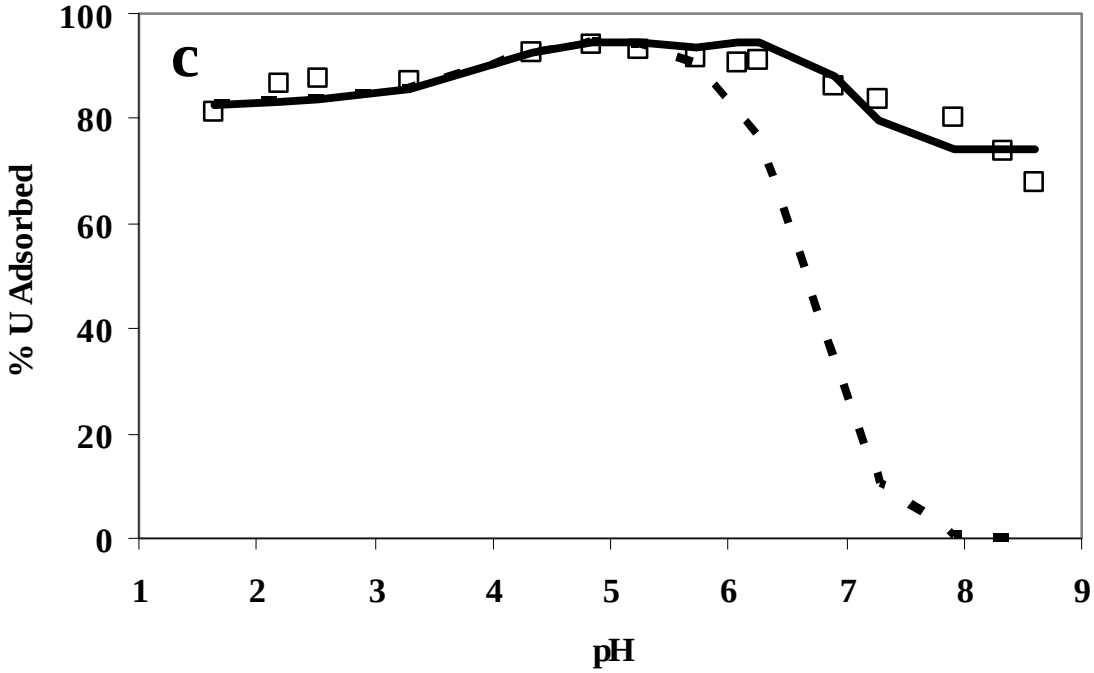

Figure 5.4: U adsorbed by *B. subtilis* as a function of pH and bacterial concentration, (a) 0.125, (b) 0.25, and (c) 0.5 g/L (wet mass), in a open system. The dashed curve (----) represents predicted adsorption in the absence of uranyl carbonate surface complexation. The solid curve (—) represents the best-fit surface complexation model (see text). Closed circles represent results from desorption experiments conducted with an initial adsorption step at pH 6.3.

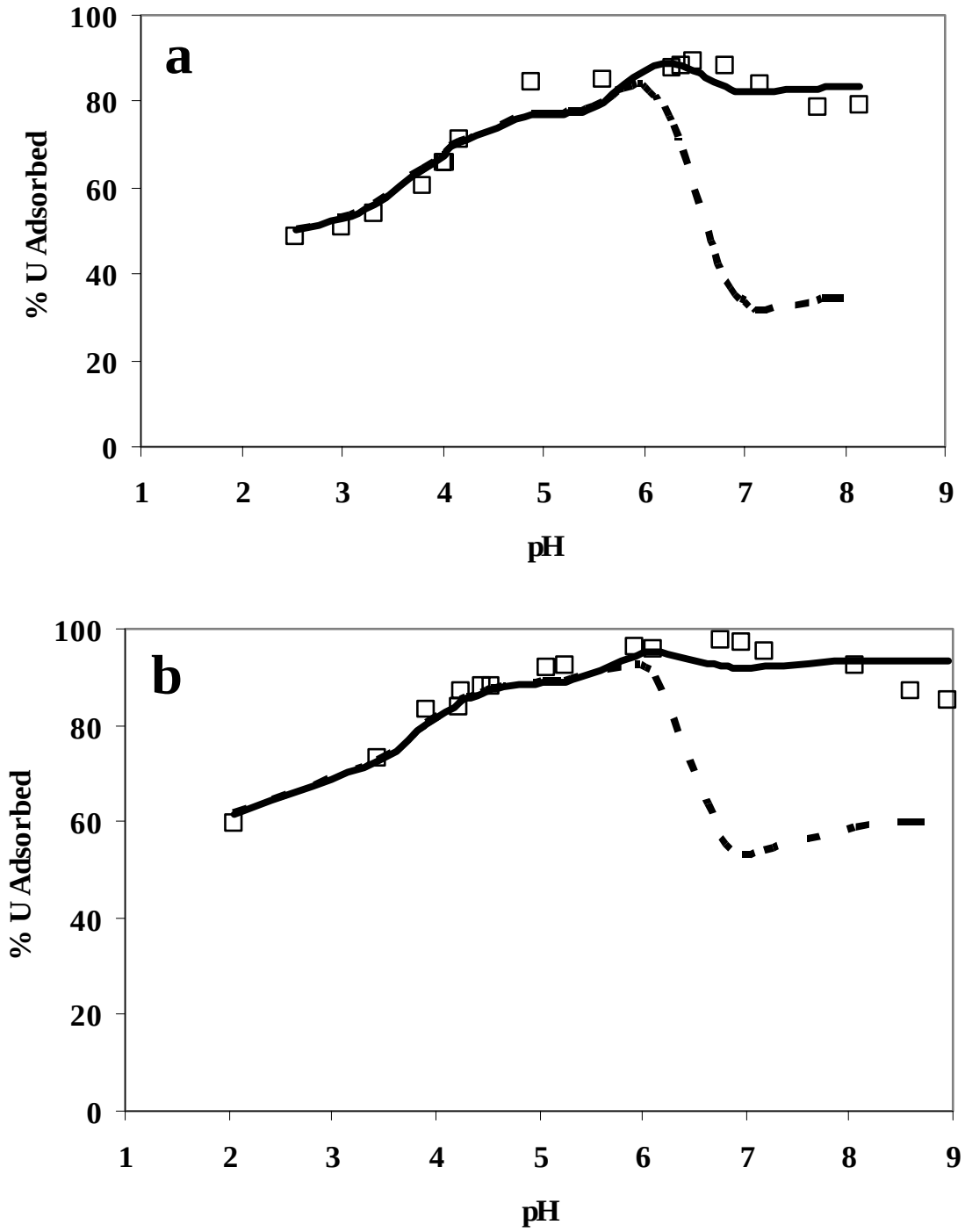

Figure 5.5: U adsorbed by *B. subtilis* as a function of pH and bacterial concentration, (a) 0.125 and (b) 0.25 g/L (wet mass), in a open system with 10mM Ca. The dashed curve (----) represents predicted adsorption in the absence of calcium uranyl carbonate surface complexation. The solid curve (—) represents the best-fit surface complexation model (see text).

All three systems exhibit extensive uranium adsorption onto *B. subtilis* over the entire pH range studied, including to pH values below 2 (Figures 5.3-5.5). The extensive adsorption observed under low pH conditions, consistent with the observations by Fowle et al. (2000) and by Haas et al. (2001), are in contrast to the typically low levels of adsorption documented for other aqueous cations under similar conditions (Fein et al., 1997). Potentiometric titrations and electrophoretic mobility experiments both indicate that below pH 2 - 3 bacterial surface sites exist dominantly in their protonated, neutral states, greatly diminishing the electrostatic contribution driving cation adsorption (Fein et al., 2005). The high degree of low pH uranium adsorption suggests that ion – dipole interactions of uranyl ion and phosphoryl groups on the bacterial surface contributes substantially to the adsorption reaction energetics.

The high extent of adsorption that occurs at mid-pH values is likely due to a range of adsorption reactions because the aqueous speciation of uranium is so complex in this pH range. The importance of uranyl ion in the aqueous uranium budget diminishes dramatically above pH 4, with uranyl-hydroxide and uranyl-carbonate complexes dominating above pH 5. The adsorption data do not mimic the decrease in activity of uranyl ion above pH 4, strongly suggesting that the other uranium complexes adsorb onto the bacterial surface to a substantial extent. Under the highest pH conditions studied here in calcium-free and calcium-bearing open atmosphere experiments, the extent of adsorption, although diminished somewhat by aqueous uranyl-carbonate and calcium-uranyl-carbonate complexation, is not diminished nearly as dramatically as is the case for mineral surfaces (Hsi and Langmuir, 1985; Lieser and Thybusch, 1988; Lieser et al.,

1992; Waite et al., 1994). The relatively high extent of adsorption under these high pH conditions is likely caused by adsorption of the uranyl aqueous complexes themselves onto the bacterial surface. Although adsorption of uranyl-carbonate complexes onto mineral surfaces has been reported recently (Bargar et al., 1999; Bargar et al., 2000; Stamberg et al., 2003), adsorption of these negatively charged aqueous uranyl complexes onto a highly negatively charged bacterial surface is particularly surprising and must reflect adsorption energetics that can overcome the high forces of electrostatic repulsion.

Desorption experiments were conducted to determine the reversibility of the U-bacteria adsorption reactions. Figures 5.3a and 5.4a depict results from desorption experiments in which a parent solution containing a U-bacterial suspension was adjusted to a pH where maximum adsorption occurs and allowed to reach an initial adsorption equilibrium. We sampled the solution after this initial adsorption step, and observed that approximately 80 % and 70 % of the U was bound to the bacteria in the CO_2-free and open atmosphere systems, respectively. Next, we took aliquots of this solution, adjusted the pH to lower and higher values, and allowed these aliquots to re-equilibrate by desorbing U from the cell walls. As shown in Figures 5.3a and 5.4a, the desorption data points exhibit excellent agreement with the adsorption measurements, providing tight constraints on the pH adsorption edge. This agreement indicates that the bacterial U adsorption reactions, like those of many other aqueous cations (Fowle and Fein, 2000), are completely reversible over the time period of the experiments, and that our adsorption measurements reflect equilibrium conditions for U partitioning between the aqueous phase and the bacterial cell walls.

The calcium adsorption experiments (without U present) indicate that Ca does not adsorb nearly as extensively onto the cell wall as does U. Adsorption is low under low pH conditions, and increases slightly with increasing pH. Maximum adsorption occurs above pH 6 and remains constant above this pH with 24 % of the total Ca adsorbed (Figure 5.6).

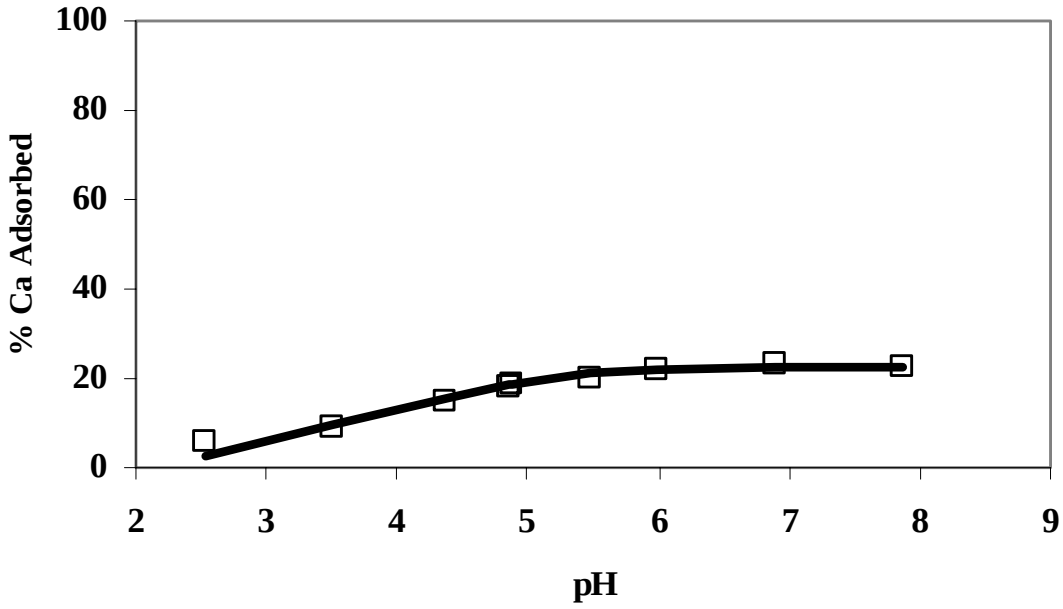

Figure 5.6: Ca adsorbed by *B. subtilis* (10 g/L wet weight) as a function of pH. The curve (—) represents the best-fit surface complexation model (see text).

5.4.2 Modeling Results

Although we have no spectroscopic data to help constrain the important binding mechanisms, adsorption measurements conducted as a function of equilibrium pH and solute:sorbent ratio can provide rigorous constraints on the stoichiometry and thermodynamic stability of the important bacterial surface species. Our approach was to model the simplest conditions first and to use those results as a foundation for models of the more complex systems. Therefore, we first modeled the low pH data in all of the systems because under low pH conditions the aqueous U speciation is dominated by the uranyl ion alone. Then we continued by modeling sequentially higher pH data, starting first with the CO_2-free system, progressing to the open atmosphere calcium-free system, and finishing with the open atmosphere calcium-bearing system. We used the program FITEQL (Herbelin and Westall, 1994) to construct models involving different uranium adsorption reactions and to determine the model that most accurately describes the observed adsorption behavior. In each calculation, we accounted for aqueous uranyl speciation using the reactions and stability constants for the important uranyl aqueous species listed in Table 5.1.

TABLE 5.1

U(VI) Aqueous Phase Reactions	Log K I = 0.0, 25°C
$UO_2^{2+} + H_2O \longleftrightarrow UO_2OH^+ + H^+$	-5.20
$UO_2^{2+} + 2H_2O \longleftrightarrow UO_2(OH)_2^\circ + 2H^+$	-12.0[a]
$UO_2^{2+} + 3H_2O \longleftrightarrow UO_2(OH)_3^- + 3H^+$	-19.2
$2UO_2^{2+} + 2H_2O \longleftrightarrow (UO_2)_2(OH)_2^{2+} + 2H^+$	-5.62[b]
$3UO_2^{2+} + 5H_2O \longleftrightarrow (UO_2)_3(OH)_5^+ + 5H^+$	-15.55
$3UO_2^{2+} + 7H_2O \longleftrightarrow (UO_2)_3(OH)_7^- + 7H^+$	-31.0
$4UO_2^{2+} + 7H_2O \longleftrightarrow (UO_2)_4(OH)_7^+ + 7H^+$	-21.9
$UO_2^{2+} + CO_3^{2-} \longleftrightarrow UO_2CO_3^\circ$	9.70
$UO_2^{2+} + 2CO_3^{2-} \longleftrightarrow UO_2(CO_3)_2^{2-}$	17.0
$UO_2^{2+} + 3CO_3^{2-} \longleftrightarrow UO_2(CO_3)_3^{4-}$	23.63
$2UO_2^{2+} + CO_3^{2-} + 3OH^- \longleftrightarrow (UO_2)_2(CO_3)(OH)_3^-$	40.82[c]

[a] From Choppin and Mathur (1991). [b] From Langmuir (1997). [c] From Tripathi (1983) All other stability constants from Grenthe (1992).

Bacterial surface speciation and aqueous uranium speciation is most simple under low pH conditions. We first considered only the data below pH 5 in all the systems, sequentially adding higher pH data and additional uranyl-bacterial surface complexes to account for the data. The model that best fits the low pH data is a 2-site model with uranyl adsorbed onto protonated *L4* sites and onto deprotonated *L2* sites. Binding onto the protonated *L4* site is used as a surrogate for adsorption onto a hypothetical site whose

pK_a is lower than those determined by Fein et al. (2005). Invoking this surrogate site is necessary in the model to account for the substantial U adsorption that occurs at pH values below the pK_a of Site 1. Under these low pH conditions, the bacterial cell wall is still proton-active, which suggests the presence of this additional site (Fein et al., 2005). However, because the pK_a and site concentration of this hypothetical site are unknown, it is impossible to model U adsorption onto it. As a surrogate for binding onto this hypothetical lowest pK_a site, we represent this reaction by including adsorption of U onto the protonated form of Site 4 in our model. Although it is unlikely that U actually binds onto a protonated site, the protonated site serves as a good surrogate because its concentration, like that of the deprotonated form of the lowest hypothetical pK_a site, does not change over the low pH range where adsorption is observed. As a function of pH and bacterial concentration, this model provides an excellent fit to all data from all systems below pH 5. The log *K* values for these U-bacterial complexes are reported with their 2σ errors as Reactions 1 and 2 in Table 5.2. As stated above, we used all of data below pH 5 from each of the 8 experimental systems to constrain these values and associated uncertainties. Each dataset (where a dataset is defined as data collected as a function of pH for a particular bacterial concentration for a particular system of interest) yields a set of best-fitting K values for these reactions. The K values reported in Table 5.2 are the averages of these calculated values, weighted to account for the number of data points in each dataset. The errors were determined by determining the range of log *K* values about these averages that results in models that encompass 95% of the data in the pH range of interest. This model is similar to that used by Fowle and Fein (2000) in that each invokes uranyl adsorption onto protonated phosphoryl and deprotonated carboxyl sites.

However, the calculated K values cannot be directly compared between these two studies because the two studies used different models for the protonation behavior of the bacterial cell wall and the choice of model directly affects calculated K values for metal adsorption reactions.

TABLE 5.2

Rxn. #	U Surface complexation reactions	Log K ± 2σ
1	UO_2^{2+} + R-HL4° $\longleftrightarrow$ R-HL4-UO_2^{2+}	5.4 ± 0.2
2	UO_2^{2+} + R-L2^{-} $\longleftrightarrow$ R-L2-UO_2^{+}	6.2 ± 0.3
3	UO_2OH^{+} + R-L3^{-} $\longleftrightarrow$ R-L3-UO_2OH°	7.1 ± 0.4
4	$(UO_2)_3(OH)_7^{-}$ + R-L4^{-} $\longleftrightarrow$ R-L4-$(UO_2)_3(OH)_7^{2-}$	8.6 ± 0.6
5	$UO_2CO_3^{\circ}$ + R-L2^{-} $\longleftrightarrow$ R-L2-$UO_2CO_3^{-}$	5.5 ± 0.6
6	$(UO_2)_2CO_3(OH)_3^{-}$ + R-L3^{-} $\longleftrightarrow$ R-L3^{-}$(UO_2)_2CO_3(OH)_3^{2-}$	7.5 ± 0.6
7	$UO_2(CO_3)_3^{4-}$ + L3^{-} $\longleftrightarrow$ R-L3-$UO_2(CO_3)_3^{5-}$	7.3 ± 0.6
8	$Ca_2UO_2(CO_3)_3^{o}$ + R-L2^{-} $\longleftrightarrow$ R-L2-$Ca_2UO_2(CO_3)_3^{-}$	5.0 ± 0.2
	Aqueous Complexation Reactions for Ca-Bearing System	
9	UO_2^{2+} + $3CO_3^{2-}$ + $2Ca^{2}$ $\longleftrightarrow$ $Ca_2UO_2(CO_3)_3$	30.45[a]
10	Ca^{2+} + HCO_3^{-} $\longleftrightarrow$ $CaHCO_3^{+}$	1.11[b]
11	Ca^{2+} + CO_3^{2-} $\longleftrightarrow$ $CaCO_3^{\circ}$	3.22[b]
	Ca Surface Complexation Reactions	
12	R-L1^{-} + Ca^{2+} $\longleftrightarrow$ R-L1-Ca^{+}	2.7 ± 0.1[c]
13	R-L2^{-} + Ca^{2+} $\longleftrightarrow$ R-L2-Ca^{+}	2.5 ± 0.1[c]

R is a bacterium to which a functional group type, Li is attached. [a]From Bernhard (2001). [b]From Wolery (1992). [c]This Work.

We used our calculated stability constants for the low pH uranyl-bacterial species to predict the extent of adsorption under higher pH conditions in the CO_2-free system. The 2-site model under estimates the observed extent of adsorption above pH 5, likely because it only involves UO_2^{+2} adsorption and neglects adsorption of the uranyl-hydroxide complexes that dominate the aqueous speciation above pH 5. Keeping the calculated stability constants from the 2-site model fixed, we tested the ability of models involving the adsorption of uranyl-hydroxide species onto deprotonated bacterial surface sites to account for the higher pH data. As an extension of our approach to modeling the low pH data, we considered sequentially higher pH ranges, including in the model additional uranyl-hydroxide bacterial surface complexes as we proceeded. The data to pH 7.5 allowed us to determine the stability of one uranyl-hydroxide bacterial surface complex; adding the data to pH 9 required the inclusion of an additional uranyl-hydroxide bacterial surface complex to the model. We tested various models involving different uranyl hydroxide species depending on their abundance in solution at the particular pH range where our model did not fit. Thus, the best-fit model for uranium adsorption in the CO_2-free system (Reactions 1 – 4 Table 5.2) involves the formation of four distinct uranyl-bacterial surface complexes, and can successfully account for the observed adsorption behavior across the pH range of this study and as a function of bacterial concentration in the CO_2-free systems (Figure 5.3). The log *K* values listed in Table 5.2 and their 2σ uncertainties are calculated as described above for Reactions 1 and 2 in Table 5.2, with K values averaged for the 3 bacterial concentration datasets depicted in Figure 5.3.

To model the open atmosphere, Ca-free experiments, we used the bacterial adsorption reactions and associated *K* values from the CO_2-free experiments to estimate the extent of adsorption expected in the CO_2-bearing system (Figure 5.4). These calculations accounted for aqueous uranyl-carbonate complexation using the stability constants for these reactions that are listed in Table 5.1. This initial model was calculated assuming that no surface complexation of the uranyl carbonate species occurred. The bacterial surface complexes defined from the CO_2-free model reasonably describe adsorption in the low- to mid-pH range for the open atmosphere experiments; however, the model under-estimates the extent of adsorption at higher pH values (Figure 5.4). This is strong evidence that uranyl-carbonate species, which dominate uranyl speciation under these higher pH conditions, adsorb onto the bacterial surface and are responsible for the enhanced adsorption relative to the estimated amount. Using the CO_2-free model as our baseline model, we tested the ability of models involving the adsorption of various uranyl-carbonate species to account for the observed bacterial adsorption. As we did in modeling the CO_2-free system, we started with the lower pH data, constrained the thermodynamic stability of the uranyl-carbonate bacterial surface complex that best accounted for those, and sequentially repeated the process with increasing pH. This process yielded a model for the open-atmosphere data that includes 3 uranyl-carbonate bacterial surface complexes in addition to the 4 reactions from the CO_2-free model (Reactions 1 – 4 Table 5.2). The overall model provides a good fit to the observed adsorption behavior in the open-atmosphere experiments over the entire pH range and for all bacterial concentrations studied. The uranyl-carbonate bacterial surface complex reactions and their log *K* values are reported with their 2σ errors as Reactions 5-7 in

Table 5.2. The log *K* values are averaged as described above, with weighted average K values determined from the 3 bacterial concentration datasets depicted in Figure 5.4.

For the calcium-bearing systems, the pertinent aqueous Ca complexation reactions (Reactions 9 – 11 Table 5.2) and Ca-bacterial complexation reactions (Reactions 12 – 13 Table 5.2) were taken into account during modeling. We modeled Ca adsorption by first testing a model involving Ca adsorption onto a depronated site 1 ($L1^-$). This model accounts for the observed adsorption up to approximately pH 4.8, but substantially under-estimates the extent of adsorption at higher pH. To account for the under-estimation above pH 4.8, we added an additional reaction to the model to account for Ca adsorption onto a depronated site 2 ($L2^-$). This 2-site model provides an excellent fit to the data over the entire pH range of the experiments (see Figure 5.6). The log *K* values are reported as Reactions 12 and 13 in Table 5.2, with their 2σ error, calculated by determining the range of log *K* values that encompasses 95% of the experimental data.

We used a similar modeling approach to that applied to the open atmosphere, Ca-free systems, to model the open atmosphere Ca-bearing system. That is, we used the bacterial adsorption reactions and associated *K* values from the CO_2-free and open atmosphere experiments (Reactions 1 – 7 Table 5.2) to estimate the extent of adsorption expected in the calcium-bearing system. The calculation of this initial model accounted for aqueous calcium-uranyl-carbonate complexation using the stability constant from Bernhard et al. (2001) (Reaction 9 Table 5.2). This initial model was calculated assuming that no surface complexation of the calcium-uranyl-carbonate species occurs

with the bacterial surface. The bacterial surface complexes defined from the CO_2-free and open atmosphere systems (Reactions 1 – 7 Table 5.2) reasonably describe adsorption in the low- to mid-pH range for the calcium-bearing experiments. However, the model dramatically under estimates the observed extent of adsorption at higher pH values (Figure 5.5), providing strong evidence that the calcium-uranyl-carbonate complex, which dominates the uranyl speciation under these higher pH conditions, adsorbs onto the bacterial surface and is responsible for the enhanced adsorption relative to the estimated amount. The inclusion of 10mM $Ca(NO_3)_2$ in these Ca-bearing experiments slightly increases the ionic strength of this system relative to the Ca-free systems, however the effect of this ionic strength increase is likely to be small and can not account for the observed enhanced adsorption in the presence of aqueous Ca. Typically, increasing ionic strength of a system causes the extent of adsorption to decrease due to the collapse of the electric double layer on the adsorbing surface. In our system, we see the opposite effect, with adsorption increasing with the addition of Ca.

To account for the enhanced adsorption behavior relative to the model we tested model fits involving calcium-uranyl-carbonate complex adsorption onto sites $L2^-$, $L3^-$, or $L4^-$. The model involving the $L2^-$ binding site alone yields a reasonable fit to the observed adsorption behavior both as a function of pH and bacterial concentration (Figure 5.5). The surface complexation reaction, its average log *K* value, and associated 2σ uncertainty are reported in Table 5.2 as Reaction 8. The averaged log *K* value with associated uncertainty are determined as described above, with a weighted average K value determined from the 2 bacterial concentration datasets depicted in Figure 5.5.

5.5 Conclusions

Our experimental approach, which measured adsorption in both CO_2-free and open atmosphere systems, is the first to provide rigorous constraints on the effect of CO_2 and calcium on bacterial adsorption of uranium, and the modeling approach that we used enabled us to differentiate between uranyl-hydroxide and uranyl-carbonate adsorption. Our results suggest that neutrally- and negatively-charged uranyl-hydroxides, uranyl-carbonates, and the calcium-uranyl–carbonate complex form highly stable surface complexes on the negatively-charged *B. subtilis* surface, leading to substantially enhanced extents of adsorption in the pH range 7 to 9. The presence of these surface complexes at higher pH is unexpected given the unfavorable electrostatic energetics between the aqueous uranyl complexes and the bacterial surface.

The stability constants of the important uranium-bacterial surface complexes that we determined in this study may help predict U adsorption onto other bacterial species (Borrok et al., 2004c) and can be incorporated into geochemical models that will help determine the potential impact of bacterial surface adsorption on the mobility of uranium in groundwater systems. Such modeling can be used to assess and predict the effects of pH, CO_2, and calcium concentration of the uranium adsorption behavior. Our discovery of uranyl-carbonate and calcium-uranyl-carbonate adsorption onto a common bacterial surface suggests that uranium may not be as mobile as is currently thought in CO_2- and calcium-bearing systems, a result that may force re-consideration of remediation and retardation strategies for uranium contamination in circumneutral bacteria-bearing aerobic systems.

CHAPTER 6

CONCLUSIONS

This dissertation provides new knowledge on the adsorption of a variety of contaminants or potential contaminants onto common geologic surfaces. The adsorption behavior of Bmim Cl, and other imidazolium based ionic liquids, suggests that if it were introduced into the subsurface, geologic retardation is unlikely unless clays with an interlayer are present. Ionic liquids do show promise for industrial replacement of solvents; however, more research investigating the adsorption of a variety of classes of ionic liquids is still necessary. This would provide a better understanding of which potentially new solvents would be the most benign to the environment in case of accidental release. Our results revealed instability of Bmim Cl under low pH conditions and further research into the altered properties or pH active impurities of Bmim Cl is necessary prior to its use in industry. Isolation and characterization of the breakdown products and their adsorptive properties would enhance the understanding of the potential impact Bmim Cl might have in case of an industrial accident.

Titration calorimetry of bacterial surface adsorption reactions is a very useful technique combined with previous used methods of studying the bacterial surface. My results compliment those findings of Fein et al. (2005) in that the data indicate that the bacterial surface functional groups are not fully protonated, even at pH values as low as 2.6. Applying a surface complexation model to the measured bulk heats in this study yields site-specific enthalpies and entropies of protonation and Cd adsorption onto *B. subtilis*. My results indicate that functional groups on the bacterial surface likely behave more like organic acids with multiple acid sites and the coordination environment Cd may be the result of multidentate complexation. These data provide new details of proton and Cd adsorption that are impossible to gain from previous methods, e.g. bulk adsorption experiments, spectroscopic studies, thermodynamic modeling, used to study the reactivity of the bacterial surface. Calorimetric measurements of other metals and studies involving different bacterial species could substantially enhance our understanding of molecular-scale mechanisms that control proton and metal adsorption onto bacteria.

Np and U exhibit very different adsorption behavior onto *B. subtilis*. Np is comparatively a weak adsorber that is highly dependent on ionic strength. Our results indicate that Np uptake is primarily the result of adsorption onto most likely phosphoryl and carboxyl functional groups on the bacterial surface under most conditions studied. Np uptake under low pH high ionic strength conditions is consistent with bacterially influenced reduction of the Np (V) to Np (IV). This unusual behavior in low pH high ionic strength conditions warrants further research and is particularly suited for an x-ray

adsorption near edge spectroscopic study to directly determine the oxidation state of the Np bound to the bacterial surface under these conditions and confirm bacterial reduction is responsible for the unusual behavior.

U, in contrast to Np, adsorbs very strongly to the bacterial surface under all conditions studied. These are rather surprising results since U speciation under circumneutral to alkaline pH conditions is dominated by neutral and negatively charged uranyl species and electrostatics would not predict these interactions. The role of Ca in enhanced adsorption at high pH open atmosphere conditions is also surprising since one might predict the aqueous complexation would compete with the bacterial surface retaining the U in solution. Further spectroscopic research investigating U adsorption at high pH, with and without Ca, could provide better constraints on the surface complexation model and confirm the role of Ca in enhanced adsorption.

One of the biggest challenges facing Earth scientists is quantifying the mobility of contaminants in the subsurface. The immense complexity and variability in subsurface systems creates unique challenges in the prediction of contaminant transport. Adsorption reactions are major controlling factors in subsurface processes. The results presented in this dissertation fill in crucial gaps in our understanding of chemical waste migration through water-rock systems and suggest future directions of research. These results will yield substantially more accurate and flexible geochemical models through the incorporation of parameters based on thermodynamic measurements.

BIBLIOGRAPHY

Ainsworth C. C., Zachara J. M., and Schmidt R. L. (1987) Quinoline sorption on Namontmorillonite: contributions of the protonated and neutral species. *Clays and Clay Miner.* **35**, 121-128.

Allen D. T. and Shonnard D. R. (2002) *Green Engineering: Environmentally Conscious Design of Chemical Processes*. Prentice Hall.

Anthony J. L., Maginn E. J., and Brennecke J. F. (2001) Solution Thermodynamics of Imidazolium-Based Ionic Liquids and Water. *Journal of Physical Chemistry B* **105**, 10942-10949.

Atun G. and Kilislioglu A. (2002) The adsorption behavior of natural sand in contact with uranium contaminated seawater. *Journal of Environmental Science and Health, Part A: Environmental Science and Engineering* **A37**(7), 1295-1305.

Banaszak J. E., Reed D. T., and Rittmann B. E. (1998) Speciation-dependent toxicity of neptunium(V) toward *Chelatobacter heintzii*. *Environmental Science and Technology* **32**(8), 1085-1091.

Banaszak J. E., Webb S. M., Rittmann B. E., Gaillard J. F., and Reed D. T. (1999) Fate of neptunium in an anaerobic, methanogenic microcosm. *Materials Research Society Symposium Proceedings* **556**(Scientific Basis for Nuclear Waste Management XXII), 1141-1149.

Bargar J. R., Reitmeyer R., and Davis J. A. (1999) Spectroscopic Confirmation of Uranium(VI)-Carbonato Adsorption Complexes on Hematite. *Environmental Science and Technology* **33**(14), 2481-2484.

Bargar J. R., Reitmeyer R., Lenhart J. J., and Davis J. A. (2000) Characterization of U(VI)-carbonato ternary complexes on hematite: EXAFS and electrophoretic mobility measurements. *Geochimica et Cosmochimica Acta* **64**(16), 2737-2749.

Bencheikh-Latmani R., Leckie J. O., and Bargar J. R. (2003) Fate of Uranyl in a Quaternary System Composed of Uranyl, Citrate, Goethite, and *Pseudomonas fluorescens*. *Environmental Science and Technology* **37**(16), 3555-3559.

Bernhard G., Geipel G., Reich T., Brendler V., Amayri S., and Nitsche H. (2001) Uranyl(VI) carbonate complex formation: validation of the $Ca_2UO_2(CO_3)_3$(aq.) species. *Radiochimica Acta* **89**(8), 511-518.

Bethke C. M. and Brady P. V. (2000) How the Kd approach undermines ground water cleanup. *Ground Water* **38**(3), 435-443.

Beveridge T. J. and Murray R. G. E. (1976) Uptake and retention of metals by cell-walls of *Bacillus subtilis*. *Journal of Bacteriology* **127**, 1502-1518.

Beveridge T. J. and Murray R. G. E. (1980) Sites of metal deposition in the cell wall of *Bacillus subtilis*. *Journal of Bacteriology* **141**(2), 876-87.

Boily J. F. and Fein J. B. (2000) Proton binding to humic acids and sorption of Pb(II) and humic acid to the corundum surface. [Erratum to document cited in CA133:119775]. *Chemical Geology* **171**(1-2), 145-146.

Borrok D., Fein J. B., and Kulpa C. F. (2004a) Proton and Cd adsorption onto natural bacterial consortia: Testing universal adsorption behavior. *Geochimica et Cosmochimica Acta* **68**(15), 3231-3238.

Borrok D., Fein J. B., Tischler M., O'Loughlin E., Meyer H., Liss M., and Kemner K. M. (2004b) The effect of acidic solutions and growth conditions on the adsorptive properties of bacterial surfaces. *Chemical Geology* **209**(1-2), 107-119.

Borrok D. M., Fein J. B., and Kulpa C. F., Jr. (2004c) Cd and Proton Adsorption onto Bacterial Consortia Grown from Industrial Wastes and Contaminated Geologic Settings. *Environmental Science and Technology* **38**(21), 5656-5664.

Boyanov M. I., Kelly S. D., Kemner K. M., Bunker B. A., Fein J. B., and Fowle D. A. (2003) Adsorption of cadmium to *Bacillus subtilis* bacterial cell walls: A pH-dependent X-ray absorption fine structure spectroscopy study. *Geochimica et Cosmochimica Acta* **67**(18), 3299-3311.

Brady P. V. and Bethke C. M. (2000) Beyond the Kd approach. *Ground Water* **38**(3), 321-322.

Brennecke J. F. and Maginn E. J. (2001) Ionic Liquids: Innovative Fluids for Chemical processing. *AIChE Journal* **47**(11), 2384-2389.

Buck E. C., Brown N. R., and Dietz N. L. (1996) Contaminant uranium phases and leaching at the Fernald site in Ohio. *Environmental Science and Technology* **30**(1), 81-8.

Chatellier X. and Fortin D. (2004) Adsorption of ferrous ions onto *Bacillus subtilis* cells. *Chemical Geology* **212**(3-4), 209-228.

Chipera S. J. and Bish D. L. (2001) Basline studies of the Clay Minerals Society source clays: powder x-ray diffractions analysis. *Clays and Clay Miner.* **49**(5), 398-409.

Choppin G. R. (1997) Factors in Ln(III) complexation. *Journal of Alloys and Compounds* **249**(1-2), 1-8.

Choppin G. R. and Kullberg L. (1978) Protonation thermodynamics of humic acid. *Journal of Inorganic and Nuclear Chemistry* **40**, 651-654.

Choppin G. R. and Mathur J. N. (1991) Hydrolysis of actinyl(VI) cations. *Radiochimica Acta* **52-53**(Pt. 1), 25-8.

Christensen J. J., Hansen L. D., and Izatt R. M. (1976) *Handbook of Proton Ionization Heats and Related Thermodynamic Quantities*. Wiley-Interscience.

Christensen J. J., Izatt R. M., and Hansen L. D. (1967) Thermodynamics of proton ionization in dilute aqueous solution. VII. ΔH and ΔS values for proton ionization from carboxylic acids at 25°. *Journal of the American Chemical Society* **89**, 213-222.

Cox J. S., Smith D. S., Warren L. A., and Ferris F. G. (1999) Characterizing heterogeneous bacterial surface functional groups using discrete affinity spectra for proton binding. *Environmental Science and Technology* **33**(24), 4514-4521.

Daughney C. J. and Fein J. B. (1998a) The effect of ionic strength on the adsorption of H^+, Cd^{2+}, Pb^{2+}, and Cu^{2+} by *Bacillus subtilis* and *Bacillus licheniformis*: a surface complexation model. *Journal of Colloid and Interface Science* **198**(1), 53-77.

Daughney C. J. and Fein J. B. (1998b) Sorption of 2,4,6-Trichlorophenol by *Bacillus subtilis*. *Environmental Science and Technology* **32**(6), 749-752.

Daughney C. J., Siciliano S. D., Rencz A. N., Lean D., and Fortin D. (2002) Hg(II) adsorption by bacteria: A surface complexation model and its application to shallow acidic lakes and wetlands in Kejimkujik National Park, Nova Scotia, Canada. *Environmental Science and Technology* **36**(7), 1546-1553.

Do D. D. and Do H. D. (2002) Characterization of micro-mesoporous carbonaceous materials. Calculations of adsorption isotherm of hydrocarbons. *Langmuir* **18**(1), 93-99.

Earle M., J. and Seddon K., R. (2000) Ionic liquids. Green solvents for the future. *Pure and Applied Chemistry* **72**(7), 1391-1398.

Economopoulou A. A. and Economopoulos A. P. (2002) Air pollution in Athens basin and health risk assessment. *Environmental Monitoring and Assessment* **80**(3), 277-299.

Fahey J. A. (1986) Neptunium. In *The Chemistry of the Actinide Elements* (ed. J. J. Katz,

G. T. Seaborg, and L. R. Morss), pp. 443-498. Chapman Hall.

Fein J. B., Boily J. F., Guclu K., and Kaulbach E. (1999) Experimental study of humic acid adsorption onto bacteria and Al-oxide mineral surfaces. *Chemical Geology* **162**(1), 33-45.

Fein J. B., Boily J.-F., Yee N., Gorman-Lewis D., and Turner B. F. (2005) Potentiometric titrations of *Bacillus subtilis* cells to low pH and a comparison of modeling approaches. *Geochimica et Cosmochimica Acta* **69**(5), 1123-1132.

Fein J. B., Daughney C. J., Yee N., and Davis T. A. (1997) A chemical equilibrium model for metal adsorption onto bacterial surfaces. *Geochimica et Cosmochimica Acta* **61**(16), 3319-3328.

Fein J. B. and Delea D. (1999) Experimental study of the effect of EDTA on Cd adsorption by Bacillus subtilis: a test of the chemical equilibrium approach. *Chemical Geology* **161**(4), 375-383.

Fein J. B., Fowle D. A., Cahill J., Kemner K., Boyanov M., and Bunker B. (2002) Nonmetabolic reduction of Cr(VI) by bacterial surfaces under nutrient-absent conditions. *Geomicrobiology Journal* **19**(3), 369-382.

Fein J. B., Martin A. M., and Wightman P. G. (2001) Metal adsorption onto bacterial surfaces: development of a predictive approach. *Geochimica et Cosmochimica Acta* **65**(23), 4267-4273.

Ferris F. G., Schultze S., Witten T. C., Fyfe W. S., and Beveridge T. J. (1989) Metal interactions with microbial biofilms in acidic and neutral pH environments. *Applied and Environmental Microbiology* **55**(5), 1249-57.

Fowle D. A. and Fein J. B. (1999) Competitive adsorption of metal cations onto two gram positive bacteria: testing the chemical equilibrium model. *Geochimica et Cosmochimica Acta* **63**(19/20), 3059-3067.

Fowle D. A. and Fein J. B. (2000) Experimental measurements of the reversibility of metal-bacteria adsorption reactions. *Chemical Geology* **168**(1-2), 27-36.

Fowle D. A., Fein J. B., and Martin A. M. (2000) Experimental study of uranyl adsorption onto *Bacillus subtilis*. *Environmental Science and Technology* **34**(17), 3737-3741.

Garelick H., Dybowska A., Valsami-Jones E., and Priest N. D. (2005) Remediation technologies for arsenic contaminated drinking waters. *Journal of Soils and Sediments* **5**(3), 182-190.

Giblin A. M., Batts B. D., and Swaine D. J. (1981) Laboratory simulation studies of uranium mobility in natural waters. *Geochimica et Cosmochimica Acta* **45**(5), 699-709.

Gorman-Lewis D., Elias P. E., and Fein J. B. (2005a) Adsorption of Aqueous Uranyl Complexes onto Bacillus subtilis Cells. *Environmental Science and Technology* **39**(13), 4906-4912.

Gorman-Lewis D., Fein Jeremy B., Soderholm L., Jensen M. P., and Chiang M. H. (2005b) Experimental Study of Neptunyl Adsorption onto *Bacillus Subtilis*. *Geochimica et Cosmochimica Acta* **29**(20), 4837-4844.

Gorman-Lewis D. J. and Fein J. B. (2004) Experimental Study of the Adsorption of an Ionic Liquid onto Bacterial and Mineral Surfaces. *Environmental Science and Technology* **38**(8), 2491-2495.

Grenthe I., Fuger J., Konings R. J., Lemire R. J., Muler A. B., Nguyen-Trung C., and Wanner H. (1992) *Chemical Thermodynamics of Uranium*. Elsevier.

Grenthe I., Ots H., and Ginstrup O. (1970) A calorimetric determination of the enthalpy of ionization of water and the enthalpy of protonation of THAM at 5, 20, 25, 35, and 50 °C. *Acta Chemica Scandinavica* **24**, 1067-1080.

Guillaume B., Begun G. M., and Hahn R. L. (1982) Raman spectrometric studies of "cation-cation" complexes of pentavalent actinides in aqueous perchlorate solutions. *Inorganic Chemistry* **21**(3), 1159-66.

Haas J. R., Dichristina T. J., and Wade R. (2001) Thermodynamics of U(VI) sorption onto *Shewanella putrefaciens*. *Chemical Geology* **180**(1-4), 33-54.

Haderlein S. B., Weissmahr K. W., and Scharwzenbach R. P. (1996) Specific adsorption of nitroaromatic explosives and pesticides to clay minerals. *Environ. Sci. Tech.* **30**, 612-622.

Hale J. D., Izatt R. M., and Christensen J. J. (1963) A calorimetric study of the heat of ionization of water at 25°. *Journal of Physical Chemistry* **67**, 2605-2608.

Hayes K. F., Redden G., Wendell E., and Leckie J. O. (1991) Surface Complexation Models: An Evaluation of Model Parameter Estimation Using FITEQL and Oxide Mineral Titration Data. *J. Colliod Interface Sci.* **142**(2), 448-469.

Hennig C., Panak P. J., Reich T., Rossberg A., Raff J., Selenska-Pobell S., Matz W., Bucher J. J., Bernhard G., and Nitsche H. (2001) EXAFS investigation of uranium(VI) complexes formed at *Bacillus cereus* and *Bacillus sphaericus* surfaces. *Radiochimica Acta* **89**(10), 625-631.

Herbelin A. and Westall J. C. (1994) FITEQL 3.1, A computer program for determination of chemical equilibrium constants from experimental data. Dept. of Chem. Oregon St. Univ.

Holm P. E., Rootzen H., Borggaard O. K., Moberg J. P., and Christensen T. H. (2003) Correlation of cadmium distribution coefficients to soil characteristic. *J. Envron. Qual.* **32**, 138-145.

Hsi C. K. D. and Langmuir D. (1985) Adsorption of uranyl onto ferric oxyhydroxides: application of the surface complexation site-binding model. *Geochimica et Cosmochimica Acta* **49**(9), 1931-41.

Iler R. K. (1979) *The chemistry of Silica*. Wiley.

Jensen M. P., Morss L. R., Beitz J. V., and Ensor D. D. (2000) Aqueous complexation of trivalent lanthanide and actinide cations by N,N,N',N'-Tetrakis(2pyridylmethyl)ethylenediamine. *J. Alloys Compd.* **303/304**, 137-141.

Jensen M. P. and Nash K. L. (2001) Thermodynamics of dioxoneptunium(V) complexation by dicarboxylic acids. *Radiochimica Acta* **89**(9), 557-564.

Jespersen N. D. and Jordan J. (1970) Thermometric enthalpy titration of proteins. *Analytical Letters* **3**, 323-334.

Johnston J. H. and Cardile C. M. (1987) Iron substitution in montmorillonite, illite, and glauconite by Fe-57 mossbauer-spectroscopy. *Clays and Clay Minerals* **35**(3), 170-176.

Keller C. (1971) Neptunium. In *The Chemistry of the Transuranium Elements*, Vol. 3, pp. 197-204. V C H Publishers.

Kelly S. D., Kemner K. M., Fein J. B., Fowle D. A., Boyanov M. I., Bunker B. A., and Yee N. (2002) X-ray absorption fine structure determination of pH-dependent Ubacterial cell wall interactions. *Geochimica et Cosmochimica Acta* **66**(22), 38553871.

King E. J. (1965) *Acid-Base Equilibria*. Macmillan.

Koretsky C. (2000) The significance of surface complexation reactions in hydrologic systems: a geochemist's perspective. *Journal of Hydrology (Amsterdam)* **230**(3-4), 127-171.

Kraepiel A. M. L., Keller K., and Morel F. M. M. (1999) A model for metal adsorption onto montmorillonite. *Journal of Colloid and Interface Science* **210**, 43-54.

Langmuir D. (1979) Techniques of estimating thernodynamic properties for some aqueous complexes of geochemical interest. In *Chemical Modeling in Aqueous Systems* (ed. E. A. Jenne), pp. 353-387. Amer. Chem. Soc.

Langmuir D. (1997) *Aqueous Environmental Geochemistry*. Prentice Hall Inc.

Lee J. U. and Fein J. B. (2000) Experimental study of the effects of *Bacillus subtilis* on gibbsite dissolution rates under near-neutral pH and nutrient-poor conditions. *Chemical Geology* **166**(3-4), 193-202.

Lemire R. J., Fuger J., Nitsche H., Rand M. H., Potter P., Rydberg J., Spahiu K., Sullivan

J. C., Ullman W. J., Vitorage P., and Wanner H. (2001) *Chemica*l *Thermodynamics of Neptunium and Plutonium*. Elsevier.

Lieser K. H., Quandt-Klenk S., and Thybusch B. (1992) Sorption of uranyl ions on hydrous silicon dioxide. *Radiochimica Acta* **57**(1), 45-50.

Lieser K. H. and Thybusch B. (1988) Sorption of uranyl ions on hydrous titanium dioxide. *Fresenius' Journal of Analytical Chemistry* **332**(4), 351-7.

Lloyd J. R., Yong P., and Macaskie L. E. (2000) Biological reduction and removal of Np(V) by two microorganisms. *Environmental Science and Technology* **34**(7), 1297-1301.

Longmire P., Turney W. R., Mason C. F. V., Dander D., and York D. (1994) Predictive geochemical modeling of uranium and other contaminants in laboratory columns in relatively oxidizing, carbonate-rich solutions. *Technology and Programs for Radioactive Waste Management and Environmental Restoration*(Vol. 3), 2081-5.

Macaskie L. E. and Basnakova G. (1998) Microbially-enhanced chemical sorption of heavy metals: A method for the bioremediation of solutions containing long-lived isotopes of neptunium and plutonium. *Environmental Science and Technology* **32**, 2049-2059.

Markai S., Andres Y., Montavon G., and Grambow B. (2003) Study of the interaction between europium (III) and *Bacillus subtilis*: fixation sites, biosorption modeling and reversibility. *Journal of Colloid and Interface Science* **262**(2), 351-361.

Martell A. E., Smith R. M., and Motekaitis R. J. (1998) Critically Selected Stability Constants of Metal Complexes Database Version 5.0. In *NIST Standard Reference Database*, Vol. 46. NIST Standard Reference Data.

Martinez R. E., Smith D. S., Kulczycki E., and Ferris F. G. (2002) Determination of intrinsic bacterial surface acidity constants using a Donnan shell model and a continuous pKa distribution method. *Journal of Colloid and Interface Science* **253**(1), 130-139.

Masjedi M. R., Jamaati H. R., Dokouhaki P., Ahmadzadeh Z., Taheri S. A., Bigdeli M., Izadi S., Rostamian A., Aagin K., and Ghavam S. M. (2003) The effects of air pollution on acute respiratory conditions. *Respirology.* **8**(2), 213-230.

McKinley J. P., Zachara J. M., Smith S. C., and Turner G. D. (1995) The influence of uranyl hydrolysis and multiple site-binding reactions on adsorption of U(VI) to montmorillonite. *Clays and Clay Minerals* **43**(5), 586-98.

Molhave L. (2003) Organic compounds as indicators of air pollution. *Indoor Air.* **13**(Suppl 6), 12-19.

Nakajima A., Horikoshi T., and Sakaguchi T. (1982) Studies on the accumulation of heavy metal elements in biological systems. XXI. Recovery of uranium by immobilized microorganisms. *European Journal of Applied Microbiology and Biotechnology* **16**(2-3), 88-91.

Nancollas G. H. (1966) *Interactions in Electrolyte Solutions*. Elsevier.

Nash K. L., Rao L. F., and Choppin G. R. (1995) Calorimetric and laser induced fluorescence investigation of the complexation geometry of selected europium-gem-diphosphonate complexes in acidic solutions. *Inorganic Chemistry* **34**, 27532758.

Ngwenya B. T., Sutherland I. W., and Kennedy L. (2003) Comparison of the acid-base behaviour and metal adsorption characteristics of a gram-negative bacterium with other strains. *Applied Geochemistry* **18**(4), 527-538.

Panak P. J., Knopp R., Booth C. H., and Nitsche H. (2002) Spectroscopic studies on the interaction of U(VI) with *Bacillus sphaericus*. *Radiochimica Acta* **90**(9-11), 779-783.

Paris D. F., Steen W. C., Baughman G. L., and Barnett Jr. J. T. (1981) 2nd-Order Model to Predict Microbial-Degradation of Organic-Compounds in Natural-Waters. *Applied and Environmental Microbiology* **41**(3), 603-609.

Perdue E. M. (1978) Solution thermochemistry of humic substances-I. Acid-base equilibria of humic acid. *Geochimica et Cosmochimica Acta* **42**, 1351-1358.

Plette A. C. C., van Riemsdijk W. H., Benedetti M. F., and Van der Wal A. (1995) pH dependent charging behavior of isolated cell walls of a Gram-positive soil bacterium. *Journal of Colloid and Interface Science* **173**(2), 354-63.

Rao L. and Choppin G. R. (1995) Thermodynamic study of the complexation of neptunium(V) with humic acids. *Radiochim. Acta* **69**, 87-95.

Rheinlander T., Klumpp E., and Schwuger M. J. (1998) On the adsorption of hydrophobic pollutants on surfactant/clay complexes: Comparison of the influence of a cationic and a nonionic surfactant. *Journal of Dispersion Science and Technology* **19**(2-3), 379-398.

Rittmann B. E., Banaszak J. E., and Reed D. T. (2003) Reduction of Np(V) and precipitation of Np(IV) by an anaerobic microbial consortium. *Biodegradation* **13**(5), 329-342.

Rizkalla E. N. and Choppin G. R. (1992) Hydration of lanthanides and actinides in solution. *Journal of Alloys and Compounds* **180**, 325-36.

Runde W. (2002) Geochemical interactions of actinides in the environment. *Geochemistry of Soil Radionuclides* **SSSA Special Publication**(59), 21-44.

Sar P. and D'Souza S. F. (2001) Biosorptive uranium uptake by a *Pseudomonas* strain: characterization and equilibrium studies. *Journal of Chemical Technology & Biotechnology* **76**(12), 1286-1294.

Sasaki T., Zheng J., Asano H., and Kudo A. (2001) Interaction of Pu, Np and Pa with anaerobic microorganisms at geologic repositories. *Radioactivity in the Environment* **1**, 221-232.

Skanthakumar S., Gorman-Lewis D., Locock A., Chiang M. H., Jensen M. P., Burns P. C., Fein J., Jonah C. D., Attenkofer K., and Soderholm L. (2004) Changing Np redox speciation in the synchrotron beam. *Materials Research Society Symposium Proceedings* **802**, 151-156.

Soderholm L., Williams C. W., Antonio M. R., Tischler M. L., and Markos M. (2000) The influence of *Deulfovibrio desulfuricans* on neptunium chemistry. *Materials Research Society Symposia Proceedings* **590**, 27-32.

Sokolov I., Smith D. S., Henderson G. S., Gorby Y. A., and Ferris F. G. (2001) Cell surface electrochemical heterogeneity of the Fe(III)-reducing bacterium *Shewanella putrefaciens*. *Environmental Science and Technology* **35**(2), 341-347.

Songkasiri W., Reed D. T., and Rittman B. E. (2002) Bio-sorption of neptunium(V) by *Pseudomonas fluorescens*. *Radiochimica Acta* **90**, 785-789.

Sposito G. (1984) *The Surface Chemistry of Soils*. Oxford Univeristy Press.

Stamberg K., Venkatesan K. A., and Vasudeva Rao P. R. (2003) Surface complexation modeling of uranyl ion sorption on mesoporous silica. *Colloids and Surfaces, A: Physicochemical and Engineering Aspects* **221**(1-3), 149-162.

Stewart M. A., Jardine P. M., Brandt C. C., Barnett M. O., Fendorf S. E., McKay L. D., Mehlhorn T. L., and Paul K. (2003) Effects of contaminant concentration, aging, and soil properties on the bioaccessibility of Cr(III) and Cr(VI) in soil. *Soil & Sediment Contamination* **12**(1), 1-21.

Stipp S. L. S., Hansen M., Kristensen R., Hochella M. F., Bennedsen L., Dideriksen K., Balic-Zunic T., Leonard D., and Mathieu H. J. (2002) Behaviour of Fe-oxides relevant to contaminant uptake in the environment. *Chemical Geology* **190**(1-4), 321-337.

Stout B. E. and Choppin G. R. (1993) Cation-cation complexes of neptunyl. *Radiochimica Acta* **61**(2), 65-7.

Stoyer N. J., Hoffman D. C., and Silva R. J. (2000) Cation-cation complexes of PuO_2^{+} and NpO_2^{+} with Th^{4+} and UO_2^{2+}. *Radiochimica Acta* **88**(5), 279-282.

Sullivan J. C., Hindman J. C., and Zielen A. J. (1961) Specific interaction between Np(V) and U(VI) in aqueous perchloric acid media. *Journal of the American Chemical Society* **83**, 3373-8.

Sverjensky D. A. (1994) Zero-point-of-charge prediction from crystal chemistry and solvation theory. *Geochimica et Cosmochimica Acta* **58**(14), 3123-3129.

Sverjensky D. A. and Sahai N. (1996) Theoretical prediction of single-site surface-protonation equilibrium constants for oxides and silicates in water. *Geochimica et Cosmochimica Acta* **60**(20), 3773-3797.

Takeda S. and Usui S. (1987) Adsorption of dodecylammonium ion on quartz in relation to its flotation. *Colliods Surf.* **23**, 15-28.

Tripathi V. S. (1983). Ph.D. Dissertation, Stanford University.

Turner G. D., Zachara J. M., McKinley J. P., and Smith S. C. (1996) Surface-charge properties and UO_2^{2+} adsorption of a subsurface smectite. *Geochimica et Cosmochimica Acta* **60**(18), 3399-3414.

Turney W. R., Mason C. F. V., Longmire P., Dander D. C., York D. A., Chisholm-Brause

C. J., and Thomson B. M. (1994) Carbonate heap leach of uranium-contaminated soils. *Technology and Programs for Radioactive Waste Management and Environmental Restoration*(Vol. 3), 2087-90.

VanBriesen J. M. (1998) Modeling Coupled Biogeochemical Processes in Mixed Waste Systems. Ph. D. thesis, Northwestern Univ.

Vanderzee C. E. and Swanson J. A. (1963) The heat of ionization of water. *Journal of Physical Chemistry* **67**, 2608-2612.

Waite T. D., Davis J. A., Payne T. E., Waychunas G. A., and Xu N. (1994) Uranium(IV) adsorption to ferrihydrite: application of a surface complexation model. *Geochimica et Cosmochimica Acta* **58**(24), 5465-78.

Weerasooriya R., Aluthpatabendi D., and Tobschall H. J. (2001) Charge distribution multi-site complexation (CD-MUSIC) modeling of Pb(II) adsorption on gibbsite. *Colliods Surf. A.* **189**, 131-144.

Weerasooriya R., Dharmasena B., and Aluthpatabendi D. (2000) Copper-gibbsite interactions: and application of 1-pK surface complexation model. *Colliods Surf. A.* **170**, 65-77.

Weerasooriya R., Wijesekara H. K. D. K., and Bandara A. (2002) Surface complexation modeling of cadmium adsorption on gibbsite. *Colloid and Surface A* **207**, 13-24.

Welton T. (1999) Room-Temperature Ionic Liquids. Solvents for Synthesis and Catalysis. *Chemical Review* **99**, 2071-2083.

Weppen P. and Hornburg A. (1995) Calorimetric studies on interactions of divalent cations and microorganisms or microbial envelopes. *Thermochimica Acta* **269/270**, 393-404.

Wightman P. G., Fein J. B., Wesolowski D. J., Phelps T. J., Benezeth P., and Palmer D. A. (2001) Measurement of bacterial surface protonation constants for two species at elevated temperatures. *Geochimica et Cosmochimica Acta* **65**(21), 3657-3669.

Wolery T. J. (1992) EQ3NR, a computer program for geochemical aqueous speciation-solubility calculations: theoretical manual, user's guide and related documentation (Version 7.0): Part 3, pp. 259 pp. Livermore Natl. Lab.,Livermore,CA,USA.

Yanase N., Payne T. E., and Sekine K. (1995) Groundwater geochemistry in the Koongarra ore deposit, Australia (II). Activity ratios and migration mechanisms of uranium series radionuclides. *Geochemical Journal* **29**(1), 31-54.

Yee N. and Fein J. (2001) Cd adsorption onto bacterial surfaces: A universal adsorption edge? *Geochimica et Cosmochimica Acta* **65**(13), 2037-2042.

Yee N. and Fein J. B. (2002) Does metal adsorption onto bacterial surfaces inhibit or enhance aqueous metal transport? Column and batch reactor experiments on Cd-Bacillus subtilis-quartz systems. *Chemical Geology* **185**(3-4), 303-319.

Yee N., Fowle D. A., and Ferris F. G. (2004) A Donnan potential model for metal sorption onto *Bacillus subtilis*. *Geochimica et Cosmochimica Acta* **68**(18), 36573664.

Zachara J. M., Ainsworth C. C., Cowan C. E., and Thomas B. L. (1987) Sorption of binary mixtures of aromatic nitrogen heterocyclic compounds on subsurface materials. *Environmental Science and Technology* **21**, 397-402.

Zachara J. M., Ainsworth C. C., Felice L. J., and Resch C. T. (1986) Quinoline sorption to subsurface materials: Role of pH and rention of the organic cation. *Environmental Science and Technology* **20**, 620-627.

Zachara J. M., Ainsworth C. C., and Smith S. C. (1990) The sorption of N-heterocyclic compounds on reference and subsurface smectite clay isolates. *Journal of Contaminant Hydrology* **6**, 281-305.

Zekany L. and Nagypal I. (1985) A Comprehensive Program for the Evalution of Potentiometric and/or Spectrophotometric Equilibrium Data Using Analytical Derivatives. In *Computational Methods for the Determination of Formation Constansts*. Plenum Press.

Zhang P.-C., Krumhansl J. L., and Brady P. V. (2002) Introduction to properties, sources and characteristics of soil radionuclides. *SSSA Special Publication* **59**(Geochemistry of Soil Radionuclides), 1-20.